Femtosecond Fluorescence Studies of Intramolecular Reorientational Motions.

van der Meer, M.J.

Publication date
2000
Document Version
Final published version

Femtosecond Fluorescence Studies

of

Intramolecular Reorientational Motions

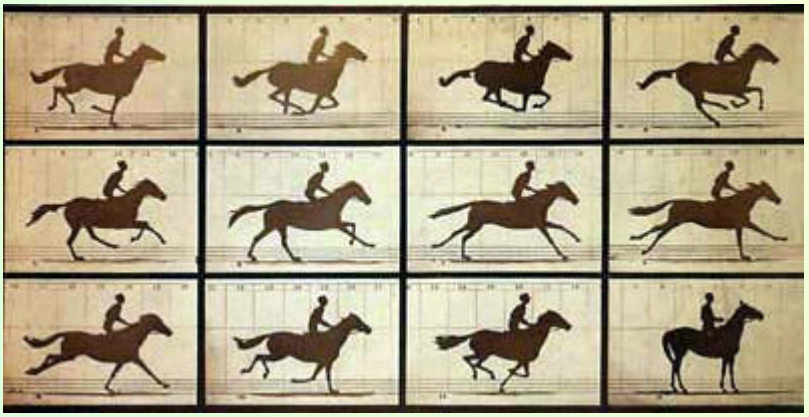

M.J. van der Meer

Femtosecond Fluorescence Studies

of

Intramolecular Reorientational Motions

M.J. van der Meer

Cover photo: Eadweard Muybridge 1878. This photo was a first ‘time-resolved’ study of a galloping horse. It settled a bet of $25.000 over the question whether a galloping horse at any time has all four hooves in the air.

Femtosecond Fluorescence Studies
of
Intramolecular Reorientational Motions

ACADEMISCH PROEFSCHRIFT

ter verkrijging van de graad van doctor
aan de Universiteit van Amsterdam
op gezag van Rector Magnificus
Prof. dr J.J.M. Franse
ten overstaan van een door college voor promoties ingestelde
commissie, in het openbaar te verdedigen in de Aula der Universiteit
op dinsdag 21 november 2000, te 10:00 uur

door

Michiel Jacobus van der Meer

geboren te Leiden

Promotor : Prof. dr M. Glasbeek

Faculteit der Natuurwetenschappen, Wiskunde en Informatica

Promotiecommissie : Prof. dr C.A. de Lange
Prof. dr K.J. Hellingwerf
Prof. dr N.M.M. Nibbering
Prof. dr H. Schenk
Dr H.J. Bakker
Prof. dr J.I. Dijkhuis

List of publications

The work described in this thesis has in part appeared in the following articles:

Chapter 3

P. Changenet, H. Zhang, M.J. van der Meer, M. Glasbeek, P. Plaza, M.M. Martin,
Ultrafast twisting dynamics of photoexcited auramine in solution,
J. Phys. Chem. A **102**, 6716-6721 (1998).

Chapter 4

M.J. van der Meer, H. Zhang, M. Glasbeek,
Femtosecond fluorescence upconversion studies of barrierless bond twisting of auramine in solution,
J. Chem. Phys. **112**, 2878-2887 (2000).

Chapter 5

M.J. van der Meer, H. Zhang, W. Rettig, M. Glasbeek,
Femto- and picosecond fluorescence studies of solvation and non-radiative deactivation of ionic styryl dyes in liquid solution,
Chem. Phys. Lett. **320**, 673-680 (2000).

Chapter 6

P. Changenet, H. Zhang, M.J. van der Meer, K.J. Hellingwerf, M. Glasbeek,
Subpicosecond fluorescence upconversion measurements of primary events in yellow protein,
Chem. Phys. Lett. **282**, 276-282 (1998).

In addition, the author participated in the following papers:

M. Glasbeek, H. Zhang, M.J. van der Meer,
Femtosecond studies of barrierless bond twisting in solution,
Proceedings of Femtochemistry IV, Leuven July 1999.

P. Changenet, H. Zhang, M.J. van der Meer, M. Glasbeek, P. Plaza, M.M. Martin,
Fluorescence quenching of auramine in fluid solution: a femtosecond spectroscopy study,
J. Fluoresc. **10**, 155-160 (2000).

M. Glasbeek, H. Zhang, M.J. van der Meer,
Femtosecond studies of barrierless rotamers in solution,
J. Chin. Chem. Soc. TAIP. **47**, 715-719 (2000).

M. Glasbeek, H. Zhang, M.J. van der Meer,
Femtosecond studies of twisting dynamics of auramine in solution,
J. Mol. Liq. **86**, 123-126 (2000).

Contents

Chapter 1

Introduction

1.1 General

Studies of chemical reaction dynamics are of fundamental importance for a better understanding of chemical reaction mechanisms on a molecular level [Refs.1-4, and references therein]. A common concept in discussions of reaction dynamics is the reaction potential energy function. Figure 1.1 displays an example for such a function. The free energy of the system of interest is plotted as a function of a reaction coordinate [2,5]. The reaction coordinate is usually mainly determined by intramolecular vibrational modes and, in the case the molecules are in solution, by motions of solvent molecules. The first minimum (R) of the function in Figure 1.1 corresponds to the initial state of the reactants, the second minimum (P) is the product state.

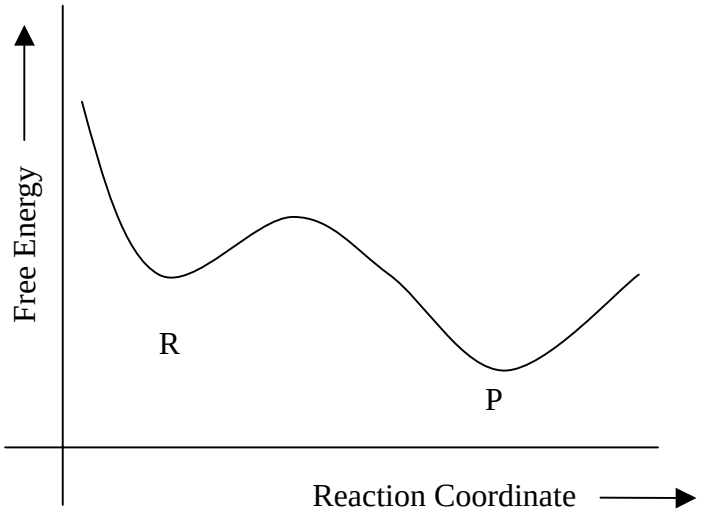

Figure 1.1. Free energy function of the reactant- and product state as a function of the reaction coordinate.

Chemical reaction dynamics in solution is characterized by various entities [4,6,7]. In many cases the nature of the solvent has a major effect on the shape of the potential energy function. The polarity and viscosity of the solvent, for instance, could affect the energy of the minima and the height of the activation barrier.

In this thesis we focus on the dynamics of first-order photo-induced reactions in solution. Photo-induced chemical reactions are of great importance to many chemical and biological systems and applications. Examples are laser dyes [8,9], photoactive proteins [10] and liquid crystal displays [11]. Rate constants of photo-induced chemical reactions may vary over a wide range. While charge transfer processes in solution may occur on a (sub-)picosecond time scale, backbone reorganisational motions in protein systems extend over seconds or even minutes. Photo-induced reaction dynamics can be probed using time-resolved spectroscopy [12-14]. With the advent of ultrafast laser technology it has become possible to study reaction dynamics with a (sub-)picosecond time resolution. Because of this time resolution ultrafast processes, such as charge transfer, can now be monitored in real-time.

In this thesis intramolecular conformational changes are of central interest. We study the role of intramolecular conformational changes in ultrafast photo-induced excited-state reaction dynamics in solution. The main issues of reaction dynamics are the nature of the reaction coordinate and the shape of the potential energy surface. Influences of different solvent properties, such as polarity and viscosity, on the shape of the potential energy function are investigated. We focus on characterizing the electronic excited state(s) of the molecular system which is/are involved in the fluorescent excited state potential. In order to probe ultrafast photo-induced excited-state reaction dynamics, experiments are conducted by means of time-resolved fluorescence spectroscopy with a (sub)-picosecond time resolution. In some cases model simulations, based on a theoretical description of the potential energy function, are performed to get a better understanding of the physics underlying the experimentally observed phenomena.

The review of solvation dynamics given in Section 1.2 is meant to give some background information to the discussion of the experimental results given in Chapter 5. Several aspects of intramolecular vibrational modes, important in the discussion of the experimental results of Chapters 3 and 4, are presented in Section 1.3. Introductory information on isomerization dynamics in (biological) systems, i.e., the topic of Chapters 6 and 7, is given in Section 1.4. Finally an outline of this thesis is presented in Section 1.5.

1.2 Solvation dynamics

Numerous research activities have focused on the study of solvation dynamics ever since the first reports by Bakshiev, Mazurenko and Ware et al. [16-18]. These studies involved time-resolved spectroscopic measurements of molecules in polar solvents. To clarify some of the principles, we consider a molecule in the ground state in equilibrium with the surrounding solvent molecules. If the dipole moments of the solute (in a polar solvent), in the ground- and excited states respectively, are largely different ($\mu_g << \mu_e$), impulsive photo-excitation will instantaneously change the dipole moment of the solute molecule. The solvent molecules surrounding the solute are now no longer in an equilibrium situation. After the pulsed excitation the solvent molecules will start to reorient in order to reach the new excited state equilibrium situation. This is illustrated in Figure 1.2.

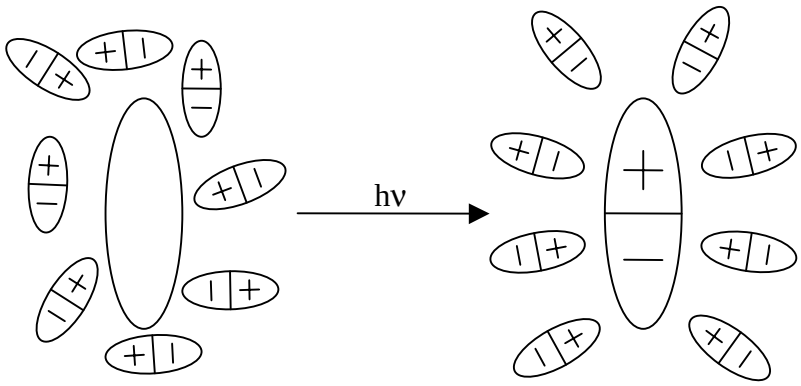

Figure 1.2. Reorientation of the solvent molecules after photo-excitation. On the right-hand side it is shown that the dipole moment of the solute has changed and that the solvent molecules are no longer randomly distributed around it.

In the theoretical treatment of the solvent molecular relaxation by van der Zwan and Hynes [19], it is assumed that the solute molecule in the excited state is not polarizable (μ_e is constant during solvation) and that excited state reactions do not occur. In this approach it is assumed that linear response theory applies for the solute/solvent system [20]. In Figure 1.3, the energy as a function of the reaction coordinate is drawn for the electronic ground- and excited-states of such a system [7]. In the ground state the population distribution as a function of the reaction coordinate is considered to be Gaussian under equilibrium conditions. Pulsed photo-excitation excites this distribution to the excited state potential. The vertical excitation, shown in

Figure 1.3, reflects the fact that the electronic distribution changes much faster than the nuclear motions (Franck-Condon principle). The reaction coordinate of the solvation process is considered to be represented by a so-called generalized solvation coordinate. In the case of a polar solvent the reaction coordinate is a measure for the nuclear solvent polarization that can be considered to be in equilibrium with an effective dipole moment $\mu(t)$ of the solute molecule. Normalization leads to the relative coordinate $x(t)$, given as,

$$x(t) = \frac{\mu(t) - \mu_g}{\mu_e - \mu_g} \qquad (1.1)$$

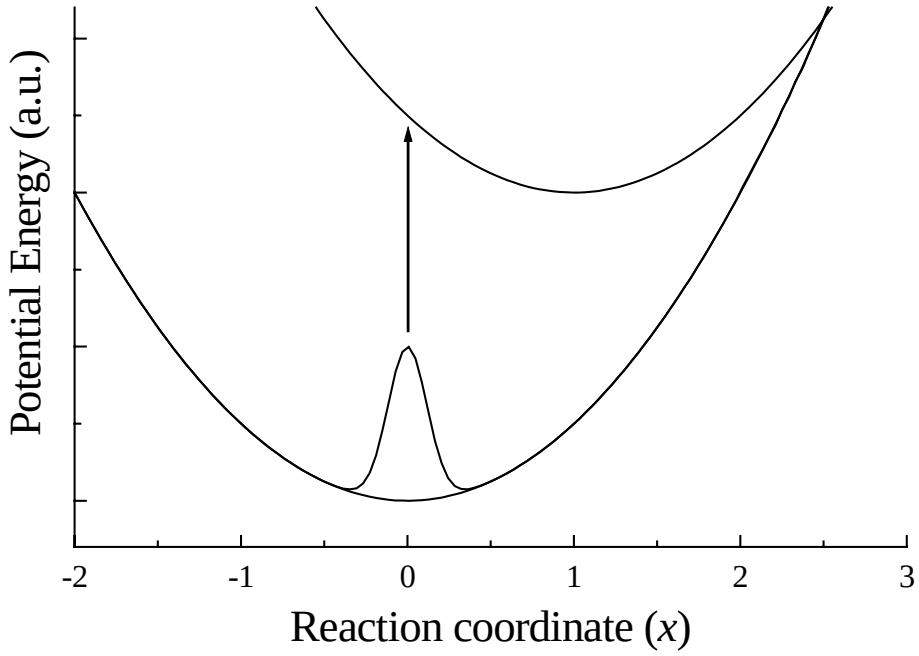

Figure 1.3. Illustration of the potential energy curves of the ground and first electronic excited state as a function of a reaction coordinate *x*.

The relaxation of the excited state population is usually studied by following the temporal characteristics of the spectral response function (dynamic Stokes shift):

$$S(t) = \frac{\nu(t) - \nu(\infty)}{\nu(0) - \nu(\infty)} \qquad (1.2)$$

The time-dependence of the emission frequency of the solute molecule ($\nu(t)$) is a measure for the shift of the excited state population (Figure 1.4).

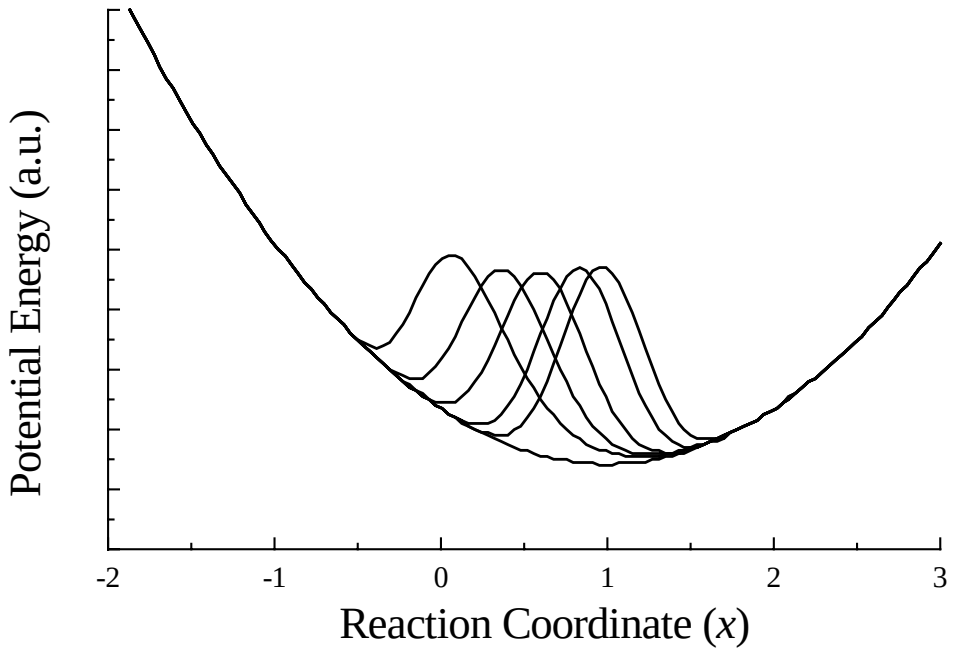

Figure 1.4. Progression of the excited state population over the potential energy surface at several times after pulsed excitation.

The spectral response function can also be written as:

$$S(t) = \frac{E_{sol}(t) - E_{sol}(\infty)}{E_{sol}(0) - E_{sol}(\infty)} \qquad (1.3)$$

in which $E_{sol}(t)$ is the time-dependent solvation energy of the solute. This energy may be composed of several components [6]:

$$E_{sol}(t) = E_p(t) + E_{np}(t) + E_{vibr}(t) + E_{solv}(t) \qquad (1.4)$$

$E_p(t)$ is the electrostatic interaction between the solute and the solvent molecules. The non-polar (e.g. van der Waals) solute-solvent interaction energy is $E_{np}(t)$, the relaxation of intramolecular vibrational modes is denoted by $E_{vibr}(t)$. The change in the solvent-

solvent interaction induced by the change in dipole moment of the solute molecule is represented by $E_{solv}(t)$. For rigid solute molecules, dissolved in a polar solvent, with a large difference in ground- and excited-state dipole moment, the spectral dynamics generally is predominantly determined by $E_p(t)$. The other three terms in Expression 1.4 are in this case negligible. Examples of such fluorescent probes are 4-dicyanomethylene-2-methyl-6-(p-dimethylaminostyryl)-4H-pyran (DCM) [21], coumarin 153 [13,22,23], 7-dimethylamino-4-coumarin-acetic acid (DMACAA) [13]. The experimentally obtained spectral response functions have been fitted to multi-exponential decay functions. Time constants and pre-exponential factors of these fit-functions have been tabulated for numerous solvents [22,23]. In Chapter 5, in the discussion of our experimental results for the DPD family (unbridged and bridged diphenyl derivatives of 1- or 4-(4'-dimethylaminostyryl)pyridinium dyes), we determine the time constants for the solvation in ethanol, decanol and benzonitrile, and compare these values with those reported in the literature [24].

Whereas in the first theoretical studies of solvation (e.g. the continuum dielectric model of Debye-Onsager [25]) a single exponential solvation relaxation is predicted, in many experimental studies, however, non-exponential behavior has been observed [13,21-23]. The non-exponential behavior indicates that the continuum models are not adequate to describe the dynamics of solvation. An improved theory is the mean spherical approximation by Wolynes [26], or the theory of Chandra and Bagchi, which includes both rotational and diffusional motions of the solvent [27]. A recent theoretical survey has been given by Bagchi et al.[6].

1.3 Intramolecular modes

In many reactions, the reaction coordinate involves intramolecular reorganisational modes. For example, intramolecular twisting, bending or stretching modes may trigger chemical reactions.

Many time-resolved spectroscopic studies have been performed for molecules showing intramolecular conformational changes. Well-known examples are DMABN [28-32], 9,9'-bianthryl [33-37], and di- and triphenylmethane dye molecules like crystal violet [38-47], ethyl violet [48,49] and malachite green [49-52]. The focus of these studies has been on the nature of the reaction coordinate. The experimental

results of DMABN (dimethyl-aminobenzonitrile) and derivatives have raised considerable controversy regarding the nature of the reaction coordinate for these molecules. A point of great dispute has been whether the excited charge transfer state is twisted (TICT) with respect to the planar ground state [28-30] or whether a pyramidalization (of the amino nitrogen) coordinate was involved [31,32]. Advanced theoretical descriptions of the photo-induced TICT reactions in the case of DMABN, where both intramolecular twisting and solvent molecule motions were taken into account, gave evidence for a solvent dependent reaction path over a two-dimensional potential energy surface [53]. In a recent study, which included many DMABN derivatives, it was shown that both a twisting and an 'anti'-pyramidalization coordinate are important entities in the intramolecular reaction coordinate [54]. A recent experimental study of 9,9'-bianthryl and analogues has also revealed a two-coordinate (internal twisting and solvent motion) relaxation model [55]. The relative importance of these coordinates were found to be strongly solvent dependent. The reaction coordinate in the di- and triphenylmethane dye molecules [38-52] involves twisting of the phenyl rings. The dynamics are strongly influenced by the viscosity of the solvent.

In Chapter 3 and 4 we present a study of a di-phenyl methane dye (auramine). The mechanism of the photo-excited reaction involving the twisting of the phenyl rings is not fully understood. The main issues are the nature of the reaction coordinate as well as the characterization of the excited state(s), or more generally, the relevant shape of the excited state potential energy surface. We have performed a time-resolved spectroscopic study to obtain a better understanding of the mechanism of the reaction dynamics. Our experimentally observed phenomena could not be explained on the basis of an existing theoretical model, which has been used for similar molecular systems [56,57]. Therefore simulations of the time-resolved fluorescence spectra, based on a different model of the excited state potential energy surface, have been conducted to obtain better insight in the physics underlying the observed phenomena [58].

1.4 Isomerization

The photochemistry of photoactive proteins has received widespread attention in recent years [59]. Especially bacteriorhodopsin (bR), which acts as a light-driven

trans-membrane proton pump, is of great interest in chemistry and biology [59-62]. The photocycle of this protein starts with light absorption by the retinal chromophore molecule attached to the protein backbone. The primary step of the photocycle of bacteriorhodopsin has been found to be a *13,14-trans* to *cis* photoisomerization process of retinal [61]. Ultrafast time-resolved fluorescence spectroscopy has proven to be useful for measuring the dynamics of such isomerization processes. The advantage of this method compared to transient absorption spectroscopy, is that only the dynamics of the population of the fluorescent excited state is probed. In transient absorption spectroscopy ground-state populations and higher lying excited-state populations are also probed. In the determination of the molecular mechanism of the photo-isomerization process of bR several models have been discussed to obtain a better understanding of the physics underlying the experimentally observed phenomena [61,62].

In Chapters 6 and 7 of this thesis we focus on another membrane protein, photoactive yellow protein (PYP). PYP also contains a chromophore with a double bond, coumaric acid [63,64]. It is believed that the initial step in the photocycle of PYP is a multibond-isomerization process similar to the primary event in retinal in bR. With ultrafast fluorescence spectroscopy the initial events in PYP are monitored. To study the influence of the environment of the chromophore molecule on the isomerization process, Chosrowjan et al. modified the backbone of the protein by site-directed mutagenesis [65]. In order to obtain a better understanding of the mechanism of the isomerization process in the chromophore molecule, we performed time–resolved fluorescence measurements on PYP and derivatives [66]. In these derivatives we varied the chromophore, by changing functional groups of the coumaric acid molecule, to study the effect on the isomerization process. Major changes in the fluorescence decay rates have been observed for the different derivatives of PYP.

1.5 Outline of thesis

In this thesis a time-resolved fluorescence study of several compounds in solution is presented. Dynamic Stokes shift and lifetime measurements have been performed in the femto- and picosecond time domains. Technical details about the experiments are presented in Chapter 2. In Chapter 3 a study of the excited state

dynamics of auramine in solution is presented. A major result is a dynamic Stokes shift of a few hundred wavenumbers accompanied by a drop in the integrated fluorescence intensity in all solvents. The rate of the dynamic Stokes shift was found to be dependent on the viscosity of the solvent. In Chapter 4 the dynamics of the excited-state population of auramine is studied as a function of temperature. In an attempt to more quantitatively analyse the results, a model is proposed in which two excited states are involved in the excited-state dynamics. With this model it is possible to simulate the experimentally obtained time-resolved fluorescence spectra. In Chapter 5 a comparative study of the excited state dynamics of a few bridged and unbridged ionic styryl dyes, with flexible phenyl groups, is given. By bridging one or two single bonds in the molecule the influence of the flexibility of the phenyl groups on the excited state dynamics is studied. Dynamic Stokes shift measurements are performed on the bridged and unbridged molecules in different solvents. Comparisons are made between the experimentally determined dynamic Stokes shift and time-constants of solvation dynamics from the literature. Bridging of the single bonds is found to strongly affect the lifetime of the emissive state. In Chapter 6 and 7 the primary step in the photocycle of photoactive yellow protein (PYP) is investigated. Several functional groups of the chromophore molecule inside the protein pocket are varied. The effect of the changes of the chromophore on the fluorescence decay rate are studied. The experimental results are discussed with respect to a model in which the first step in the photocycle involves a *trans-cis* isomerization of the double bond of the chromophore molecule.

References

[1] A.H. Zewail, Science **242**, 1645 (1988).

[2] R.D. Levine, R.B. Bernstein, Molecular Reaction Dynamics and Chemical Reactivity, Oxford Univ. Press, New York, 1987.

[3] R.B. Bernstein, A.H. Zewail, J. Chem. Phys. **90**, 829 (1989).

[4] G.R. Fleming, T. Joo, Adv. Chem. Phys. **101**, 829 (1997).

[5] H.A. Kramers, Physica **7**, 284 (1940).

[6] B. Bagchi, R. Biswas, Adv. Chem. Phys. **109**, 207 (1999).

[7] R.A. Marcus, Adv. Chem. Phys. **101**, 391 (1997); R.A. Marcus, J. Phys. Chem. **38**, 1858 (1963).

[8] A.H. Zewail (ed.), Femtochemistry: Ultrafast Dynamics of the Chemical Bond, World Scientific, Singapore, 1994.

[9] W. Rettig, B. Strehmel, S. Schäder, H. Seifert (Eds.), Applied Fluorescence in Chemistry, Biology and Medicine, Springer, Berlin, 1998.

[10] G.G. Kocherdoerfer, R.A. Mathies, Israel J. Chem. **35**, 211 (1996).

[11] C.W. Tang, S.A. VanSlyke, C.H. Chen, J. Appl. Phys. **65**, 3610 (1989).

[12] G.R. Fleming, Chemical applications of Ultrafast Spectroscopy, Oxford University Press, Berlin, 1998.

[13] P.F. Barbara, W. Jarzeba, Adv. Photochem. **15**, 1 (1990).

[14] R. Jimenez, G.R. Fleming, P.V. Kumar, M. Maroncelli, Nature (London) **369**, 471 (1994).

[15] M. Maroncelli, J. Mol. Liq. **57**, 1 (1993).

[16] N.G. Bakshiev, Opt. Spectrosc. **21**, 446 (1964).

[17] Yu. T. Mazurenko, N.G. Baksiev, Opt Spectrosc. **28**, 490 (1970).

[18] W.R. Ware, P. Chow, S.K. Lee, Chem. Phys. Lett. **2**, 356 (1968).

[19] G. van der Zwan, J.T. Hynes, J. Phys. Chem. **89**, 4181 (1985).

[20] A. Chandra, B. Bagchi, Chem. Phys. Lett. **165**, 93 (1990).

[21] H. Zhang, A.M. Jonkman, P. van der Meulen, M. Glasbeek, Chem. Phys. Lett. **224**, 551 (1994).

[22] M. Maroncelli, G.R. Fleming, J. Chem. Phys. **86**, 6221 (1987).

[23] M.L. Horng, J.A. Gardecki, A. Papazyan, M. Maroncelli, J. Phys. Chem. **99**, 17311 (1995).

[24] M.J. van der Meer, H. Zhang, W. Rettig, M. Glasbeek, Chem. Phys. Lett. **320**, 673 (2000).

[25] L. Onsager, J. Am. Chem. Soc. **58**, 1485 (1935).

[26] P.G. Wolynes, J. Phys. Chem. **86**, 5133 (1987).

[27] A. Chandra, B. Bagchi, J. Phys. Chem. **94**, 3177 (1991).

[28] E. Lippert, W. Lüder, H. Boos, in: A. Mangini (Ed.), Advances in Molecular Spectroscopy, Pergamon, Oxford, 1962, p.443.

[29] Z.R. Grabowski, J. Dobkowski, Pure Appl. Chem. **55**, 245 (1983).

[30] W. Rettig, G. Germuth, E. Lippert, Ber. Bunsenges. Phys. Chem. **83**, 692 (1997).

[31] K.A. Zachariasse, T. von der Haar, A. Hebecker, U. Leinhos, W. Kühnle, Pure Appl. Chem. **65**, 1745 (1993).

[32] T. von der Haar, A. Hebecker, Y. Il'ichev, Y.-B. Jiang, W. Kühnle, K.A. Zachariasse, Trav. Chim. Pays-Bas **114**, 430 (1995).

[33] F. Schneider, E. Lippert, Ber. Bunsenges. Phys. Chem. **72**, 1155 (1968).

[34] N. Nakashima, M. Murakawa, N. Mataga, Bull. Chem. Soc. Jpn. **49**, 845 (1976).

[35] M. Mataga, H. Yao, T. Okada, W. Rettig, J. Phys. Chem. **93**, 3383 (1989).

[36] T.J. Kang, W. Jarzeba, P.F. Barbara, T. Fonseca, Chem. Phys. **149**, 81 (1990).

[37] K. Elich. M. Kitazawa, T. Okada, R. Wortmann, J. Phys. Chem. A **101**, 2010 (1997).

[38] V. Sundström, T. Gillbro, H. Bergstrom, Chem. Phys. **73**, 439 (1982).

[39] D.A. Cremers, M.W. Windsor, Chem. Phys. Lett. **71**, 27 (1980).

[40] W. Yu, F. Pellegrino, M. Grant, R.R. Alfano, J. Chem. Phys. **67**, 1766 (1977).

[41] J.M. Grzbowski, S.E. Sugamori, D.F. Williams, R.W. Yip, Chem. Phys. Lett. **65**, 456 (1979).

[42] M. Ishikawa, J.Y. Ye, Y. Maruyama, H. Nakatsuka, J. Phys. Chem. A **103**, 4319 (1999).

[43] F. W. Wise, M. J. Rosker, C. Tang, J. Chem. Phys. **86**, 2827 (1987).

[44] D. Ben-Amotz, C.B. Harris, J. Chem. Phys. **86**, 4856 (1987); ibid **86**, 5433 (1987); D. Ben-Amotz, R. Jeanloz, C.B. Harris, J. Chem. Phys. **86**, 6119 (1987).

[45] M. Ishikawa, Y. Maruyama, Chem. Phys. Lett. **219**, 416 (1994).

[46] R. Menzel, C.W. Hoganson, M.W. Windsor, Chem. Phys. Lett. **120**, 29 (1985).

[47] A. Mokhtari, L. Fini, J. Chesnoy, J. Chem. Phys. **87**, 3429 (1987).

[48] M.D. Hirsch, H. Mahr, Chem. Phys. Lett. **60**, 299 (1979).

[49] M. Vogel, W. Rettig, Ber. Bunsenges. Phys. Chem. **91**, 1241 (1987); ibid **89**, 962 (1985).

[50] M. Canva, G. Lesaux, P. Georges, F. Chaput, JP. Boilot, Chem. Phys. Lett. **176**, 495 (1991).

[51] J.Y. Ye, T. Hattori, H. Inouye, H. Ueta, H. Nakatsuka, Y. Maruyama, M. Ishikawa, Phys. Rev. B **53**, 8349 (1996).

[52] K.M. Abedin, J.Y. Ye, H. Inouye, T. Hattori, H. Sumi, H. Nakatsuka, J. Chem. Phys. **103**, 6414 (1995).

[53] T. Fonseca, H.J. Kim, J.T. Hynes, J. Photochem. Photobiol. A: Chem. **82**, 67 (1994).

[54] W. Rettig, B. Zietz, Chem. Phys. Lett. **317**, 187 (2000).

[55] M. Jurczok, P. Plaza, M.M. Martin, Y.H. Meyer, W. Rettig, Chem. Phys. **253**, 339 (2000).

[56] B. Bagchi, G.R. Fleming, D.W. Oxtoby, J. Chem. Phys. **78**, 7375 (1983); B. Bagchi, G.R. Fleming, Phys. Chem. **94**, 9 (1990).

[57] P. Changenet, H. Zhang, M.J. van der Meer, M. Glasbeek, P. Plaza, M.M. Martin, J. Phys. Chem. A **102**, 6716 (1998).

[58] M.J. van der Meer, H. Zhang, M. Glasbeek, J. Chem. Phys. **112**, 2878 (2000).

[59] G.G. Kochendoerfer, R.A. Mathies, Israel J. Chem. **35**, 211 (1996).

[60] G. Haran, K. Wynne, A. Xie, Q. He, M. Chance, R.M. Hochstrasser, Chem. Phys. Lett. **261**, 389 (1996).

[61] R.A. Mathies, C.H.B. Cruz, W.T. Pollard, C.V. Shank, Science **240**, 777 (1988).

[62] K.C. Hasson, F. Gai, P.A. Anfinrud, Proc. Natl. Acad. Sci. USA **93**, 15124 (1996).

[63] W.D. Hoff, P. Dux, K. Hard, B. Devreese, I.M. Nugterenroodzant, W. Crielaard, R. Boelens, R. Kaptein, J. Van Beeumen, K.J. Hellingwerf, Biochemistry **33**, 13959 (1994).

[64] M. Baca, G.E.O. Borgstahl, M. Boissinot, P.M. Burke, D.R. Williams, K.A. Slater, E.D. Getzoff, Biochemistry **33**, 14369 (1994).

[65] H. Chosrowjan, N. Mataga, Y. Shibata, Y. Imamoto, F. Tokunaga, J. Phys. Chem. B **102**, 7695 (1998).

[66] P. Changenet, H. Zhang, M.J. van der Meer, K.J. Hellingwerf, M. Glasbeek, Chem. Phys. Lett. **282**, 276 (1998).

Chapter 2

Experimental

2.1 Introduction

A description of the techniques and equipment, used in the studies discussed in Chapters 3 to 7, is given in this Chapter. In Section 2.2 the setup to measure steady-state absorption and emission spectra is described. In Section 2.3 an overview of the picosecond time-correlated single-photon counting setup is given. The femtosecond fluorescence up-conversion technique and setup is presented in Section 2.4. Details of the samples and used solvents are given in Section 2.5. General information about time-resolved spectroscopy is also provided in several textbooks [1,2].

2.2 Steady state spectra

The steady-state absorption spectra were measured by means of a Shimadzu UV-Vis spectrophotometer (UV-240). It is a double-beam spectrometer with an iodine-tungsten lamp and a deuterium lamp. The wavelength range is from 190 to 900 nm. The monochromator has a holographic grating with a spectral resolution of 2 nm.

The steady-state emission spectra were measured using the time-correlated single-photon counting setup, which is described in Section 2.3. The intensity of the fluorescence at a particular wavelength is measured by accumulating the amount of photons for a fixed period of time. The obtained intensity is corrected for the sensitivity of the monochromator and photomultiplier at that particular wavelength, using an experimentally determined calibration curve [3].

2.3 Time-Correlated Single-Photon Counting

A time-correlated single-photon counting setup was used to measure time-resolved fluorescence transients in a time range from 10 picoseconds to 50 nanoseconds. The setup consisted of an excitation laser system, which produced

picosecond light pulses and a time-correlated single-photon counting detection system. In Figure 2.1 an overview of the setup is shown.

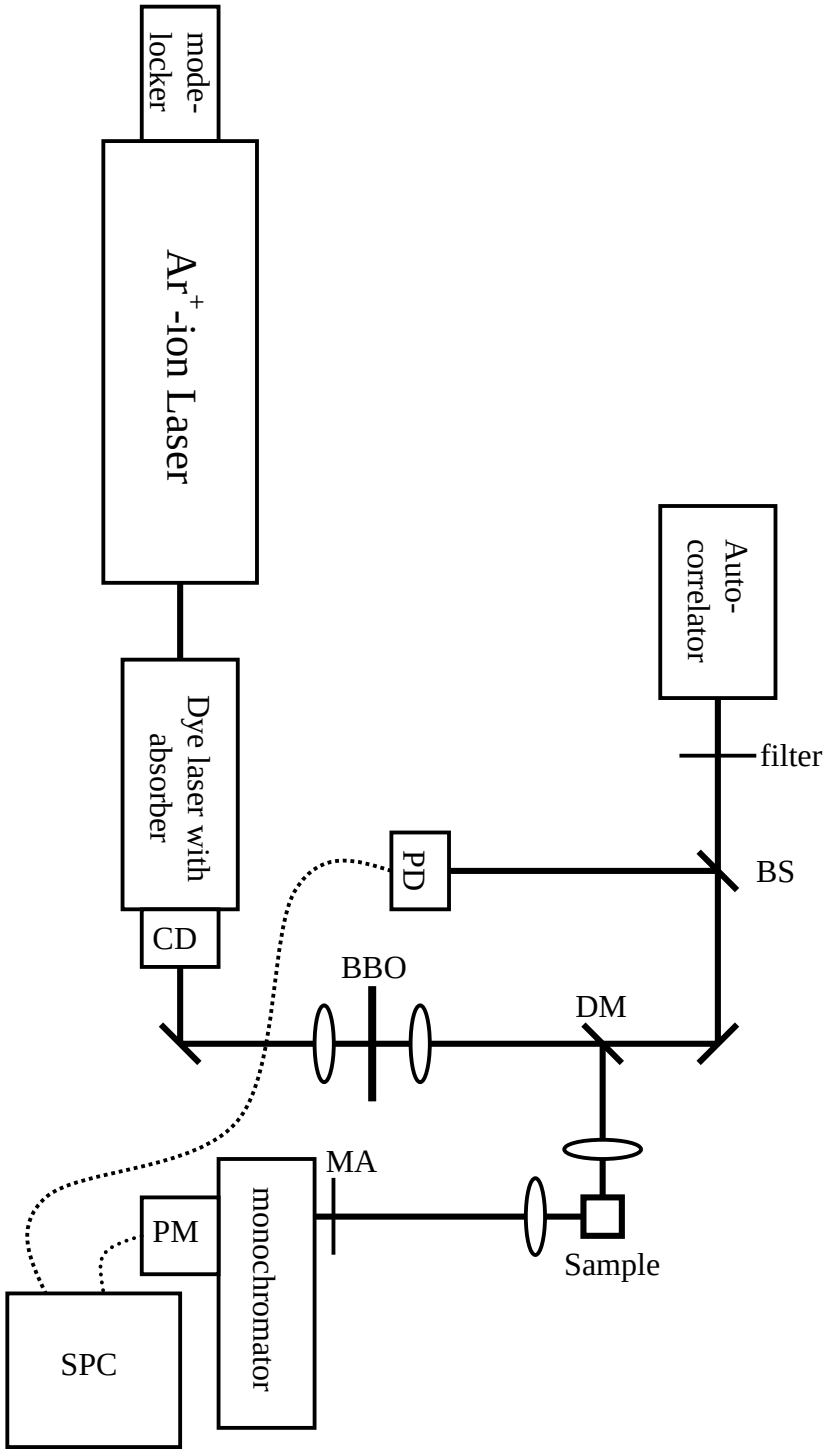

Figure 2.1. Overview of the time-correlated single-photon counting setup. CD = cavity dumper, DM = dichroic mirror, BS = beam splitter, PD = photo diode, MA = magic angle polarizer (54.7°), PM = photo-multiplier and SPC = time-correlated single-photon counting detection system.

The excitation source in the time-correlated single-photon counting setup was a Coherent Innova 200-15 Watt Ar^+-ion laser, which was mode-locked by a Coherent 468 mode-locker. The laser system produced pulses of about 80 ps with a repetition rate of 76 MHz (λ=514.5 nm). These pulses were used to excite a Coherent 700 jet dye laser in which DCM-spezial was used as the laser dye. The synchronously pumped dye laser system was extended with a cavity dumper (Coherent 7200, CD in Figure 2.1). The purpose of this cavity dumper was to increase the power per pulse and reduce the repetition rate. In general the cavity dumper was set to reduce the repetition rate from 76 MHz to 3.8 MHz (a factor 20). To shorten the laser pulses a saturable absorber jet was used in the dye laser system. In our case a mixture of DQTCI and DTDCI dissolved in ethylene glycol (at an optimal concentration) was used. The dye laser system with the saturable absorber and cavity dumper created pulses with a duration of 1 picosecond and an energy of 25 nJ. These pulses were tunable over a wavelength-range from 620 to 680 nm. The pulses were frequency doubled by a 6 mm thick BBO crystal to create wavelengths from 310 to 340 nm. The dichroic mirror (DM, Figure 2.1) separated the frequency-doubled laser beam from the beam at the fundamental frequency. The residue of the beam at fundamental frequency was directed to a photodiode (PD) and an autocorrelator. The autocorrelation function of the laser pulses were measured in an autocorrelator. The photodiode is connected to the time-correlated single-photon counting detection system, which will be discussed later. The frequency-doubled beam (UV) was used to photo-excite the sample. The fluorescence perpendicular to the excitation beam was focused on the slit of a Zeiss M20 grating monochromator by a lens. It first passed a polarizer, set to the magic angle (MA=54.7°), to get rid of the fluorescence decay due to rotational motions of the solute molecules. The fluorescence intensity, dispersed by the monochromator, was detected by a Hamamatsu R3809 U (S-20) microchannel plate photomultiplier. The signal from this photomultiplier, amplified by a Hewlett Packard 8347 A amplifier, was directed into the time-correlated single-photon counting detection system [4]. The amplified signal was sent into a Tennelec TC454 constant fraction discriminator producing a start pulse for the Tennelec TC 864 time-to-amplitude converter (TAC). The stop pulses for the time-to-amplitude converter were produced by another Tennelec constant fraction discriminator (TC 455) which got its signal from the photodiode (PD, Figure 2.1). These pulses were directed into the TAC via a Tennelec TC 412A delay generator. The output signal of the TAC, producing

pulses with a amplitude proportional to the time interval between start and stop pulses was sent into a EG&G Ortec 918 multichannel buffer (MCB) connected to a personal computer. In the MCB a time histogram of the fluorescence decay was created. When measurements were performed in a 5 nanosecond time range, the channel of the buffer had a width of 1.25 picoseconds per channel (4096 channels). The system response function, which is necessary for the deconvolution of the fluorescence transients, was determined by measuring the Raman scattered light of a water cell at a wavelength approximately 40 nm longer than the excitation wavelength. The full width at half maximum of this function was typically 17 picoseconds.

2.4 Fluorescence Up-conversion technique

The fluorescence up-conversion setup was used to measure time-resolved fluorescence transients with a time resolution in the femtosecond time range. In Figure 2.2 an overview of the setup is shown. The principle of the fluorescence up-conversion is based on the mixing of the frequencies of the incoherent fluorescence and a gating laser pulse in a non-linear BBO crystal [5]. By delaying the gating pulse with an optical delay line, with respect to the fluorescence beam, the fluorescence can be measured time-resolved. The up-conversion signal, which is created in the BBO crystal, has a photon frequency given by

$$\omega_{sum} = \omega_{laser} + \omega_{fl} \qquad (2.1)$$

implying,

$$\frac{1}{\lambda_{sum}} = \frac{1}{\lambda_{laser}} + \frac{1}{\lambda_{fl}} \qquad (2.2)$$

The intensity of the sum-frequency signal (=up-converted signal) is given as [5],

$$I_{sum}(\tau) = \int_{-\infty}^{\infty} I_{fl}(t) I_{laser}(t-\tau) dt \qquad (2.3)$$

in which τ is the time delay between the fluorescence and the gating pulse. The system response function of the setup, necessary for the deconvolution of the fluorescence transients, is proportional to the cross correlation function of two laser pulses.

Experimentally, a full width at half maximum of about 120 femtoseconds is found for the cross correlation function of laser pulses at 840 nm and 420 nm.

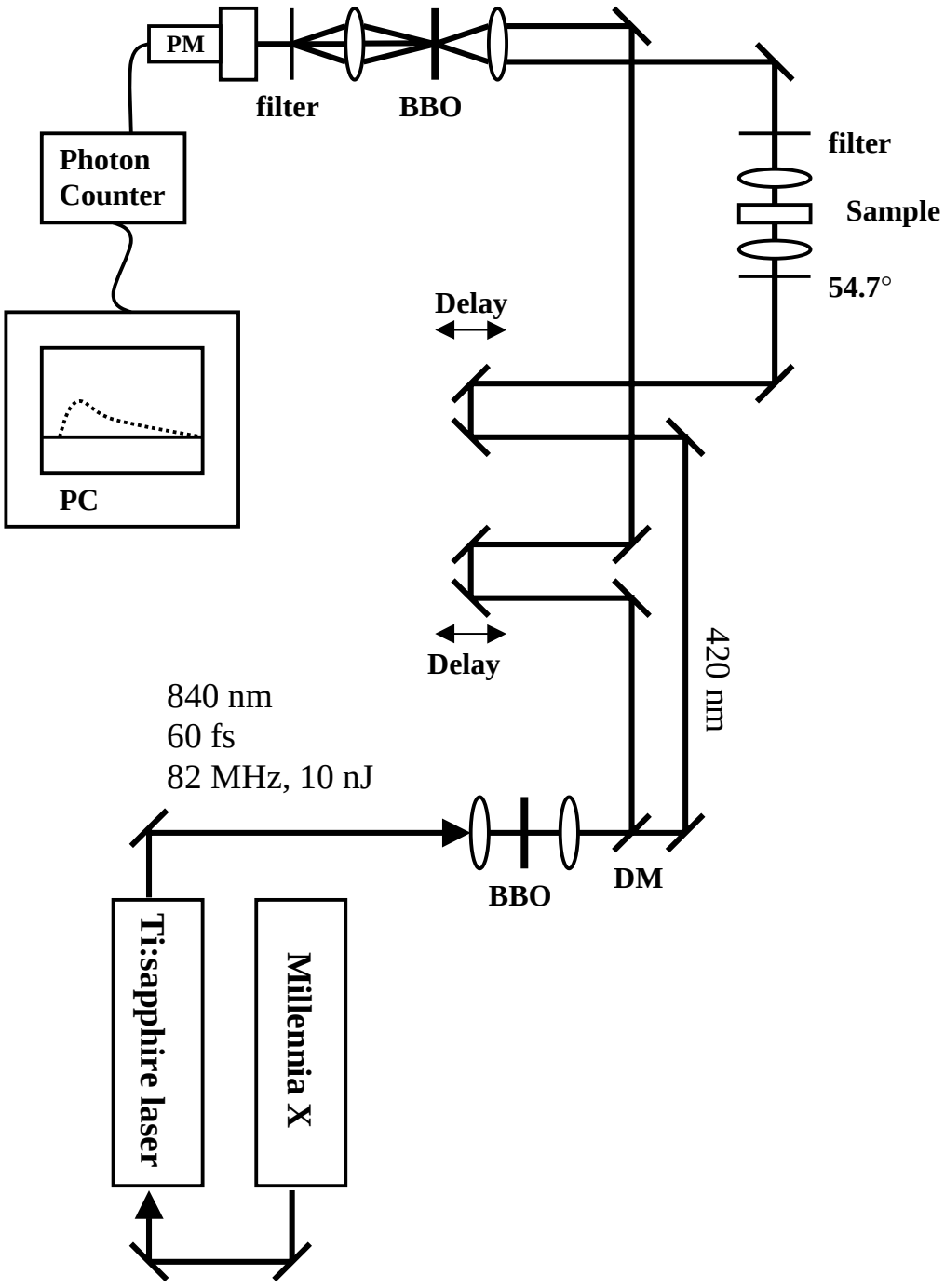

Figure 2.2. Overview of the fluorescence up-conversion setup. DM = dichroic mirror, PM = photo-multiplier.

The excitation source in the fluorescence up-conversion setup was a Spectra Physics Millennia X (10 Watt) continuous wave diode laser. This laser was used to pump a mode-locked Ti:sapphire laser (Spectra Physics Tsunami). Laser pulses in a tunable wavelength range from 790 to 840 nm were produced at a repetition rate of 82 MHz. The energy per pulse was about 10 nJ and the full width half maximum of the autocorrelation function of pulses at the fundamental frequency was about 60 femtoseconds. The pulses were focused onto a BBO crystal to create frequency-doubled pulses. A dichroic mirror separated the beam at fundamental frequency from the second-harmonic (=frequency-doubled). The frequency-doubled pulses were used to photo-excite the sample. The sample was a 1 mm quartz cell containing the solution. The sample was driven by a motor to perform a circular motion in a plane perpendicular to the excitation beam to prevent heating of the probe by the laser pulses. A polarizer, set to the magic angle (54.7°), was used to circumvent the influence of rotational diffusion of the solute molecules on the decay of the fluorescence. The fluorescence beam was focused on a type I phase-matching BBO crystal (=sum frequency crystal). The beam at fundamental frequency was directed to an optical delay line by a dichroic mirror. A translational stage was driven by a stepper motor with an accuracy of 0.1 μm. Each step of the translational stage changes the optical path length of the pulses by 0.2 μm, thus delaying the pulses 0.66 femtoseconds per step.

Pulses at the fundamental frequency were used as the gating pulses in the sum frequency crystal. To observe an up-converted signal, one has to fulfill phase-matching conditions,

$$k_{sum} = k_{fl} + k_{laser} \qquad (2.4)$$

Here k_{sum}, k_{fl}, and k_{laser} are the wave vectors of the sum-frequency light, the fluorescence beam and the laser pulses at the fundamental frequency. For each detection wavelength the phase matching angle had to be adjusted by rotation of the BBO crystal. The acceptance angle of the crystal ($\Delta\Theta$) determines the wavelength-range covered by the BBO crystal. The angle depends on the change of k_{sum} with the angle and the thickness of the crystal (L),

$$\Delta\Theta = \frac{\pi}{L}\left(\frac{\delta k_{sum}}{\delta\Theta}\right)^{-1} \qquad (2.5)$$

From Equation 2.3 it is shown that the intensity of the up-converted signal is proportional to the intensity of the fluorescence when the gating pulse intensity is constant. A fluorescence transient was recorded by measuring the intensity of the up-converted signal when scanning the translational stage. The up-converted signal was sent through a UG11 UV cutoff filter in front of a Zeiss M4 Q III prism monochromator (spectral resolution > 5nm). As a detector, an EMI 9863 QB/350 photomultiplier (PM, Figure 2.2) connected to a Princeton Applied Research photon counting system (amplifier/discriminator model 1120, photon counter model 1109) was used. A Newport MM3000 motion controller was used to run the translational stage. A personal computer was connected to the photon counting system and the translational stage to control the experiment.

2.5 Samples

In Chapters 3 and 4 we present our results for auramine. The full name of auramine O is 4,4'-(imidocarbonyl)bis(N,N-dimethylaniline-monohydrochloride). Auramine was purchased from Aldrich, with a purity of only 80%. The powder was sublimed two times to remove impurities from the sample. These impurities could be detected by measurements of the fluorescence around 350 nm.

In Chapter 5 we present our results for bridged and unbridged diphenyl derivatives of 1- or 4-(4'-dimethylaminostyryl)pyridinium dyes (DPD family). The DPD compounds were obtained from the group of Professor W. Rettig in Berlin. Details about the synthetisation are given elsewhere [6,7]. The samples were used as received.

In Chapters 6 and 7 our results are given for the study of photo-active yellow protein (PYP). PYP was isolated from the halophilic purple bacterium *Ectothiorhodospira halophila*. A description of the reconstitution of PYP with various chromophores, analogous to the wild-type chromophore, is given elsewhere [8].

A 10 mM Tris.HCL buffer with a pH of 7.5 was used as a solvent for the PYP samples. Ethanol, purchased from Merck, was used as a solvent. The purity was UV-spectroscopy grade (>99.9%). It was used without any purification. Decanol, at a purity of 99% (GC-grade) was purchased from Janssen. By means of steady-state fluorescence measurements the presence of impurities was checked. No fluorescent impurities were found in the wavelength range of our fluorescence experiments. It was used without any

further purification. Benzonitrile (Aldrich) had a HPLC-grade purity of 99.9%. It was used as purchased.

In order to perform measurements at low temperatures a home-built liquid nitrogen flow cryostat was used to control the temperature in a range from 293 to 77 K. The accuracy of the temperature control was about ± 0.5 K.

References

[1] W. Demtröder, Laser spectroscopy, Springer-Verlag, Berlin Heidelberg and New York, 1996.

[2] O. Svelto, D. C. Hanna, Principles of lasers, Plenum Press, New York and London, 1989.

[3] E.R. Middelhoek, P. van der Meulen, J.W. Verhoeven, M. Glasbeek, Chem. Phys. **198**, 373 (1995).

[4] D. Bebelaar, Rev. Sci. Instrum. **57**, 1116 (1986).

[5] M.A. Kahlow, W.Jarzeba, T.P. Dubrull, P.F. Barbara, Rev. Sci. Instrum. **59**, 1098 (1988).

[6] M. Sczepan, W. Rettig, A. I. Tolmachev, to be published.

[7] M. Sczepan, W. Rettig, Y.L. Bricks, Y.L. Slominski, A.I. Tolmachev, J. Photochem. Photobiol. A Chem. **124**, 75 (1999).

[8] A.R. Kroon, W.D. Hoff, H. Fennema, G.J. Koomen, J.W. Verhoeven, W. Crielaard, K.J. Hellingwerf, J. Biol. Chem. **271**, 31949 (1996).

Chapter 3

Ultrafast twisting dynamics of photoexcited auramine in solution*

Abstract

Subpicosecond fluorescence upconversion and transient absorption spectroscopy are applied to study the excited-state dynamics of auramine, a diphenylmethane dye, in liquid solutions. The fluorescence decays, on a time scale of a few picoseconds to a few tens of picoseconds, are found to be non-exponential and solvent viscosity dependent. They can be fitted as a sum of two exponentials in ethanol and three exponentials in decanol with a larger average lifetime in the more viscous solvent. The decays exhibit wavelength-dependent time constants, whereas the fluorescence rise time is instrument limited (150 fs) at all wavelengths. The average decay time increases with the wavelength across the steady-state emission spectrum. The spectral reconstruction indicates a few hundred wavenumbers dynamic Stokes shift accompanied by a drop in the intensity in both solvents. From transient absorption experiments, the fluorescent state population is shown to decay to an intermediate dark state and then to the ground state, with a viscosity-dependent rate. A barrierless or quasi-barrierless photoreaction involving the rotational diffusion of the phenyl rings, with a change in the radiative transition rate along the reaction path, is proposed to explain the wavelength-dependent non-exponential fluorescence decays. Both, fluorescence and transient absorption, data are discussed in support of an adiabatic photoreaction involving internal twisting and charge shift.

* The contents of this chapter has been published as an article, P. Changenet, H. Zhang, M.J. van der Meer, M. Glasbeek, P. Plaza, M.M. Martin, J. Phys. Chem. A **102**, 6716-6721 (1998).

3.1 Introduction

Oster et al reported that auramine, a substituted diphenylmethane cationic dye (Scheme 3.1), is weakly fluorescent in water and in low viscosity solvents, and highly fluorescent in the presence of DNA [1] and polymeric acids [2] or in viscous solvents [3]. Auramine forms a highly fluorescent complex with some proteins such as the horse liver alcohol dehydrogenase (1000 times more fluorescent than in water [4]) or the Ca^{2+} - liganded calmodulin [5]. It is used as a fluorescent probe for investigating protein structure and function [4-6] and also physical ageing of polymers [7,8] or dye adsorption on powdered solids [9].

SCHEME 3.1

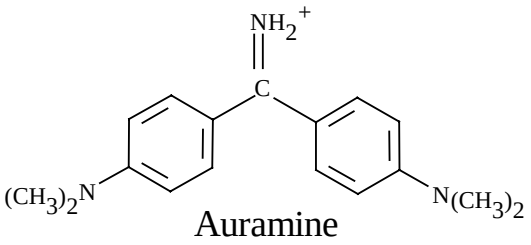

Auramine

To explain the fluorescence properties of auramine, Oster and Nishijima [3] suggested an internal conversion process via the rotational diffusion of the phenyl rings, the mobility of these large groups being affected by the surroundings. In solutions of increasing viscosity (η), they reported a linear change in the reciprocal of the fluorescence quantum yield versus T/η. Förster and Hoffmann [10] reported that the fluorescence yield of substituted triphenyl compounds such as the triphenylmethane (TPM) dyes exhibit a sublinear increase with the solvent viscosity ($\eta^{2/3}$). They proposed that rotational diffusion of the phenyl rings occurs along a barrierless potential, with a nonradiative decay rate that depends on the twist angle. They developed a theory which describes the evolution of the excited state population like a Brownian particle on a harmonic surface and were able to reproduce the observed viscosity effect on the fluorescence yield. More recently, Bagchi, Fleming and Oxtoby [11,12] (BFO) developed a theory describing the excited state population decay by a coordinate-dependent sink for the nonradiative decay and a coordinate-independent sink for the radiative decay. One of the major predictions of the BFO theory is the non-exponential character of the excited population decays, with decay functions that depend on the initial conditions. The theory also predicts fractional viscosity dependence of the fluorescence yield and viscosity effects on the non-radiative decays that depend on the form of the sink function. It is worth noting that TPM dyes were extensively investigated (see references in Ref. 11-19 and in the detailed review [20]), these molecules being considered as model compounds for the study of barrierless reaction

[11,12,14] whereas only few [19] time-resolved spectroscopic studies of auramine in liquid solution have been performed, in particular on the very short time scale.

In this chapter, we present results of time-resolved spontaneous fluorescence and transient absorption measurements of auramine in liquid solutions. Fluorescence upconversion and pump-continuum probe techniques, with subpicosecond resolution, were employed. Ethanol and decanol were used as the solvents in order to test the solvent viscosity effect. The fluorescence decays are interpreted by a solvent-viscosity dependent photoreaction, similar to that reported for TPM dyes. Furthermore, the results reveal wavelength-dependent decays without change in the fluorescence rise time. Such a behavior was previously reported for compounds which undergo barrierless or low-energetic activated trans-cis isomerization in the first excited state, as e.g., in the cases of bacteriorhodopsin [21], all-trans retinal [22] and, more recently, photoactive yellow protein [23,24]. The transient absorption experiments on auramine exhibit the rise of a non-emissive state population, concomitant with the rapid relaxation of the emissive first excited state population. It is discussed that the results support the previously proposed model of Martin et al [19] in which diffusive twisting motions of the auramine phenyl rings causes a relaxation of the population of the emissive locally excited state into a dark excited charge transfer state along an adiabatic potential.

3.2 Experimental

3.2.1. Femtosecond fluorescence upconversion set-up

Fluorescence decays of auramine were measured using the femtosecond fluorescence upconversion set-up described previously [25]. A cw Ar^+ laser pumps a Tsunami Ti:sapphire laser producing pulses, at 840 nm, with a duration of 60 fs, at a repetition rate of 82 MHz and with an output energy of about 10 nJ per pulse. The pulses are focused onto a 1 mm BBO crystal to generate the second harmonic. After splitting the pulses by a dichroic beam-splitter, they are used as the pump (λ = 420 nm) and the gating pulses (fundamental frequency). The pump beam was focused onto a 1 mm cell containing the auramine solution. The sample holder is moved back and forth, perpendicular to the excitation beam, in order to prevent heating of the sample. The photoinduced auramine fluorescence was focused together with the gating beam onto a 1 mm BBO crystal (type I phase match). The up-converted signal was filtered by an UG

11 Schott filter (with a band pass from 260 to 380 nm), focused on the entrance slit of a monochromator (spectral resolution < 5 nm) and detected by means of a photomultiplier (EMI 9863 QB/350) connected to a photon counting system. The fluorescence decays were measured under magic angle conditions to avoid the effects due to rotational diffusion of the molecule. The up-converted signal was accumulated for 1 s, for each time-delay step. Decay measurements were performed using typical step sizes of 6.6 fs, 66 fs or 264 fs. The instrumental response was estimated to be roughly 150 fs (FWHM) from the cross correlation function of the gating and pump pulses.

3.2.2. Pump-probe set-up

Time-resolved transient absorption and gain spectra were measured applying the pump-probe technique. The subpicosecond laser source was a non-mode-locked dye laser system developed at Orsay [26]. The basic system produces 500 fs pulses (400 μJ/pulse) at 610 nm from a single seeded Q-switched Nd:YAG laser (6 ns, 10 Hz). Tunable high-power subpicosecond pulses at wavelengths between 400 and 800 nm are produced by focusing the 500 fs red pulses into a 2 cm water cell. The generated white light continuum is filtered at the desired wavelength, then amplified in dye amplifiers pumped by the second or the third harmonic of the Nd:YAG laser. In this study, a first beam at 425 nm (700 fs, 20 μJ) was used to excite the sample and a second beam at 700 nm (300 fs, 200 μJ) was used to generate the continuum probe. The probe was split in two beams, one was sent through the sample, while the other passed through a reference cell. Then, the transmitted beams were focused on the entrance slit of a polychromator (Jarell-Ash, entrance slit 150 μm) through 2.50 m long optical fibers (diameter = 600 μm) and were simultaneously analyzed with a computer-controlled double-diode array detector (Princeton Instruments Inc.). The polarization of the pump light was set at the magic angle relative to the polarization of the probe light. Data were typically accumulated over 500 laser shots. The auramine solutions were contained in 1 mm flow cell and the concentration was such as to obtain an optical density of about 0.5 at the excitation wavelength. The spectra were corrected for the chirp (group velocity dispersion) of the probe pulse using the data of a two-photon absorption experiment in 1-chloronaphthalene.

3.2.3. Samples

Auramine, 4,4'-(imidocarbonyl)bis(N,N-dimethylaniline-monohydrochloride), was purchased from Aldrich (80%) and purified by several sublimations to eliminate a fluorescent impurity which could be detected when auramine solutions were excited near 350 nm. The solvents used were UV-spectroscopy grade ethanol (Merck, $\varepsilon = 24.5$, $\eta = 1.08$ cP) and 99% decanol (Janssen, $\varepsilon = 8.1$, $\eta = 14.3$ cP). The absence of detectable impurity in decanol was checked by steady state fluorescence measurements. The sample concentration was chosen to be larger than 10^{-4} M in order to avoid deprotonation of auramine. In fluorescence decay experiments, we checked that the results were not affected when the solutions were diluted by a factor of 2. All measurements were carried out at room temperature.

3.3 Results

3.3.1. Time-resolved spontaneous fluorescence

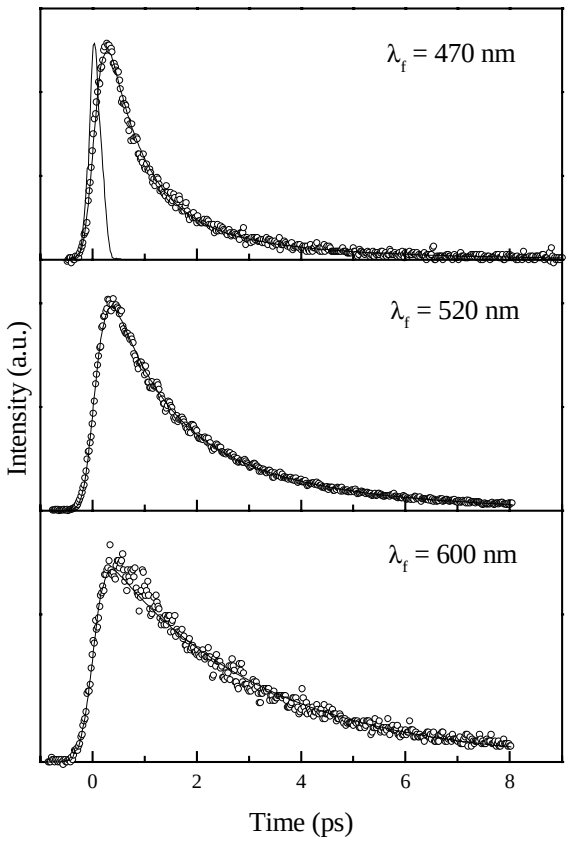

Figure 3.1. Representative fluorescence decays of auramine in ethanol at room temperature, after 80 fs pulsed excitation, at 420 nm, at three different detection wavelengths. The apparatus response function is included in the figure.

Representative fluorescence upconversion decays, measured for auramine in ethanol and decanol are shown in Figures 3.1 and 3.2. As illustrated by the transients of these figures, the fluorescence decays are dependent on the wavelength at which the emission is detected. Each fluorescence decay could be fitted to a multi-exponential decay function convoluted with the system response function. The data for various wavelengths over the 465-600 nm spectral range are collected in Table 3.1, for auramine dissolved in ethanol (a) and decanol (b). It is seen that the weighted average lifetime increases gradually when the detection wavelength is increased. The variation of the two time constants for the fluorescence decay of auramine in ethanol over the whole spectral range is from 0.7 ps up to about 1.9 ps and from 2.7 ps up to 4.6 ps, respectively. In decanol, three time constants are required, the ranges of which are given as 0.9 - 1.1 ps, 15 - 50 ps and 50 - 130 ps. Thus, for the fluorescence decay components, the lifetimes (as well as the amplitudes) are wavelength dependent: the contribution of the fastest decay decreases progressively when the detection wavelength is increased. In the more viscous solvent, decanol (η=14.3 cP), for wavelengths longer than 560 nm, the fastest decay component has disappeared. Also, the weighted average lifetime is longer than in the low viscosity ethanol (η=1.08 cP). In all fluorescence transients, the initial rise was determined by the system response function, i.e., the fluorescence rise following the laser pulse is faster than the time resolution of the experiments (150 fs). No change in the lifetimes (or the amplitudes) was observed when the excitation wavelength was tuned to higher energy, i.e. to 400 nm instead of 420 nm. Using the spectral reconstruction method of Maroncelli and Fleming [27], the time-resolved fluorescence spectra displayed in Figure 3.3 were obtained for auramine. The spectra in this figure show the best-fit results of the point-to-point reconstructed spectra to a lognormal function at various times after the excitation pulse.

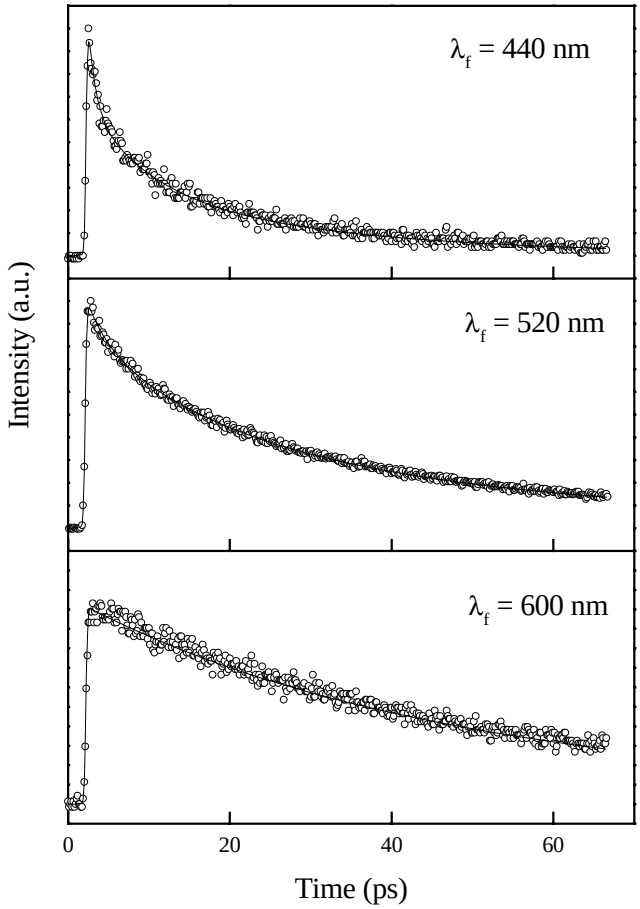

Figure 3.2. Representative fluorescence decays of auramine in decanol at room temperature, after 80 fs pulsed excitation, at 420 nm, at three different detection wavelengths.

Table 3.1

Fluorescence exponential decay components for auramine dissolved in (a) ethanol and (b) decanol Relative amplitudes of the exponential components are indicated between brackets.

λ_f nm	τ_1 ps (%)	τ_2 ps (%)	τ_3 ps (%)
		(a) ethanol	
465	0.7 (75)	2.7 (25)	
490	0.8 (65)	2.8 (35)	
515	1.4 (65)	3.8 (35)	
545	1.9 (55)	3.3 (45)	
570	1.7 (65)	4.3 (35)	
600	1.5 (55)	4.6 (45)	
		(b) decanol	
465	0.9 (35)	16.5 (40)	51.5 (25)
490	1.1 (25)	19.5 (40)	52.0 (35)
515	1.1 (15)	22.0 (40)	51.0 (45)
545	1.1 (10)	25.5 (50)	65.5 (40)
570	-	31.0 (55)	79.0 (45)
600	-	49.5 (80)	131.5 (20)

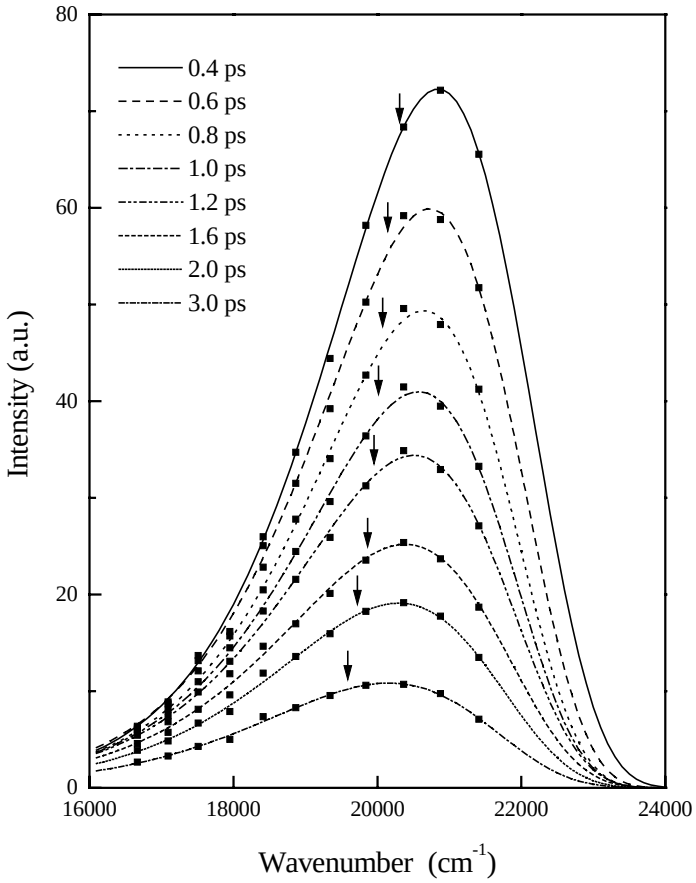

Figure 3.3. Log-normal fits to the reconstructed spectra of auramine in ethanol from fluorescence decays. Dots represent the reconstructed intensity data points from the experimental fluorescence transients. Arrows indicate position of first moment of the frequency.

3.3.2. Time-resolved absorption, bleaching and gain spectra

The pump-probe spectra, measured for auramine in decanol in the 370-650 nm spectral range after excitation at 425 nm with a 700 fs pulse, are given in Figure 3.4 for several pump-probe delays between 2 ps and 300 ps. The steady-state absorption and fluorescence spectra are also shown in the figure. The spectral changes in the differential optical density (ΔD) look similar to those reported previously for auramine in ethanol [19], except that in decanol the changes occur on a longer time scale.

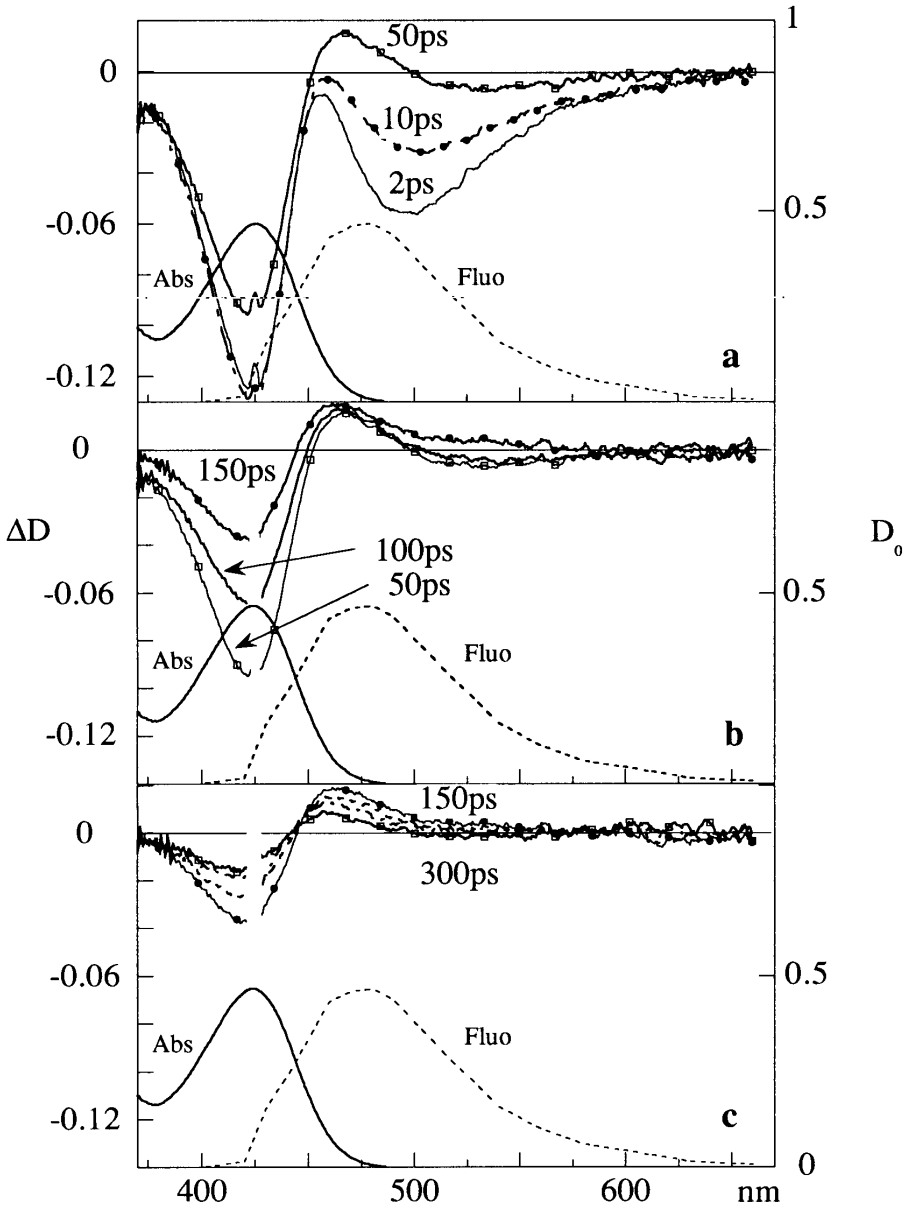

Figure 3.4. Time-resolved differential absorption (ΔD left scale) of auramine in decanol at room temperature after 700 fs pulsed pumping at 425 nm. Pump-probe delays are included; (a) 2-50 ps, (b) 50-150 ps, and (c) 150-300 ps. The right scale refers to the steady-state absorption D_0 and emission spectra of auramine in decanol (normalized).

We distinguish three stages, displayed in Figure 3.4a, b, and c, respectively. Following the excitation pulse, the differential optical density (ΔD) is negative (Figure 3.4a, Δt = 2 ps) in the whole spectral range. Below 450 nm, the spectrum is dominated by the bleaching of the sample absorption. Above 470 nm, where fluorescence is expected and where the ground state does not absorb, the negative ΔD values show that

gain is dominant over the contributions (to the differential absorption) of excited state absorption in this wavelength region (*vide infra*). For Δt = 2-50 ps, a fast decrease of the gain signal below 500 nm occurs simultaneously with the rise of a transient absorption band around 465 nm, indicating the formation of a transient state from the fluorescent state. At longer delays (Figure 3.4b) the remaining part of the gain band above 500 nm vanishes and a weak transient absorption band is seen below 550 nm when $\Delta t \cong 150$ ps. This change, from gain to transient absorption, looks similar to that observed at 465 nm, but at a slower rate, in agreement with the results obtained in the fluorescence up-conversion experiments, when detection is at the red edge of the fluorescence band. The bleaching signal remains practically constant during the first 10 ps after excitation; subsequently it shows a decay (Figure 3.4a and b). Finally, for Δt = 150-300 ps (Figure 3.4c), both transient absorption and bleaching signals decay and an isosbestic point around 450 nm with $\Delta D \approx 0$ is obtained, showing that the transient state population is relaxing to the ground state.

Kinetics are illustrated in Figure 3.5 at three probe wavelengths, one in the bleaching band (415 nm) and two in two different regions of the gain band (490 nm and 545 nm). It is seen that the decay of the bleaching signal, i.e. the ground state repopulation, measured at 415 nm, for $\Delta t > 10$ ps, is well described by a single exponential function with a time constant of 130 ps. At 490 nm and 545 nm both the decay of the fluorescent state and the rise and decay of the transient state are assumed to be probed, although the contribution of the latter is almost negligible at 545 nm. It is seen that the time-resolved differential optical density $\Delta D(t)$ is well fitted as a sum of 4 exponentials, by fixing the values of the time constants equal to the three fluorescence decay components given at these wavelengths in Table 3.1b (although the fastest component of ≈ 1 ps does not have much meaning for a fit without convolution of the instrumental time response), plus the 130 ps component measured at 415 nm. The fit gives, as expected, a different sign for the pre-exponential factor of the 130 ps transient-state decay component and a weaker contribution of this component at 545 nm. Also, the fit confirms that this transient state is formed through the fluorescent state decay. By fixing only the 130 ps component, a rough bi-exponential fit gives an average first time constant of 19 ± 3 ps at 490 nm and 40 ± 15 ps at 545 nm, in reasonable agreement with the weighted average fluorescence decay times measured at these wavelengths.

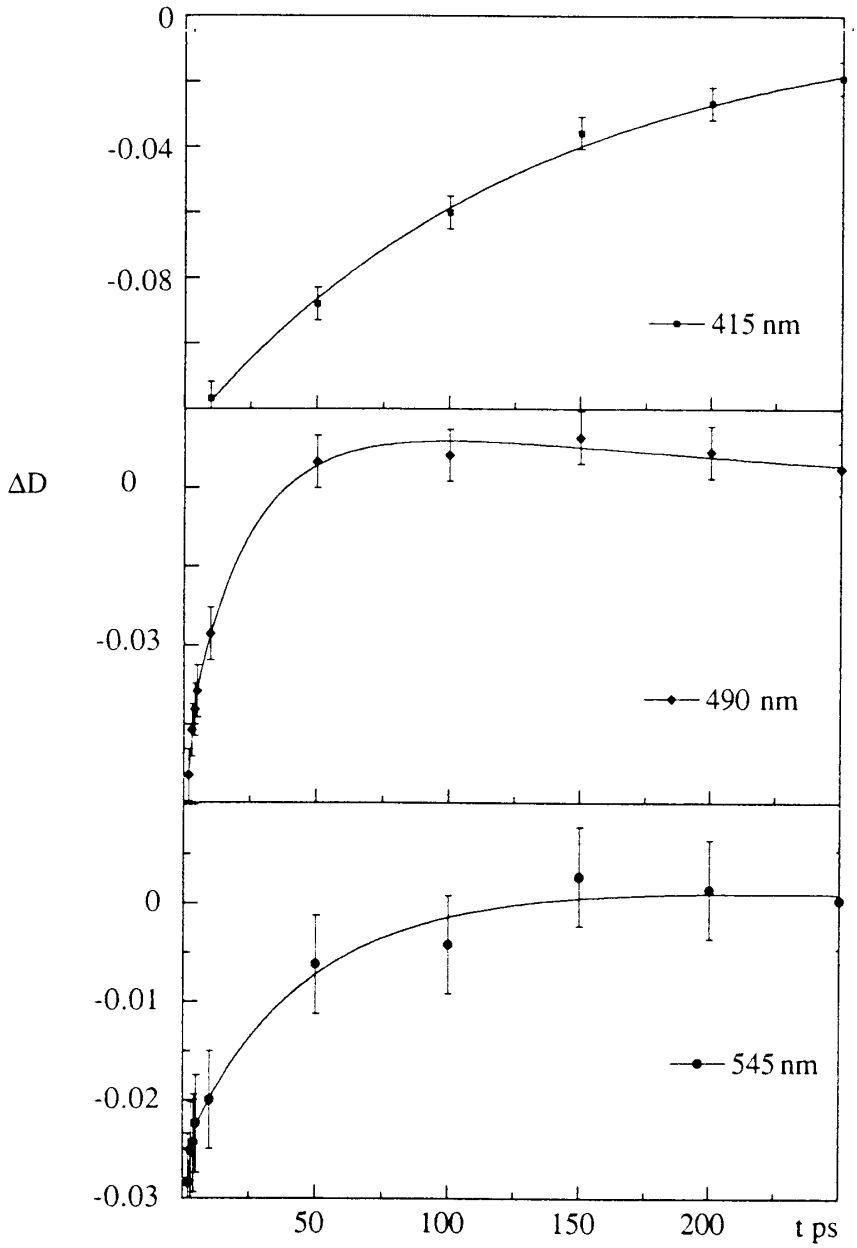

Figure 3.5. Kinetics of the time-resolved differential absorption ΔD(t) measured at 415 nm, 490 nm and 545 nm, for auramine in decanol after excitation with a 700 fs pulsed excitation at 425 nm. At 415 nm, after a lag of 10 ps, the fit gives an exponential decay of the bleaching with a time constant of 130 ps. The fits shown for 490 and 545 nm were done by using a four exponential function and fixing one time-constant at 130 ps and using the data obtained from the fluorescence decay at the same wavelength (Table 3.1b) for the three other ones.

3.4 Discussion

3.4.1. Non-exponential fluorescence decays

The fluorescence upconversion experiments allow a direct observation of the relaxation of the locally excited state without any interference of the ground-state and excited-state absorptions. The fast non-exponential decays of the spontaneous emission and the strong viscosity effect on the lifetimes (Figures 3.1-3.2, Table 3.1) suggest that a barrierless photoreaction similar to that reported in the early studies for TPM dyes [3,10] occurs in auramine. In detail, there are some differences, however. In decanol, which is roughly 13 times more viscous than ethanol, the weighted average lifetimes at the selected wavelengths (Table 3.1a and b) are increased by a factor of about 14 ± 3, except at 600 nm where the disappearance of the fastest component leads to a larger effect. This increase is about twice that found for the TPM dyes ethyl violet [15,17] and crystal violet [14] in the same solvents. On the basis of the BFO theory [11,12,19], the difference in the observed viscosity effects would indicate that the sink functions, i.e. the reaction coordinate-dependence of the nonradiative decay rate, are different. However, the BFO theory predicts an excitation wavelength dependence of the excited state relaxation dynamics, which was not observed for TPM dyes (see references in Refs. [12,16]) and has not been found here for auramine, either. The absence of an excitation wavelength effect also allows us to exclude that the observed dynamics are complicated by concurrent vibrational redistribution.

3.4.2. Wavelength-dependent fluorescence decays

The experiments reveal that the weighted average fluorescence lifetime of auramine, in both solvents, increases with the emission wavelength; a rise in the red wing of the fluorescence spectrum remained unobserved. Non-exponential and wavelength dependent decay behavior of the spontaneous fluorescence was also reported for compounds, which undergo barrierless or low-energetic activated trans-cis isomerization in the first excited state, as e.g., the 1,1’-diethyl-4,4’-cyanine dye [28,29], bacteriorhodopsin [21], all-trans retinal [22] and, more recently, photoactive yellow protein [23,24]. No variation of the lifetime with the emission wavelength was observed in the case of the cis-stilbene isomerization [30], however. The absence of a temporal rise in the red wing of the fluorescence band of auramine is similar to the results for the

trans-cis isomerization studies cited above [21-24], but unlike that for the 1,1'-diethyl-4,4'-cyanine dye molecule for which a rise in the red part of the emission was found [28,29].

Alternatively, the wavelength dependence of the fluorescence transients is reflected in the temporal behavior of the emission spectrum. The position of the band maximum in the reconstructed spectra of auramine (cf Figure 3.3) shows a slight dynamic red shift of about 800 cm^{-1} in ethanol (approximately 500 cm^{-1} in decanol) and the total fluorescence intensity is rapidly reduced as time progresses. In Figure 3.3, the dynamic Stokes shift, as represented by the arrows that show the first moment of the log-normal functional fits at the various delay times, is included. A viscosity-dependent ultrafast spectral shift of the fluorescence band was reported for the cyanine dye [28,29], whereas a change in the amplitude of the fluorescence spectrum with a weak change in the peak position, spectral width and shape, with time up to 5 ps, was reported for bacteriorhodopsin [21]. In the case of the photoactive yellow protein, the wavelength-dependent decays [23] and the reconstructed spectra [24] exhibit an initially fast decaying (fs/ps) narrowed spectrum that shows a broadening and further decay in the long time range (ps/ns) of the red edge, with very little spectral shift.

By comparison with the TPM dyes, internal twisting, through rotation of the phenyl groups, is likely to be the photoreaction which causes the observed fluorescence behavior of auramine. We consider the rapid decay component at the blue wing of the auramine emission band as typical of the motion, on the excited-state potential, of the excited-state population out of the Franck-Condon region. On the basis of the BFO theory, one could suggest that the rapid decrease in the fluorescence intensity as the dynamic Stokes shift progresses results from a rapid increase in the nonradiative decay rate as the excited state population moves along the reaction path, i.e. as the excited molecules twist, the minimum of the excited state potential being supposed to be strongly nonradiatively coupled to the ground state [11,12]. However, in such a case, transient absorption experiments should display multi-exponential ground state repopulation kinetics, whereas after a 10 ps time-lag a single exponential function with a 130 ps time constant is found for auramine in the present study. Moreover, an increase in the nonradiative decay as the reaction proceeds, would also give rise to a shortening of the fluorescence lifetime in the long wavelength region of the emission spectrum. The opposite behavior is observed, however (cf Table 3.1). As can be seen from Figure

3.3, the overall integrated intensity of the emission band has decreased to about 17 % of its initial value after 3 ps. A slight decrease in the emission intensity is expected on the basis of the ν^3 law (Einstein's relation) for spontaneous emission, but this cannot account for the appreciable intensity decrease obtained experimentally. An alternative proposal for the fluorescence intensity decrease with time is that there is a decrease in the radiative rate while the molecule twists, as a result of the change in the degree of conjugation. Thus, the potential energy surface on which the relaxation takes place is not considered to be characteristic of a single electronic state for which the radiative character does not change with the reaction coordinate (such as in a solvation process). A decrease in the transition electric dipole moment as the relaxation takes place is expected, if the reaction path is the adiabatic curve resulting from the electronic coupling between the fluorescent locally excited state and a transient excited state of nonradiative character typical of a twisted dark photoproduct. This can indeed explain the results of the transient absorption experiments on auramine, both in the present study in decanol and in an earlier study in ethanol [19].

The ultrafast appearance, the fast non-exponential decay and the negligible red-shift of the spontaneous emission show that auramine behaves like bacteriorhodopsin (bR) [21] and photo-active yellow protein [23,24] (PYP). For both systems it has recently been proposed that the excited-state dynamics is compatible with a three-state model in which the system very rapidly decays out of the Franck-Condon regime (< 50 fs) into an almost flat potential energy surface with a small barrier [31] to form the reaction region typical of a twisted molecule. In the reactive region there is an anticrossing with another excited electronic state and fluorescence is assumed to take place predominantly when the molecule is in the reactive region. Inhomogeneous broadening due to ill-defined surroundings are held responsible for the spread in excited state lifetimes. A similar model could also be relevant in the case of auramine when it performs its torsional diffusion motions. We thus infer that the relaxation within the auramine molecule from the locally excited (fluorescent) state to the twisted dark state may either involve a barrierless decay along the adiabatic potential energy surface or may pass a small energy barrier and thus may be slightly energetically activated.

3.4.3. Transient photoproduct

In decanol, there is almost no change in the bleaching signal for probing times shorter than 10 ps (Figure 3.4a). This indicates that there is no ground state repopulation while the fluorescent state is decaying, in agreement with the aforementioned idea of the motion of the excited-state population on the excited-state potential prior to the relaxation to the ground state. A delayed onset of the ground state recovery was previously also observed for the 1,1'-diethyl-4,4'-cyanine dye and discussed in terms of a barrierless isomerization process in the excited state of the dye molecule [28,29]. For auramine, the ground state repopulation is roughly three times slower than the average fluorescent-state decay (Figure 3.5). In ethanol, the ground state repopulation kinetics was found to be about 10 times slower than the fluorescent state decay [19]. The fluorescent state relaxes to a transient dark state, although it must be noted that in decanol a fluorescence decay component close to that of the ground state repopulation (130 ps) is observed in the red tail of the emission band at 600 nm suggesting that the red part of the emission in part might be due to the transient state. This is not observed in ethanol; in that case it is thus very likely that the transient state is totally nonemissive. The present experiments do not give any direct information on the geometrical change inferred above for the probed reaction, but with respect to this one can gain insight from previous time-resolved anisotropy measurements with the TPM dye ethyl violet [18]. For the latter, a change in the direction of the $S_1 \rightarrow S_n$ transition moment direction of about 10° was deduced from time-resolved anisotropy measurements in transient absorption experiments, at a wavelength where both the locally fluorescent state and the transient dark state were probed, thus supporting a model which involves the formation of a transient state of different geometry.

For auramine in ethanol, the formation time of the dark twisted photoproduct was estimated [19] to be about 3 ps which is in good agreement with the weighted average fluorescence lifetime found in the present study in this solvent. It is remarkable that the lifetime of the dark twisted transient state is less sensitive to the solvent viscosity than the formation time. In decanol, the dark state lifetime is 4.3 times larger than in ethanol [19], whereas the formation time is increased by a factor of 14. A similar viscosity effect on the formation and decay rates of the transient twisted dark state was also noted for the TPM dye ethyl violet [15] and for a bridged triphenylmethane dye (aminorhodamine) [32]. Thus, also in the dark state decay

dynamics, the similarity between auramine and TPM derivative compounds is manifested.

It is of interest to recall that in the case of aminorhodamine, in the presence of hydrochloric acid, only a nanosecond monoexponential decay of the locally excited-state emission was observed [32], showing that upon protonation the nonradiative excited state deactivation channel is hampered. Since protonation of aminorhodamine occurs at the best electron donor site, that is the dimethyl-amino substituent attached to the phenyl group which is free to rotate in low-viscosity liquid, it was concluded that the nonradiative channel involves intramolecular charge transfer from the dimethylamino substituent to the central carbon atom. TPM dyes and analogues are organic cations and the central carbon is generally assumed to carry the positive charge in the ground state. Scheme 3.1 shows one possible form of auramine, another possible form would be that the positive charge is on the central carbon, like in TPM dyes. Thus, based on the analogous properties between the TPM derivative compounds and auramine, an intramolecular charge shift from the dimethylamino substituents to the central carbon site is likely to contribute to the photoreaction observed here for auramine.

3.5 Conclusion

The locally excited-state relaxation dynamics for auramine in ethanol and decanol has been determined by fluorescence upconversion and pump-probe transient absorption techniques. From the characteristics of the viscosity-dependent non-exponential fluorescence decays and the transient absorption data, it is concluded that the relaxation proceeds along a barrierless or low-energy activated potential energy surface by a diffusive twisting of the auramine phenyl groups. The results are discussed starting from the model of Bagchi et al [11] for a barrierless photoreaction. However, a change in the radiative rate along the reaction path is proposed to explain the wavelength-dependence of the fluorescence decays, i.e. a rapid decrease of the emission band intensity together with a small red shift, with no measurable rise time in the red wing of the band. A decrease in the transition electric dipole moment of auramine as the relaxation takes place supports the model of a photoreaction along an adiabatic potential resulting from the electronic coupling between the fluorescent locally excited state and a

dark state. The dark state is considered to be characteristic of a twisted photoproduct with charge shift.

Acknowledgement

This work was supported in part by the Netherlands Foundation for Chemical Research (SON) with financial aid from the Netherlands Organization for Scientific Research (NWO). P.P. and M.M.M. wish to thank Prof. J.T. Hynes for useful comments on the manuscript during his stay at Orsay.

References

[1] G. Oster, C. R. Hebd. Séances Acad. Sci. **232**, 1708 (1951).

[2] G. Oster, J. Polym. Sci. **16**, 235 (1955).

[3] G. Oster, Y. Nishijima, J. Am. Chem. Soc. **78**, 1581 (1956).

[4] R.H. Conrad, J.R. Heitz, L. Brand, Biochemistry **9**, 1540 (1970).

[5] R.F. Steiner, S. Albaugh, E. Nenortas, L. Norris, Biopolymers **32**, 73 (1992).

[6] J.G. Weers, A.H. Maki, Biochemistry **25**, 2897 (1986).

[7] Y. Wang, H. Morawetz, Macromolecules **19**, 1925 (1986).

[8] E.F. Meyer, A.M. Jamieson, R. Simha, J.H.M. Palmen, H.C. Booij, F.H.J. Mauer, Polymer **31**, 243 (1990).

[9] L.F. Vieira Ferreira, M. Rosario Freixo, A.R. Garcia, F. Wilkinson, J. Chem. Soc. Faraday Trans. **88**, 15 (1992).

[10] T. Förster, G. Hoffmann, Z. für Phys. Chem. NF **75**, 63 (1971).

[11] B. Bagchi, G.R. Fleming, D.W. Oxtoby, J. Chem. Phys. **78**, 7375 (1983).

[12] B. Bagchi, G.R. Fleming, J. Phys. Chem. **94**, 9 (1990).

[13] V. Sundström, T. Gillbro, J. Chem. Phys. **81**, 3463 (1984).

[14] D. Ben-Amotz, C.B. Harris, J. Chem. Phys. **86**, 4856 (1987).

[15] M.M. Martin, E. Bréhéret, F. Nesa, Y.H. Meyer, Chem. Phys. **130**, 279 (1989).

[16] M.M. Martin, P. Plaza, N. Dai Hung, Y.H. Meyer, in Ultrafast Phenomena VII, eds C.B. Harris, E.P. Ippen, G.A. Mourou, A.H. Zewail, Springer-Verlag, **53** (1990) 504.

[17] M.M. Martin, P. Plaza, Y.H. Meyer, J. Phys. Chem. **95**, 9310 (1991).

[18] M.M. Martin, P. Plaza, in Ultrafast reaction dynamics and solvent effects, eds Y. Gauduel, P.J. Rossky, American Institute of Physics, **298** (1994) 410.

[19] M.M. Martin, P. Plaza, P. Changenet, Y.H. Meyer, J. Photochem. Photobiol. A: Chem. **105**, 197 (1997).

[20] D.F. Duxbury, Chem. Rev. **93**, 381 (1993).

[21] M. Du, G.R. Fleming, Biophysical Chemistry **48**, 101 (1993).

[22] H. Kandori, H. Sasabe, Chem. Phys. Lett. **213**, 126 (1993).

[23] H. Chosrowjan, N. Mataga, N. Nakashima, Y. Imamaoto, F. Tokunaga, Chem. Phys. Lett. **270**, 267 (1997).

[24] P. Changenet, H. Zhang, M.J. van der Meer, K.J. Hellingwerf, M. Glasbeek, Chem. Phys. Lett. **282**, 276 (1998).

[25] P. van der Meulen, H. Zhang, A.M. Jonkman, M. Glasbeek, J. Phys. Chem. **100**, 5367 (1996).

[26] N. Dai Hung, P. Plaza, M.M. Martin, Y.H. Meyer, Appl. Opt. **31**, 7046 (1992).

[27] M. Maroncelli, G.R. Fleming, J. Chem. Phys. **86**, 6221 (1987).

[28] U. Åberg, E. Åkesson, J.-L. Alvarez, I. Fedchenia, V. Sundström, Chem. Phys. **183**, 269 (1994).

[29] A. Yartsev, J.-L. Alvarez, U. Åberg, V. Sundström, Chem. Phys. Lett. **243**, 281 (1995).

[30] D.C. Todd, G.R. Fleming, J. Chem. Phys. **98**, 1993 (1993).

[31] K.C. Hasson, F. Gai, P.A. Anfinrud, Proc. Natl. Acad. Sci. USA **93**, 15124 (1996).

[32] P. Plaza, N. Dai Hung, M.M. Martin, Y.H. Meyer, M. Vogel, W. Rettig, Chem. Phys. **168**, 365 (1992).

Chapter 4

Femtosecond fluorescence upconversion studies of barrierless bond twisting of auramine in solution*

Abstract

Femtosecond fluorescence upconversion studies have been performed for auramine (a diphenylmethane dye), dissolved in ethanol, as a function of temperature. It is found that the (sub)picosecond decay components in the fluorescence slow down as the temperature is lowered from 293 K to 173 K. From the observation of a residual fluorescence, with a viscosity-dependent lifetime of about 30 ps (or longer at higher viscosity), and transient absorption results, it is concluded that the two-state sink function model [B. Bagchi, G.R. Fleming, and D.W. Oxtoby, J. Chem. Phys. **78**, 7375 (1983)] does not apply in the case of auramine. Comparison of the auramine fluorescence kinetics in ethanol and decanol shows that diffusional twisting and not solvation is the main cause for the (sub)picosecond excited state relaxation. To explain the experimental results, adiabatic coupling between a locally excited emissive state (*F*) and a nonemissive excited state (*D*) is considered. Torsional diffusion motions of the phenyl groups in the auramine molecule are held responsible for the population relaxation along the adiabatic potential of the mixed state, S_1 (comprised of the *F* and *D* states). Simulation of the excited state dynamics is feasible assuming a barrierless-shaped potential energy for S_1 and applying the Smoluchowski diffusion equation. The temporal behavior of the auramine band emission was simulated for the temperature range 293 K >*T* >173 K, with the temperature, *T*, and the viscosity coefficient, η, being the only variable parameters. The simulated temporal behavior of the emission in the investigated temperature range is compatible with that obtained experimentally. The rotational diffusion coefficient for the auramine phenyl groups as extracted from the simulations is found to follow the Einstein-Stokes relation. From the numerical calculations the effective radius of the twisting phenyl groups is determined as 1.0 Å which compares well with the actual value of 1.2 Å.

* The contents of this chapter has been published as an article, M.J. van der Meer, H. Zhang, M. Glasbeek, J. Chem. Phys. **112**, 2878-2887 (2000).

4.1 Introduction

Ultrafast photoinduced intramolecular conformational changes are of great importance to many processes of chemical and biological interest [1,2]. Especially when the excited state potential energy as a function of the reaction coordinate lacks an activation barrier, very high values for the reaction rate (often in excess of 10^{12} s^{-1}) can be expected. In the condensed phase, the dynamics of barrierless reactions in *fluorescent* excited states may be studied from Time Resolved Stokes Shift (TRSS) measurements [3-5]. In the experiment, an ultrashort laser pulse prepares the molecule in the photoreactive emissive state and, as the activationless reaction in this excited state develops, the red shift of the peak of the emission band (or its first moment) is probed with time. On a picosecond time scale, the motion of the excited-state population density distribution out of the Franck-Condon region may be considered as diffusive [6]. Adopting some down-hill shape for the excited state potential energy surface, the excited state population, $\rho_e(t)$, and thus the Stokes shift is obtained by solving a diffusion-type equation [6-11]. Quite often, the lifetime of the fluorescent state is influenced by the solvent viscosity. The lifetime increases with increasing viscosity from picoseconds up to nanoseconds. The phenomenon has been observed for example for photoexcited di- and triphenylmethane dye molecules [12-40]. Examples are malachite green [15,38-40], crystal violet [12,13,16,17,24,26-28,33-35] and its julolidine analogue [23,28], ethyl violet [14,38], and parafuchsin [14,38]. To simulate the temporal behavior of $\rho_e(t)$ in such excited state systems, Bagchi, Fleming and Oxtoby [7] (BFO) considered the incorporation of a reaction-coordinate dependent (nonlocal) sink function in the Smoluchowski diffusion equation. This sink function causes an enhanced *non*radiative decay and its effect is more pronounced as the generalized reaction coordinate, $z(t)$, in the excited state approaches a value that corresponds to the excited product state. Especially, the population density of the reactive state is affected by the presence of this sink function: when the system has relaxed close to the potential energy minimum of the excited state, the population density has decreased appreciably and this is considered to be the cause for the fast drop in the fluorescence intensity.

In this chapter, we study (sub)picosecond fluorescence transients of auramine (for a picture of the molecular structure, see Scheme 4.1), in liquid solution. Auramine has long been known for its highly viscosity dependent fluorescence quantum yield

[41]. The dye is weakly fluorescent in low-viscosity solvents, like water, and highly fluorescent in viscous solvents, DNA and polymeric acids [42,43]. Auramine has recently been applied as fluorescent probe in polymers [44,45], protein systems [46], and in investigations of microviscosity and structure in micelles [47-49]. Early investigations already suggested that rotational diffusion of the phenyl groups in the auramine molecule is responsible for the drastic influence of the solvent viscosity on the fluorescence quantum yield [41,50]: in highly viscous solvents the torsional motions are impeded, thus radiationless decay is less efficient and the fluorescence is favoured [51].

SCHEME 4.1

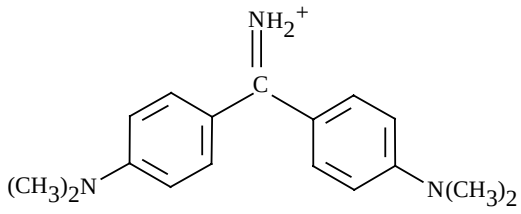

Auramine

Previous time-resolved fluorescence upconversion measurements of auramine have revealed a multi-exponential fluorescence decay for which the kinetics is detection wavelength dependent [52]. After spectral reconstruction, at room temperature two observations could be made: (a) a small dynamic Stokes shift of about 1,000 cm^{-1} in a few picoseconds, and (b) the dynamic Stokes shift is accompanied by a drastic decrease of the fluorescence intensity to about 10% of its initial value. The longer-lived residual fluorescence has a weighted average lifetime of about 30 ps in ethanol (~ 130 ps in decanol). This lifetime is thus at least one order of magnitude longer than the typical Stokes shift kinetics. Yet, no (sub)picosecond fluorescence intensity rise (characteristic of a dynamic Stokes shift) could be observed when detection is at the red part of the emission band. The absence of such a rise component is a manifestation of the fact that, concomitant with the dynamic Stokes shift, fluorescence intensity is lost and that this loss is on a time scale much faster than the 30 ps (or longer) residual lifetime. As discussed previously [52], the results can not be reconciled within an approach that follows the BFO model, because according to this model the rapid fluorescence intensity loss in a few picoseconds would imply an excited state lifetime (shortened by the presence of the sink function) of also a few picoseconds and this is in contradiction with the observed residual lifetime of at least 30 ps.

In an alternative approach, we proposed [52] that, concomitant with the torsional diffusive relaxation affecting $\rho_e(t)$, also the radiative decay rate constant, k_e^{rad}, may be z-dependent such that $k_e^{rad}(z)$ is reduced as the reaction takes place. The z-dependence

of $k_e^{rad}(z)$ was discussed to originate from an adiabatic coupling of a locally excited emissive state and a nonemissive "phantom" state. Indeed, the existence of a short-living (30 ps – 130 ps) dark excited state had been verified by means of transient absorption experiments [31,52]. In these pump-probe experiments the fast decay of the gain signal above 470 nm for *(*t = 1 – 10 ps (reflecting the fast decay of the fluorescent state) is accompanied by a simultaneous rise of a 'new' transient absorption band around 465 nm, indicating the formation of a transient state from the fluorescent state. At longer delay times (Δt = 10 – 50 ps), the 465 nm transient absorption and the bleaching of the ground state absorption around 425 nm exhibit a simultaneous decay, thus giving rise to an isosbestic point around 450 nm. These results show that the time constants for the decay of the formed transient state and the ground state recovery are the same. The long lifetime of 30 – 130 ps (depending on the solvent viscosity) of the transient intermediate state is evidence for a transient dark electronic excited state, the population of which relaxes to the ground state [52]. Twisting is accompanied by an energy relaxation along the adiabatic potential energy curve whereby the excited state radiative character is changed from radiative to nonradiative. The model could account in a natural way for the observation of short-living fluorescence components (with characteristic times of a few picoseconds) as well as the emission from the relaxed excited state with a lifetime of at least 30 ps.

In this chapter, the proposed model of adiabatically coupled emissive and dark excited states of auramine is investigated in more detail, both experimentally and theoretically. We have undertaken a systematic (sub)picosecond study of the excited-state dynamics of auramine as a function of temperature and solvent viscosity. Femtosecond fluorescence upconversion and picosecond time-correlated single-photon-counting experiments were performed to determine the time-resolved emission spectra in the temperature range from 130 K < T < 300 K. The experiments were conducted for auramine dissolved in ethanol. We include results of simulations that start from a modified Smoluchowski equation. In this equation a potential energy function representative of the adiabatic coupling between the emissive locally excited state and the dark "phantom" state is incorporated. It is shown that upon application of the adiabatic coupling model a satisfactory agreement between the simulations and the experimental data is obtained.

4.2 Experimental

Auramine, 4,4'-(imidocarbonyl)-bis (N,N-dimethylaniline) monohydrochloride, was purchased from Aldrich (80%) and purified in several sublimation steps to eliminate fluorescent impurities. The solvent ethanol was UV spectroscopic grade and used as purchased (from Merck) without further purification. The sample concentration was chosen to be larger than ~ 10^{-4} M in order to avoid deprotonation of auramine. In steady-state fluorescence measurements only auramine fluorescence could be detected showing that impurity emission is absent.

Subpicosecond fluorescence transients were measured using the femtosecond fluorescence upconversion equipment described previously [10,53]. A diode-laser-pumped Millennia X laser was used to pump a Tsunami Ti: sapphire laser (~ 60 fs pulse width) with a repetition rate of 82 MHz. The pulses were led through a 1 mm thick BBO frequency doubling crystal after which the pulses were split by a dichroic beam-splitter into two beams, the first beam being the pump beam (at a wavelength of 420 nm) and the second beam being the gating beam (at 840 nm). Pulses with an energy of about 1 nJ/pulse were used to photoexcite the sample. The solution was contained in a cell of 1 mm thickness. The gating beam passed a stepper motor-driven translational stage and was focused together with the fluorescence induced by the pump-beam onto a 1 mm thick BBO crystal (type I phase match). The upconversion signal was filtered by an UG11 filter and focused on the entrance slit of the monochromator (spectral resolution < 5 nm) and detected by means of a photomultiplier connected to a photon counting system linked to a personal computer for data storage and analysis. To circumvent effects arising from reorientational motions of the probe molecules in the solution, the transients were measured under magic angle conditions. The instrumental response function, as deduced from the measured cross-correlation function of the excitation and the gating pulses (at 420 nm and 840 nm, respectively), was determined to be about 150 fs (FWHM).

For time windows longer than 60 ps, fluorescence transients of auramine solutions were measured using the picosecond laser system and the calibrated emission spectrometer described elsewhere [10,54]. In this set-up, the laser pulses from a frequency-doubled picosecond dye laser (excitation was at 322 nm, pulse duration ~ 4 ps) synchronously pumped by a mode-locked Ar^+ - ion laser, served as the excitation pulses. In these experiments, time-correlated single-photon-counting detection was

applied, with a time resolution of 16 ps. Steady-state emission spectra were measured using the calibrated emission spectrometer.

Temperature variation of the sample was realized by use of a home-built liquid nitrogen flow cryostat [54]. The temperature was varied by means of a Cryoson 17-90B/1 temperature regulator which is attached to the liquid nitrogen supply. The temperature of the sample was measured with a thermocouple attached to the copper cuvette holder. After thermal equilibration, the accuracy of the temperature control is ± 3 K.

4.3 Results

4.3.1 Steady-state absorption and emission spectra

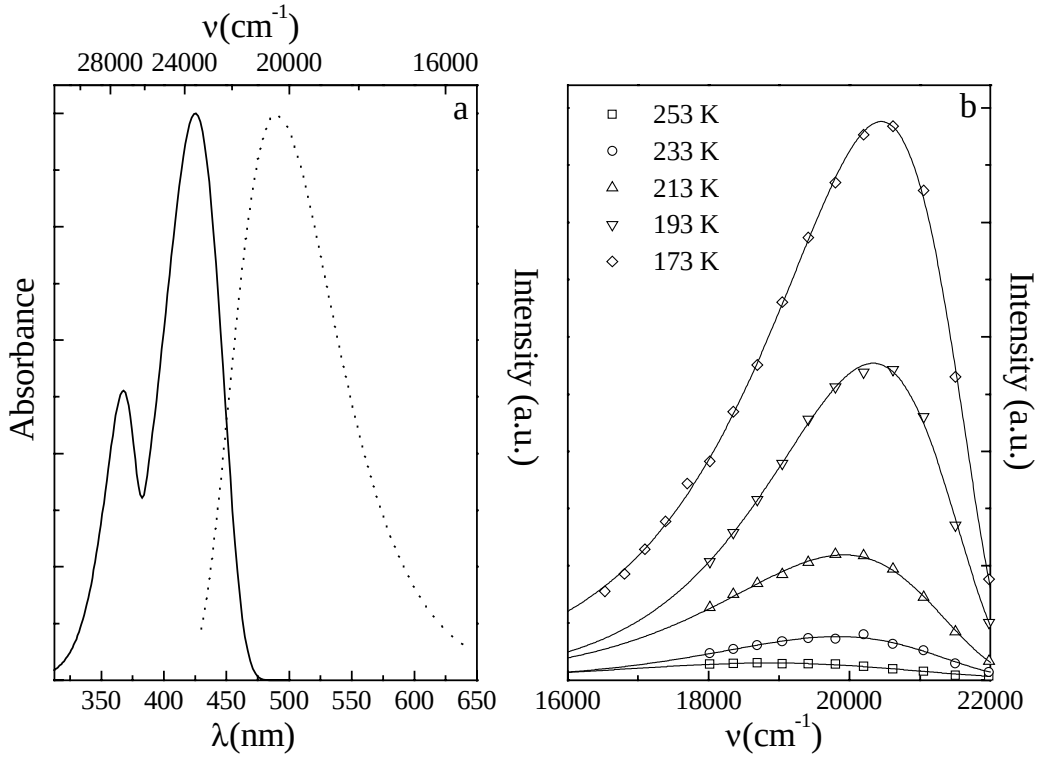

Figure 4.1. (a) Steady-state absorption (solid line) and emission (dotted line) spectra of auramine in ethanol at room temperature. (b) Steady-state emission spectra of auramine in ethanol at different temperatures as measured with photon counting ps fluorescence spectrometer. Experimental data points are indicated. Solid lines show best fits to a log-normal function.

In Figure 4.1a we show the steady-state absorption and emission spectra of auramine, dissolved in ethanol, at room temperature. Figure 4.1b shows the emission spectra of auramine, in ethanol, measured at a few temperatures. The latter figure illustrates that, at the lower temperatures, the emission band maximum is blue shifted by about 800 cm^{-1}. Also, the total band intensity rapidly increases as the temperature is lowered. This intensity increase is a characteristic feature of the auramine fluorescence and of course is a consequence of the well-known increase of the fluorescence quantum yield at the lower temperatures [41,50].

4.3.2 Femto- and picosecond fluorescence measurements

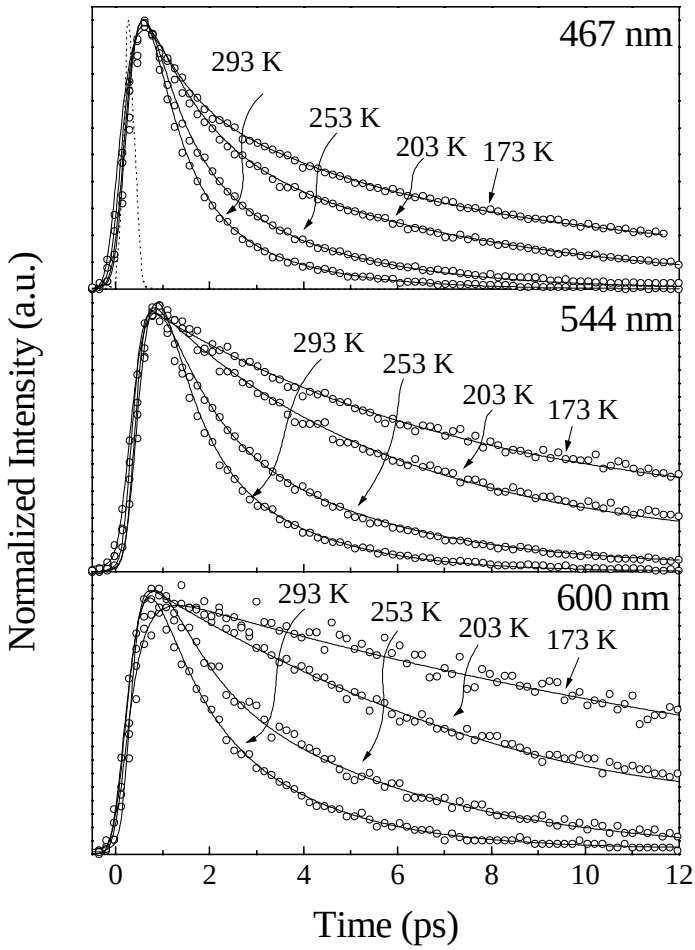

Figure 4.2. Representative fluorescence upconversion transients of auramine in ethanol for various emission wavelengths and temperatures. Open circles are measured intensities, solid lines are best fits to multiexponential decay functions as detailed in text. Dashed line in top panel shows system response function.

Fluorescence upconversion transients of auramine, dissolved in ethanol, were measured for a series of different detection wavelengths within the emission band. Typical upconversion transients at room temperature were already shown in a previous paper [52]. For convenience, however, we reproduce these transients in Figure 4.2, for T = 293 K, and a time window of 13 ps. All transients show an instantaneous rise (within the system response of about 150 fs) followed by a fast decay with a typical time of a few picoseconds.

The decay is dependent on the detection wavelength: as the wavelength is more to the red, the decay is slower. The experiments were repeated at a series of temperatures, in the range from 173 K up to 293 K, at intervals of 20 K. Figure 4.2 illustrates for the fluorescence upconversion transients, measured at 467 nm, 544 nm, and 600 nm, respectively, the variation of the kinetics with temperature. In general, as the temperature is lowered, the decay slows down.

All upconversion transients in Figure 4.2 could be fitted to a multi-exponential decay function convoluted with the system response function. The zero-intensity level for the transients measured with the fs upconversion setup was determined by equalizing the intensities at the trailing edge of the transients, measured in the time interval $\Delta t > 30$ ps, with the intensity of the transients measured with the SPC setup in the same time interval. In this way the residual long-time components in the fs transients could be obtained. Table 4.1 collects, for a few wavelengths and temperatures, best fit values for the fastest two time constants, τ_1 and τ_2 (in ps), of the decay components, their relative amplitudes, as well as the weighted average decay time. The average decay time increases from 1.2 - 2.9 ps at room temperature to 8.0 - 17.3 ps at 173 K.

At temperatures lower than about 160 K ethanol forms a glass. In Table 4.2, we present the time constants giving the best tri-exponential fit for the transients measured (not shown) with the time-correlated single-photon-counting fluorescence set-up, at 133 K. For detection wavelengths below 550 nm, the fluorescence transients initially decay with a time constant of about 55 ps (cf Table 4.2). However, for fluorescence transients detected in the red part of the emission ($\lambda \geq 550$ nm) an initial rise component with a time constant of about 55 ps is measured for auramine in ethanol glass.

Table 4.1

Best-fit values of the time constants, τ_1 and τ_2, characterizing the bi-exponential fit to the fluorescence transients, during first 15 ps, of auramine in ethanol, at several detection wavelengths and temperatures. τ_{av} is the weighted average decay time. Relative amplitudes of the two components are indicated between brackets.

T (K)	λ_{fl}(nm)	τ_1(ps)(%)	τ_2(ps)(%)	τ_{av}(ps)
293	467	0.7 (75)	2.7 (25)	1.2
	491	0.8 (65)	2.8 (35)	1.5
	544	1.9 (55)	3.3 (45)	2.5
	600	1.5 (55)	4.6 (45)	2.9
253	467	1.4 (77)	4.1 (23)	2.0
	491	1.3 (73)	3.9 (27)	2.0
	544	2.3 (82)	6.0 (18)	3.0
	600	3.6 (100)		3.6
233	467	1.6 (72)	5.2 (28)	2.6
	491	1.8 (69)	5.4 (31)	2.9
	544	2.7 (67)	6.5 (33)	3.9
	600	4.8 (100)		4.8
203	467	2.0 (63)	7.9 (37)	4.2
	491	2.3 (63)	8.9 (37)	4.7
	544	4.1 (61)	11.9 (39)	7.1
	600	6.8 (100)		6.8
173	467	2.9 (59)	15.6 (41)	8.0
	491	3.0 (59)	17.2 (41)	8.9
	544	5.3 (50)	22.4 (50)	13.8
	600	17.3 (100)		17.3

The time-dependent fluorescence spectra were reconstructed as reported previously [52]. In brief, the deconvoluted multiexponential decay function, at each detection wavelength, was normalized so that its time integrated value matched the steady-state emission intensity at the corresponding wavelength. In this way, for a set of detection wavelengths, the normalized fluorescence intensity is known at all times after the pulsed excitation. Point-to-point plots of the emission spectra at various (ps) delay times and for four different temperatures are presented in Figure 4.3. The solid lines represent the best fit of the point-to-point spectra to a log-normal line shape function. The figure clearly illustrates the salient features in the temporal dependence at the

various temperatures. First, a small dynamic Stokes shift (i.e., the red shift of the first moment of the emission band) of approximately 1,000 cm^{-1}, within the first 10 ps, is observed at room temperature.

Table 4.2

Best-fit values of the time constants, τ_1, τ_2, and τ_3, characterizing the tri-exponential fit to the fluorescence transients of auramine in ethanol, at several detection wavelengths and temperatures. τ_{av} is the weighted average decay time. Relative amplitudes of the components are indicated between brackets.

T (K)	λ_{fl}(nm)	τ_1(ps)(%)	τ_2(ps)(%)	τ_3(ps)(%)	τ_{av} (ps)
133	465	55 (32)	389 (37)	1428 (31)	463
	485	55 (17)	506 (31)	1689 (53)	907
	505	55 (18)	551 (31)	1655 (51)	863
	525	55 (3)	604 (34)	1762 (63)	1124
	545	55 (1)	822 (38)	2025 (62)	1258
	565	55 (-7)*	1177 (74)	2665 (33)	891
	585	55 (-14)*	1268 (86)	2826 (28)	810

* These are rise components; the sum of all relative amplitudes is chosen to be 100.

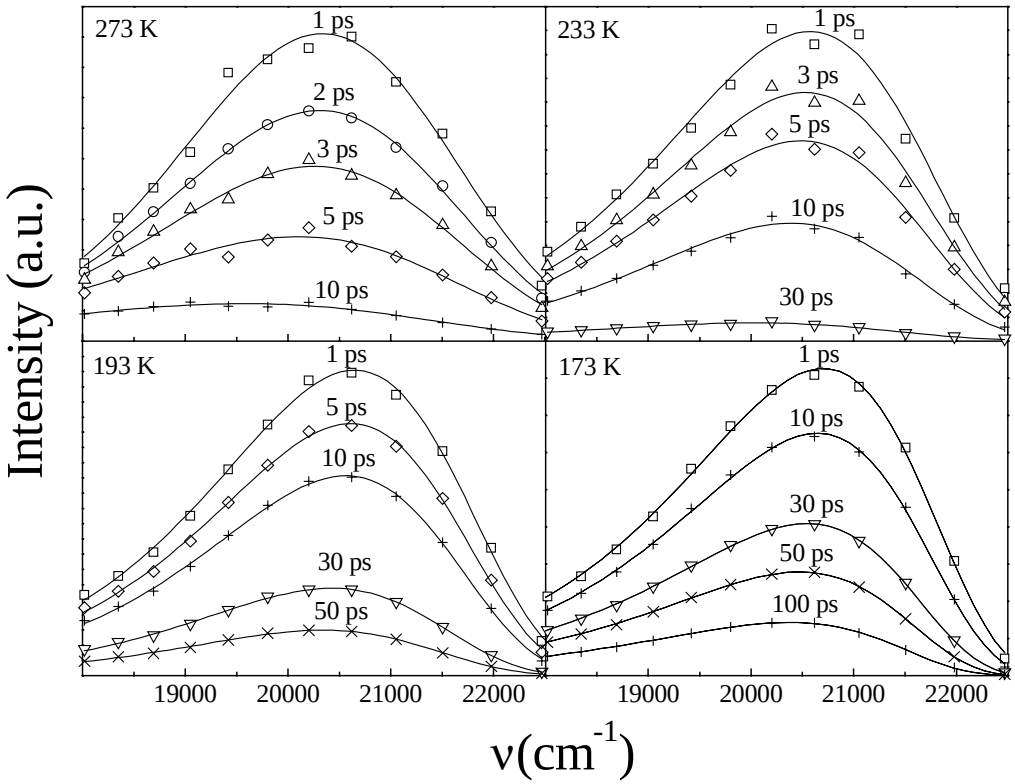

Figure 4.3. Temporal dependence of the emission spectra of auramine (dissolved in ethanol) at various temperatures. The symbols represent the experimental data after spectral reconstruction. Solid lines represent best fits to log-normal shape functions.

At 173 K, this shift is approximately 700 cm^{-1}, within 50 ps. Secondly, the dynamic Stokes shift is accompanied by a drastic drop in the total fluorescence intensity. This intensity drop is also temperature dependent: it is more pronounced at room temperature (drop of about 90% of the initial value) and much less at 170 K (drop of about 20 % of the initial value). The rate of this intensity decay is temperature dependent: as the temperature is decreased the decay rate becomes smaller. Thirdly, at room temperature, the residual fluorescence for auramine in ethanol decays with a time constant of about 30 ps. When using the more viscous solvent decanol, the residual lifetime is about 130 ps [52]. The lifetime becomes somewhat longer when the temperature is lowered to 173 K.

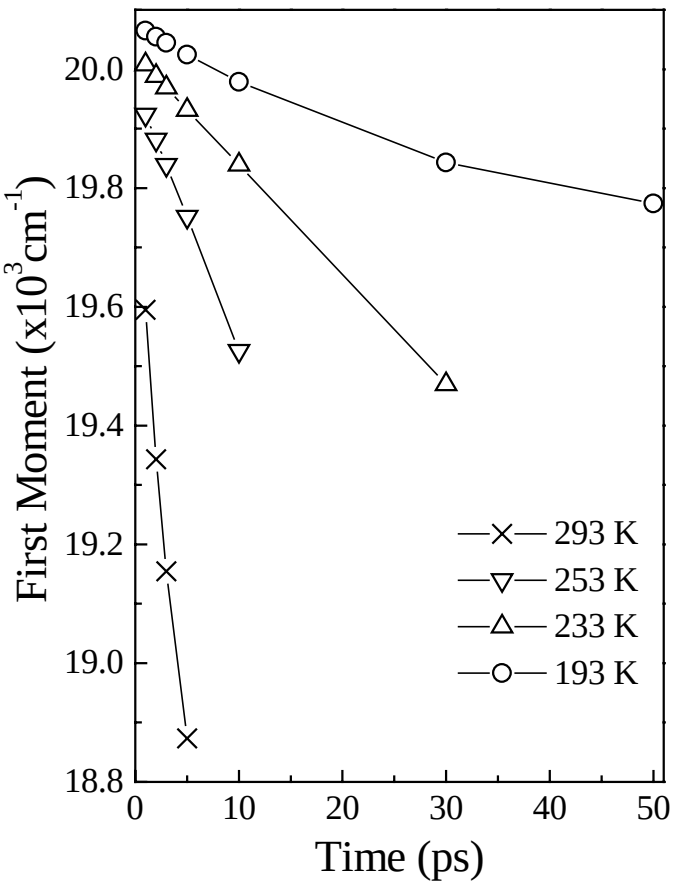

Figure 4.4. Time dependence of the first moment of the auramine emission band at the indicated temperatures.

In Figure 4.4, the temporal behavior of the first moment of the emission band is given for different temperatures. The magnitude and the rate of the shift in the first moment of the emission band are temperature dependent. The shift of the first moment (dynamic Stokes shift) is larger and faster at higher temperatures.

In Figure 4.5 plots are given for the temporal dependence of the width of the emission band at a few temperatures. Note that the auramine emission band broadens in time, but for lower temperatures the broadening is much smaller and at a smaller rate.

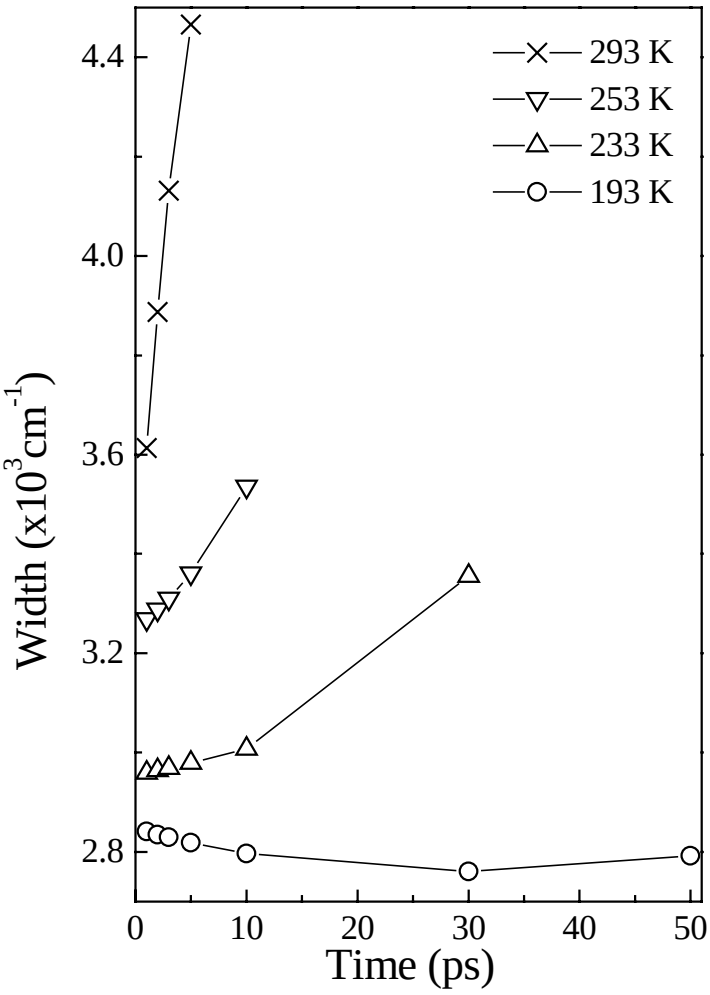

Figure 4.5. Time dependence of the width of the auramine emission band in ethanol at the indicated temperatures.

4.4 Discussion

4.4.1 Existing models

The dynamic behavior of diphenylmethane (DPM) and triphenylmethane (TPM) dyes has been extensively studied in the past [22-37]. Generally, torsional motions of the phenyl groups are held responsible for the relaxation processes observed for the molecules in the excited state. In the case of auramine, the excited state dynamics has been studied by varying the solvent viscosity [31,52]. Upon changing the solvent viscosity, but keeping the polarity almost the same, the kinetics of the fluorescence transients was affected appreciably. These observations are strong evidence that torsional motions of the auramine phenyl groups (and not solvation dynamics involving dielectric relaxation) determine the excited state dynamics of auramine. For auramine, several models have been considered previously. Oster and Nishijima (ON) [41] have measured the viscosity (η) dependence of the fluorescence quantum yield (ϕ) and found that, $1/\phi \sim T/\eta$. To interpret their results, Oster et al. assumed that the excited-state potential energy is independent of the torsional angle of the auramine phenyl groups. Twisting was considered to contribute to the broadening of the excited-state population by diffusion over a flat potential (Figure 4.6a). Through the introduction of two local sink functions, the population leaks away thus affecting the excited-state lifetime. The leakage is diffusion controlled and the ON model is compatible with the experimental behavior of $1/\phi \sim T/\eta$ [41]. Regarding the applicability of the ON model to laser-pulse excitation experiments, we remark that the model predicts a broadening of the emission band as twisting of the phenyl groups proceeds, but a drift of the population density maximum, or equivalently, a diffusion-controlled dynamic Stokes shift is not expected. Although our experiments show, on the one hand, that a dynamic broadening of the auramine emission band is present indeed (see Figure 4.5), the observed dynamic Stokes shift (see Figures 4.3 and 4.4), on the other hand, is incompatible with the ON model. In conclusion, like in the case of the results of Förster and Hoffmann [50], our results are not in agreement with the ON model.

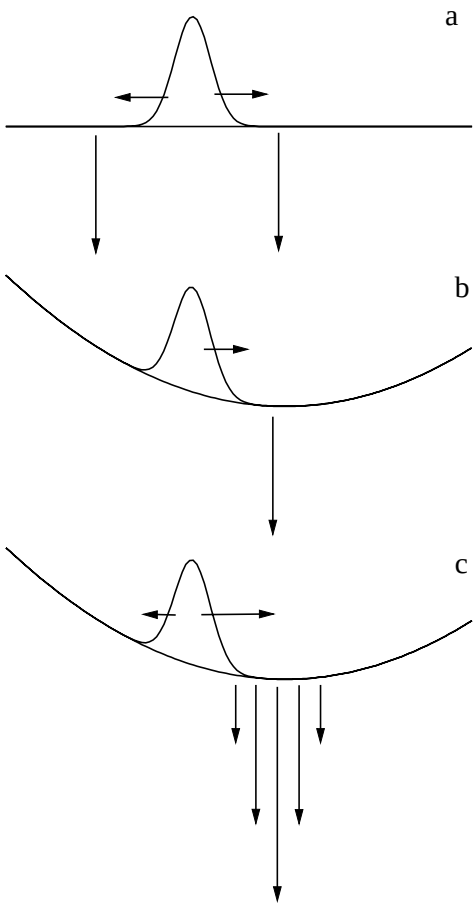

Figure 4.6. Sketch of potential energy curves and dynamics of the excited state population according to Oster and Nishijima [41] (a), Förster and Hoffmann [50] (b), Bagchi, Fleming and Oxtoby [7] (c).

Förster and Hoffmann (FH) reported a $\phi \sim \eta^{2/3}$ dependence of the auramine fluorescence quantum yield, ϕ, as a function of the solvent viscosity, η, in a series of different solvents [50]. To explain this behavior, FH considered relaxation along a parabolically shaped excited-state potential (see Figure 4.6b). In the FH model, the viscosity of the solvent exerts a high enough friction so that the motion along the potential energy surface is overdamped. Furthermore, a sink function at the potential energy minimum (cf Figure 4.6b) is introduced to warrant that the rate for radiationless decay to the ground state becomes dependent on the torsional coordinate. Förster and Hoffmann derived a $\phi \sim \eta^{2/3}$ viscosity dependence of the fluorescence quantum yield after time-integration of the derived expression for the time-dependent decay rate constant. In an analogous approach, Bagchi, Fleming and Oxtoby (BFO) have

considered the *dynamics* of the twisting processes in TPM molecules [7]. The parabolically shaped potential energy function as well as the non-local sink function (see Figure 4.6c) were now used as input functions for solving the population density in the excited state from the Smoluchowski diffusion equation. Phenomenologically, both approaches, FH and BFO, lead to a dynamic Stokes shift after ultrashort laser excitation of the photoactive molecules. The main difference would be that FH gives rise merely to a dynamic Stokes shift without emission band broadening, whereas according to BFO both a Stokes shift and a band broadening are expected. Both models have in common that there is one radiative excited state for which the eventual lifetime is determined by the decay rate imposed by the sink function. It is to be expected that if these models would be applicable for the auramine results discussed in this paper, the shortening of the excited-state lifetime predicted by the models (due to the twisting dependent radiationless decay) should be responsible for the observed drop in the total fluorescence intensity with time (cf Figure 4.3).

Recent transient absorption [31,52] and femtosecond fluorescence upconversion [52] experiments for auramine in liquid solution have shown, however, that the picosecond decay of the initially excited state is into a dark (non-emissive) “phantom” state with a lifetime of about 30 ps (in ethanol, at room temperature). The observations cannot be explained by considering rotational diffusion alone, without additional effects. This is seen as follows. If only rotational diffusion would take place, this would cause relaxation along the excited state potential energy curve, but during this process the electronic part of the wave function would not change. Consequently, the optical transition moment would not be influenced by the twisting process and the total integrated emission intensity at all times would follow a ν^3-dependence, in accordance with Einstein’s expression for spontaneous emission.

As illustrated in Figure 4.7, this clearly is not the case. While rotational diffusion occurs in the excited state, the ν^3-law does not apply in the case of auramine, and in fact the total integrated intensity decays much faster than predicted by this law.

If this enhanced decay were due to ‘sink function effects’, the auramine results show then that the characteristic time associated with this additional sink function decay would be only a few picoseconds. Since in the BFO model the sink function represents a radiationless decay to the ground state, this would, of course, also mean that the total excited state lifetime would be of the order of a few picoseconds. The latter is not

corroborated by the experimental results: for auramine a residual excited state lifetime of at least 30 ps is measured, both in transient absorption [31,52] and emission [52]. We conclude that the BFO and FH models are not applicable for auramine.

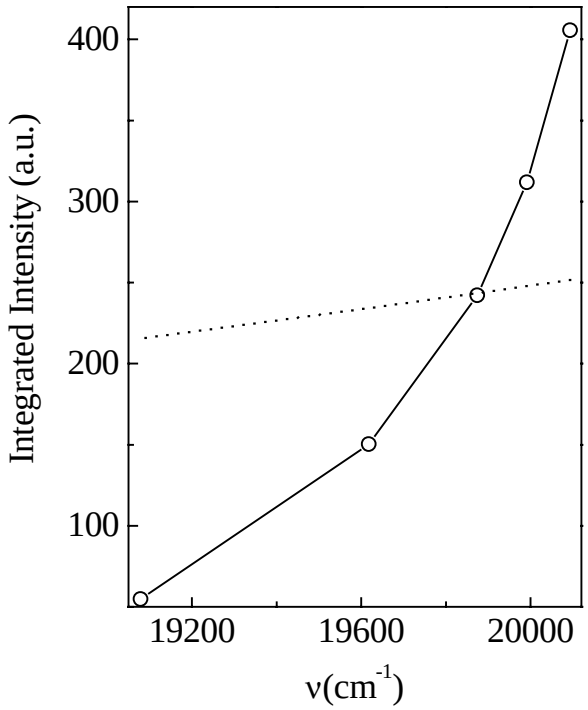

Figure 4.7. Integrated fluorescence intensity of auramine dissolved in ethanol at room temperature as a function of the first moment of the emission spectrum. Open circles represent the experimental data and the dotted line is the best fit of the data points to a function of the form, $f(\nu) = \alpha\nu^3$.

Alternatively, a decrease in k_e^{rad}, as the phenyl group twisting takes place, may be considered as a possible explanation for the initial ps fluorescence decay. In the next section we consider a three-state model, in which the three states refer to the electronic ground state and two electronically excited states, the upper of which is emissive, the lower being non-emissive. Adiabatic coupling between the two excited states is assumed. Due to the two-state coupling, the radiative decay constant and the lifetime of the resulting lower excited state become dependent on the phenyl-bond twisting angle. The dynamics of a barrierless decay along the lower excited-state potential is considered starting from a Smoluchowski equation. The simulations yield the temporal dependence of the auramine fluorescence. The results are in reasonable agreement with the experimental data.

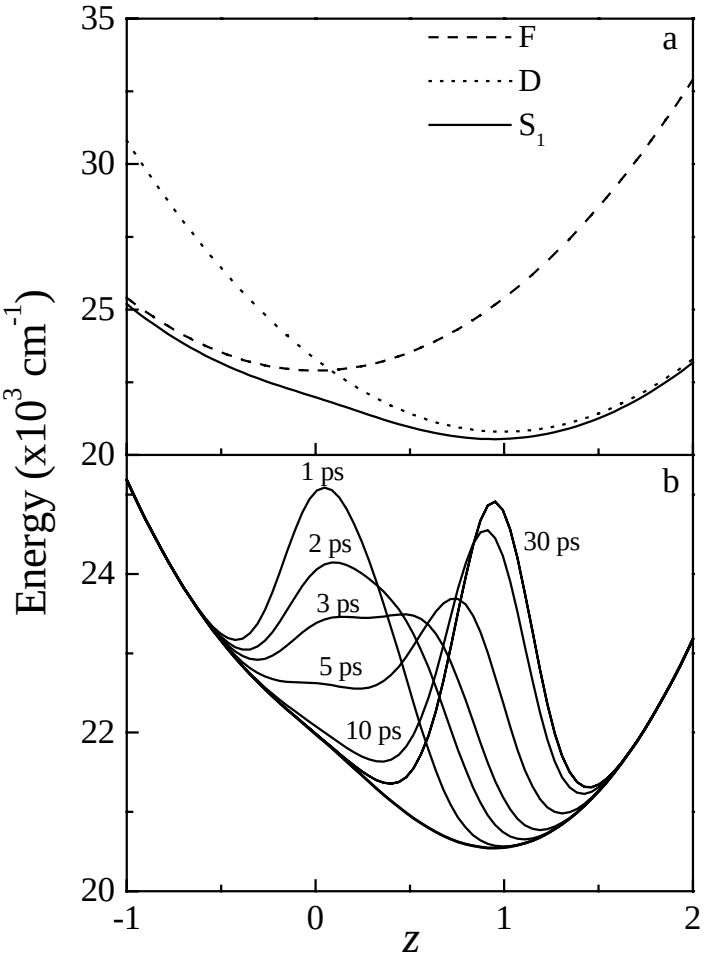

Figure 4.8. (a) Potential energies of mixed excited state (S_1) and the zero order emissive excited (*F*) and non-emissive excited (*D*) states. (b) Simulated time dependence of the population distribution in the excited S_1 state at room temperature.

4.4.2 Adiabatic coupling model

Figure 4.8a shows a sketch of the functional dependence on some relative twisting coordinate, *z*, for the energies of the three-state system we are considering. The relative twisting coordinate, *z*, is defined in terms of the time-dependent twisting angle, $\varphi(t)$, as,

$$z = \frac{\varphi(t) - \varphi(0)}{\varphi(\infty) - \varphi(0)} \qquad (4.1)$$

The energies of the ground state (*G*) and the fluorescent state (*F*) and the dark state (*D*) as a function of the twisting coordinate *z* are, in zero order, taken as,

$$G(z) = \frac{1}{2} kz^2 \qquad (4.2)$$

$$F(z) = F_{eq} + \frac{1}{2} kz^2 \qquad (4.3)$$

$$D(z) = D_{eq} + \frac{1}{2} k(1-z)^2 \qquad (4.4)$$

The parameter k is the rotation force constant and has the dimension of energy. For simplicity the harmonicity in ground and excited states is taken to be the same. F_{eq} and D_{eq} correspond to the zero-order minimum energies of the fluorescent and dark state, respectively. The zero order energies for $F(z)$ and $D(z)$ are sketched in Figure 4.8a as dashed and dotted curves, respectively. We now consider an adiabatic coupling of the two excited states, so that the energy of the lowest of the two mixed states becomes,

$$S_1(z) = \frac{1}{2}(F(z) + D(z)) - \frac{1}{2}\sqrt{(F(z) - D(z))^2 + 4C^2}, \qquad (4.5)$$

where C is the coupling strength parameter. The energy of the resulting excited state, S_1, is given as a solid curve in Figure 4.8a. Since the S_1 state is a z-dependent mixture of fluorescent and non-fluorescent zero order states, the transition moment for the optical transition to the ground state is also z-dependent. Normalizing the optical transition moment for $F(z)$ to a value of 1 and that for $D(z)$ to a value of 0, one readily obtains for the transition moment, $M(z)$, for the optical $G \leftarrow S_1$ transition,

$$M(z) = \cos^2\left(\frac{1}{2}\arctan\left(\frac{2C}{F(z) - D(z)}\right)\right) \qquad (4.6)$$

The variation of $M(z)$ with z is plotted in Figure 4.9.

Prior to the photoexcitation of the auramine molecule, the system is in the electronic ground state in thermal equilibrium with the bath of solvent molecules. Immediately after the assumed impulsive excitation to the excited state S_1, the population distribution will no longer be in equilibrium with the bath. Excitation is at least 2100 cm^{-1} above the 0-0 transition and the effects of fast vibrational relaxation within the pulse duration time have to be considered also. The simulations appear to give relatively poor fittings with the experimental data when the initial population distribution in the excited S_1 state, $\rho(z, 0)$, is Gaussian.

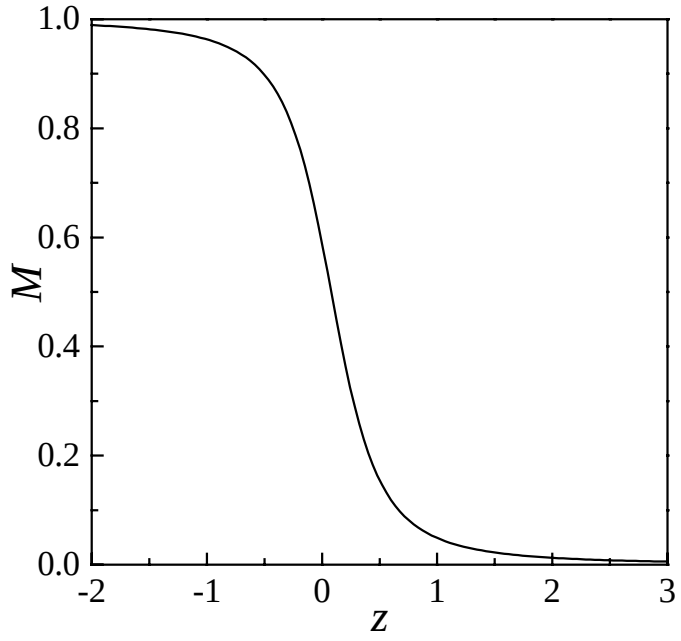

Figure 4.9. Moment for radiative transition as a function of the normalized twisting coordinate, *z*.

Good agreement (see later) is obtained assuming that the initial population distribution is no longer a symmetric function of *z*. We take a distribution according to an asymmetric log-normal shape function, represented as,

$$\rho(z,0) = \begin{cases} \exp\left(-\ln(2)\left(\dfrac{\ln(1+2bz/\left(2\sqrt{k_B T/k}\right)}{b}\right)^2\right) \\ \qquad if \quad 2bz/\left(2\sqrt{k_B T/k}\right) > -1 \\ \qquad else \quad 0 \end{cases} , \tag{4.7}$$

k_B is the Boltzmann constant, T is temperature and b is the asymmetry factor. We consider that the time evolution of $\rho(z, 0)$ follows the Smoluchowski equation [7],

$$\frac{\partial \rho(z,t)}{\partial t} = D_r \frac{\partial^2 \rho(z,t)}{\partial z^2} + \frac{D_r}{k_B T}\frac{\partial}{\partial z}\left\{\frac{\partial}{\partial z} S_1(z)\rho(z,t)\right\} , \tag{4.8}$$

with D_r being the diffusion coefficient characteristic of the rotation diffusion motions of the auramine phenyl groups. The first term on the right hand side is the diffusion term that gives rise to a spreading of the population distribution function in the excited state. The second term on the r.h.s. of Eq. (4.8) represents the density flow as determined by the frictional parameter $D_r/(k_BT)$. Finally, the temporal dependence of $\rho(z, t)$, as calculated from Eq. (4.8), gives rise to a time-dependent fluorescence spectrum for which the intensity as a function of the emission frequency, ν, and time, t, is proportional to [9,11],

$$I_{fl}(\nu,t) \propto \int dz \; g\left(\nu_0(z), \nu-\nu_0(z)\right)\left|M(z)\right|^2 \rho(z,t)\nu^3 \qquad (4.9)$$

In this expression, $g(\nu_0(z),\nu\text{-}\nu_0(z))$ is a line shape function characteristic of the Franck-Condon factor, and $\nu_0(z)$ is the torsional-angle-dependent energy gap between the excited state and the ground state. Eq. (4.9) reflects that the simulated spectrum results from the convolution of the inhomogeneously broadened emission band with the homogeneous line shape of the emission. Here, inhomogeneous broadening is due to the dispersion of the population density distribution $\rho(z, t)$ with z and homogeneous broadening is due to the Franck-Condon factor.

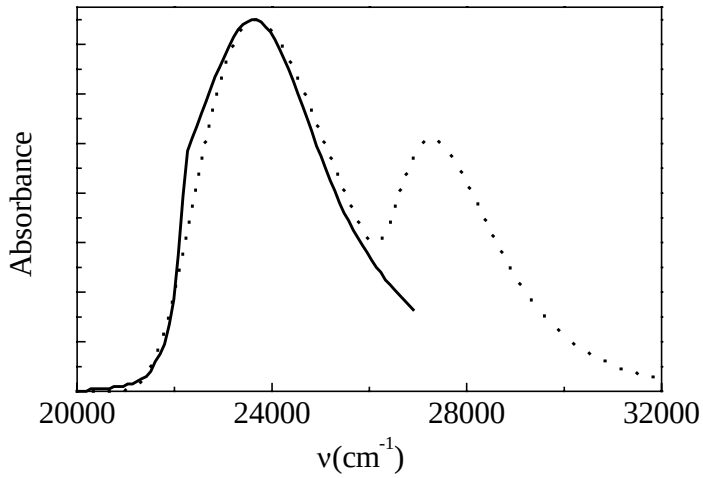

Figure 4.10. Simulated (solid line) and measured (dotted line) absorption spectrum of auramine in ethanol at room temperature.

In the numerical calculations of the emission spectra according to Eq. (4.9), some of the parameters were determined from the experimental steady-state absorption

and emission spectra. The energy for the 0 – 0 transition to the excited state S_1 is then found as 21,700 cm^{-1}. The best-fit calculation for the broad absorption band was obtained for k equal to 3,500 cm^{-1} and a width (FWHM) of the Lorentzian shaped function, $g(\nu_0(z),\nu\text{-}\nu_0(z))$, of 3,500 cm^{-1}. The auramine absorption spectrum, at room temperature, simulated with these parameter values, is given in Figure 4.10 (solid curve). The values for the remaining parameters, $F_{eq,}$ D_{eq}, C, and D_r, were obtained from the best-fit results for the time-resolved emission data. Optimized simulation results were obtained for the following values: F_{eq} = 22,600 cm^{-1}, C = 800 cm^{-1}, D_{eq} = 21,700 cm^{-1}, and b = 0.6, whereas, at a temperature of 273 K, the best-fit value for D_r was found to be 0.045 ps^{-1}. With these parameter values, we have simulated the fluorescence spectrum at various times assuming impulsive photoexcitation of the auramine solute. The Smoluchowski differential equation was numerically solved using the Runge-Kutta method [55].

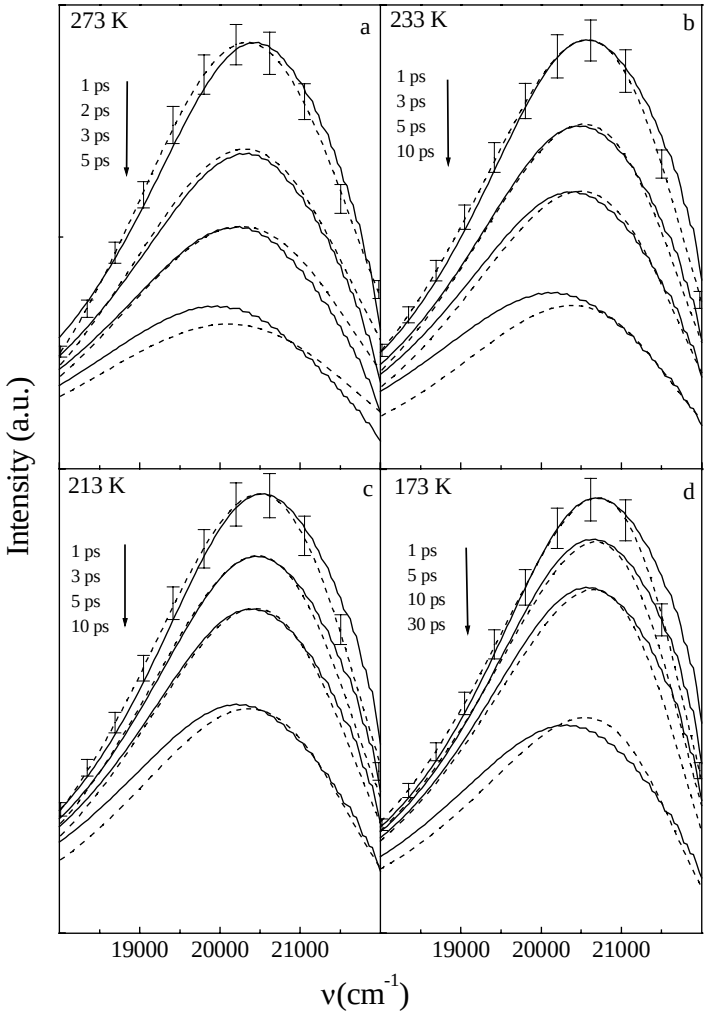

Figure 4.11. Solid lines: simulated time-resolved emission spectra at 273 K (a), 233 K (b), 213 K (c) and 173 K (d). Dotted lines: log-normal shaped time-resolved emission spectra obtained after spectral reconstruction from the fluorescence transients.

Figure 4.11a shows the results of the simulated fluorescence spectra for auramine at 273 K. For comparison we have included the experimental spectra of Figure 4.3a. The development with time of the population distribution in the excited state corresponding to the simulated fluorescence spectra of Figure 4.11a is shown in Figure 4.8b. It is noted that on account of the (quasi-) barrierless shape of the excited-state potential, the population dynamics, and thus the dynamic Stokes shift, is on the (sub)picosecond time scale, in agreement with the experimental results.

The time-resolved emission spectra at lower temperatures were simulated keeping the values for all of the parameters used in the simulations of the room temperature results the same, with the exception of the values for D_r and $D_r/(k_B T)$. The latter two parameters were varied to obtain the best fit with the temporal fluorescence behavior as reconstructed from the experimental transients. The results obtained in this way at T = 233 K, 213 K, and 173 K are given in Figures 4.11b-d. As illustrated by these figures, at these temperatures, the time dependence of the emission spectrum can be simulated reasonably well until the fluorescence intensity maximum has decayed to about 20 % of its initial value. At later times, additional factors like lifetime decay (which during the initial few picoseconds could be disregarded) and changes in Franck-Condon factor, when emission shifts to the red, might become important. However, in view of the approximations of the simulations (twisting represented by just one generalized reaction coordinate, relaxation along adiabatic potential of mixed state, validity of diffusion approximation, no change of Franck-Condon factor during relaxation, no loss of excited-state population), the simulated spectra show reasonable agreement with the spectra reconstructed from the experimental data. We conclude that the excited-state adiabatic coupling model provides a satisfactory simple framework to account for the observed dynamic Stokes shift, the strong drop in the fluorescence intensity within a few picoseconds and the existence of a longer-lived excited state with a lifetime of about 30 ps or longer.

The applied fitting procedure provides us with best-fit values for the diffusion coefficient parameter, D_r, as a function of temperature. In Figure 4.12 we plot these best-fit values for D_r as a function of T/η, where the values for η were taken from Ref. 56. The plot displayed in Figure 4.12 illustrates that the diffusion coefficient parameter, D_r, extracted from the simulations, shows an almost linear T/η dependence. This indicates that the Einstein-Stokes relation for a sphere, subject to a rotational diffusion

motion, $D_r = k_B T/\zeta$, where ζ is the total friction coefficient, is found to hold here on a molecular level. If we take into account the twisting of both phenyl groups, then $\zeta = 2\zeta_r$ and $\zeta_r = 6V\eta$, where V is the volume of the diffusing sphere [57]. From the slope of the best-fit linear dependence of D_r on T/η in Figure 4.12, the friction coefficient, ζ, and thus also V, can be determined. The radius of the twisting sphere is then estimated as 1.0 Å which should be compared with the effective radius of 1.2 Å of each of the auramine phenyl groups. This result further validates that torsional motions of the auramine phenyl groups determine the excited-state dynamics of auramine.

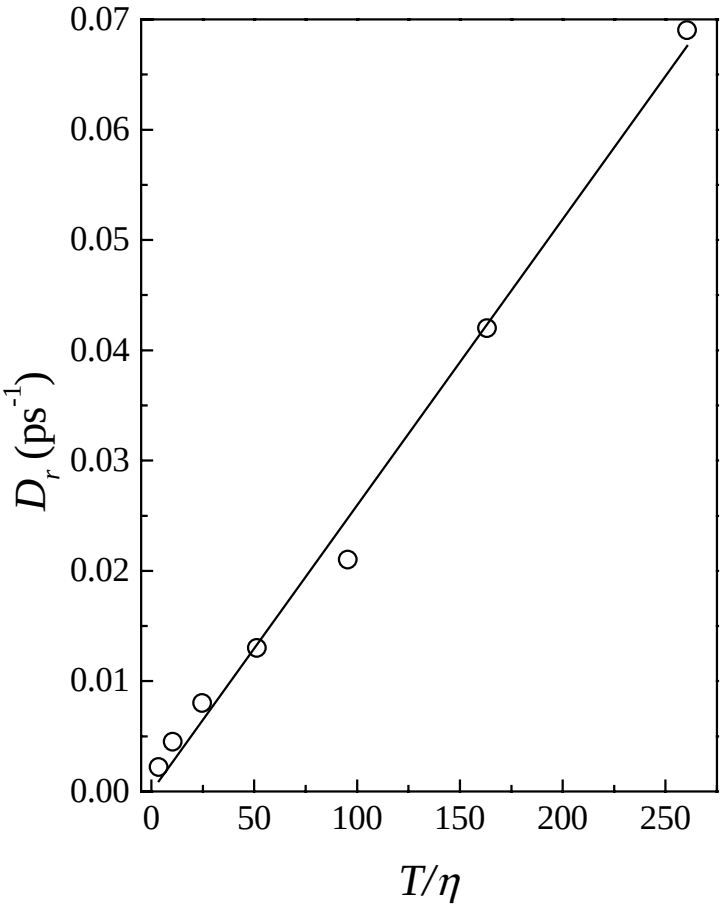

Figure 4.12. Diffusion coefficient (D_r), as numerically evaluated from the simulations, as a function of T/η. The solid line represents the best linear fit.

As mentioned in Sec. 4.3, the fluorescence transients, for auramine in the ethanol glass (T < 170 K), display a 55 ps rise component when detection is in the red part of the emission. Such a rise is typical of a dynamic Stokes shift. Note that for

auramine in liquid solution the fluorescence transients showed an *instantaneous* rise at all detection wavelengths; a 'slow' rise in the red emission region, as in the glass, was not observed. Yet, in liquid solution a dynamic Stokes shift could be inferred, but this was possible only after spectral reconstruction. For auramine in the glass environment, however, a dynamic Stokes shift can immediately be concluded from the ps decay in the blue and a concomitant ps rise component in the red regions of the emission. The difference with the liquid solution results may reflect that the initial excitation population distribution for auramine in a glass, as a function of *z*, is not broad but relatively narrow and therefore the red part of the emission is not observed instantaneously upon short-pulse excitation. Furthermore, as rotational diffusion takes place in the highly 'viscous' glass, the trajectory traversed by *z* is not as long and therefore the quenching of the fluorescence intensity is less pronounced. Consequently, the dynamic Stokes shift is not accompanied by a drastic drop in fluorescence intensity. Thus, for auramine in a glass, the characteristics normally observed for a dynamic Stokes shift [10,53,58], are observed. A relatively narrow initial population distribution in the excited state, immediately after impulsive excitation from the ground state, is indicative that *k* (cf Eqs. (4.1) to (4.3)) for auramine in the glass attains larger values than in liquid solution. A larger *k* value illustrates that 'caging' in the glass is more pronounced than in liquid solution. On the other hand, the size of the cavity available for the auramine molecules in the glass is still large enough for the molecule to be still flexible and to undergo twisting motions in its excited state.

In summary, the measurements of the temporal behavior of the fluorescence, in the temperature range from 293 K to 173 K, show that the initial picosecond decay kinetics slows down appreciably. The time dependence of the reconstructed fluorescence spectra could be simulated on the basis of a model that assumes the adiabatic coupling of two excited states, the locally excited emissive state, *F*, and the lower lying non-emissive state, *D*. It has been discussed that good agreement with the experimental data can be obtained starting from a barrierless potential shape, as a function of the twisting angle of the phenyl groups, and adopting the validity of the application of the Smoluchowski equation.

References

[1] B. Bagchi, R. Biswas, Adv. Chem. Phys. **109**, 207 (1999).

[2] A.H. Zewail, J. Phys. Chem. 100, 12701 (1996); A.H. Zewail (ed.), *Femtochemistry: Ultrafast Dynamics of the Chemical Bond*. World Scientific, Singapore, 1994.

[3] P.F. Barbara, W. Jarzeba, Adv. Photochem. **15**, 1 (1990).

[4] G.R. Fleming, *Chemical Applications of Ultrafast Spectroscopy*, Oxford University Press, Oxford, 1986.

[5] R. Jimenez, G.R. Fleming, P.V. Kumar, M. Maroncelli, Nature **369**, 471 (1994).

[6] U. Åberg, E. Åkesson, J.-L. Alvarez, I. Fedchenia, V. Sundström, Chem. Phys. **183**, 269 (1994).

[7] B. Bagchi, G.R. Fleming, D.W. Oxtoby, J. Chem. Phys. **78**, 7375 (1983); B. Bagchi, G.R. Fleming, Phys. Chem. **94**, 9 (1990).

[8] M. Du, G.R. Fleming, Biophys. Chem. **48**, 1010 (1993).

[9] K. Tominaga, G.C. Walker, W. Jarzeba, P.F. Barbara, J. Phys. Chem. **95**, 10475 (1991); K. Tominaga, G.C. Walker, T.J. Kang, P.F. Barbara, T. Fonseca, J. Phys. Chem. **95**, 10485 (1991).

[10] P. van der Meulen, H. Zhang, A.M. Jonkman, M. Glasbeek, J. Phys. Chem. **100**, 5367 (1994).

[11] P. van der Meulen, A.M. Jonkman, M. Glasbeek, J. Phys. Chem A. **102**, 1906 (1998).

[12] V. Sundström, T. Gillbro, H. Bergstrom, Chem. Phys. **73**, 439 (1982).

[13] D.A. Cremers, M.W. Windsor, Chem. Phys. Lett. **71**, 27 (1980).

[14] M.D. Hirsch, H. Mahr, Chem. Phys. Lett. **60**, 299 (1979).

[15] M. Canva, G. Lesaux, P. Georges, F. Chaput, JP. Boilot, Chem. Phys. Lett. **176**, 495 (1991).

[16] W. Yu, F. Pellegrino, M. Grant, R.R. Alfano, J. Chem. Phys. **67**, 1766 (1977).

[17] J.M. Grzbowski, S.E. Sugamori, D.F. Williams, R.W. Yip, Chem. Phys. Lett. **65**, 456 (1979).

[18] W. Rettig, Appl. Phys. B **45**, 145 (1988).

[19] E.P. Ippen, C.V. Shank, A. Bergman, Chem. Phys. Lett. **46**, 588 (1977).

[20] G.E. Bush, P.M. Rentzepis, Science **194**, 276 (1976).

[21] D. Magde, M.W. Windsor, Chem. Phys. Lett. **24**, 144 (1974).

[22] A. Migus, A. Antonetti, J. Etchepare, D. Hulin, A. Orszag, J. Opt. Soc. Am. B **2**, 584 (1985).

[23] M. Jurczok, P. Plaza, M.M. Martin, W. Rettig, J. Phys. Chem. A **103**, 3372 (1999).

[24] M. Ishikawa, J.Y. Ye, Y. Maruyama, H. Nakatsuka, J. Phys. Chem. A **103**, 4319 (1999).

[25] Y. Maruyama, M. Ishikawa, H. Satonozo, J. Am. Chem. Soc. **118**, 6257 (1996).

[26] F. W. Wise, M. J. Rosker, C. Tang, J. Chem. Phys. **86**, 2827 (1987).

[27] D. Ben-Amotz, C.B. Harris, J. Chem. Phys. **86**, 4856 (1987); ibid **86**, 5433 (1987).

[28] D. Ben-Amotz, R. Jeanloz, C.B. Harris, J. Chem. Phys. **86**, 6119 (1987).

[29] M.M. Martin, E. Bréhéret, F. Nesa, Y.H. Meyer, Chem. Phys. **130**, 279 (1989).

[30] M.M. Martin, P. Plaza, Y. H. Meyer, J. Phys. Chem. **95**, 9310 (1991).

[31] M.M. Martin, P. Plaza, P.Changenet, Y.H. Meyer, J. Photochem. Photobiol. A **105**, 197 (1997).

[32] P. Plaza, N. Dai Hung, M. M. Martin, Y. H. Meyer, M. Vogel, W. Rettig, Chem. Phys. **168**, 365 (1992).

[33] M. Ishikawa, Y. Maruyama, Chem. Phys. Lett. **219**, 416 (1994).

[34] R. Menzel, C.W. Hoganson, M.W. Windsor, Chem. Phys. Lett. **120**, 29 (1985).

[35] A. Mokhtari, L. Fini, J. Chesnoy, J. Chem. Phys. **87**, 3429 (1987).

[36] V. Sundström, T. Gillbro, J. Chem. Phys. 81, 3463 (1984).

[37] D.F. Duxbury, Chem. Rev. **93**, 381 (1993).

[38] M. Vogel, W. Rettig, Ber. Bunsenges. Phys. Chem. **91**, 1241 (1987); ibid **89**, 962 (1985).

[39] J.Y. Ye, T. Hattori, H. Inouye, H. Ueta, H. Nakatsuka, Y. Maruyama, M. Ishikawa, Phys. Rev. B **53**, 8349 (1996).

[40] K.M. Abedin, J.Y. Ye, H. Inouye, T. Hattori, H. Sumi, H. Nakatsuka, J. Chem. Phys. **103**, 6414 (1995).

[41] G. Oster, Y. Nishijima, J. Am. Chem. Soc. **78**, 1581 (1956).

[42] R.H. Conrad, J.R. Heitz, L. Brand, Biochemistry **9**, 1540 (1970).

[43] R.F. Steiner, S. Albaugh, E. Nenortas, L. Norris, Biopolymers **32**, 73 (1992).

[44] S.K. Chatterjee, N. Misra, J. Macromol. Sci. Pure Appl Chem. A **36**, 85 (1999).

[45] Z.A. Dreger, G. Yang, J.O. White, Y. Li, H.G. Drickamer, J. Phys. Chem. A **101**, 9511 (1997).

[46] Y.L. Zhang, R.A. Agbaria, I.M. Warner, Supramol. Chem. **8**, 309 (1997).

[47] S. Miyagishi, H. Kurimoto, T. Asakawa, Langmuir **11**, 2951 (1995).

[48] S. Miyagishi, H. Kurimoto, Y. Ishihara, T. Asakawa, Bull. Chem. Soc. Jpn. **67**, 2398 (1994).

[49] R. Hasegawa, T. Sugimura, Y. Suzaki, Y. Shindo, A. Kitahara, J. Phys. Chem. **98**, 2120 (1994).

[50] T. Förster, G.J. Hoffmann, Z. Phys. Chem. **75**, 63 (1971).

[51] P. Gautam, A. Harriman, J. Chem. Soc. Faraday Trans. **90**, 697 (1994).

[52] P. Changenet, H. Zhang, M.J. van der Meer, M. Glasbeek, P. Plaza, M.M. Martin, J. Phys. Chem. A **102**, 6716 (1998).

[53] H. Zhang, A.M. Jonkman, P. van der Meulen, M. Glasbeek, Chem. Phys. Lett. **224**, 551 (1994).

[54] E.R. Middelhoek, P. van der Meulen, J.W. Verhoeven, M. Glasbeek, Chem. Phys. **198**, 373 (1995).

[55] G. B. Arfken and H. J. Weber, Mathematical methods for physicists, 4th Ed. p.530, Academic Press, San Diego, 1995.

[56] R.C. Weast, M.J. Astle, W.H. Beyer (Eds.), Handbook of Chemistry and Physics, 64th edn., CRC press, New York, 1984, F-40.

[57] A. Einstein, Ann. Phys. **19**, 371 (1906).

[58] M.L. Horng, J.A. Gardecki, A. Papazyan, M. Maroncelli, J. Phys. Chem. **99**, 17311 (1995).

Chapter 5

Femto- and picosecond fluorescence studies of solvation and non-radiative deactivation of ionic styryl dyes in liquid solution*

Abstract

A comparative study of the solvation and non-radiative relaxation dynamics of bridged and unbridged ionic styryl dye compounds is reported. Femto- and picosecond fluorescence transient measurements reveal solvation dynamics on a picosecond time scale of the solutes in ethanol, benzonitrile and decanol. Bridging is found to strongly affect the lifetime of the emissive state. It is shown that the presence of unbridged styryl-group single bonds allows for an effective nonradiative decay process. This decay process is suppressed by double chemical bridging.

* The contents of this chapter has been published as an article, M.J. van der Meer, H. Zhang, W. Rettig, M. Glasbeek, Chem. Phys. Lett. **320**, 673-680 (2000).

5.1 Introduction

Studies of luminescent ionic styryl dyes have received widespread interest [1]. In particular, ionic styryl dyes have been studied in a variety of contexts. In part, the interest stems from the application of these dye molecules as spectral sensitizer [2], laser dye [3], fluorescent probe [4] or biosensor [5]. The emissive state of ionic styryl dyes (e.g., compounds **1** to **4** of Figure 5.1) is characterized by a charge shift from the styryl group to the pyridinium acceptor. This charge shift is (in a multipole expansion) accompanied by a change of the dipole moment of the ionic dye system and this, consequently, provides for the driving force for polar solvent molecules to reorient to new configurations around the solute molecules. In polar solvents, typical Stokes shifts, corresponding to the solvation of the ionic styryl dyes, of about 5,000 cm^{-1} have been measured [6,7]. Following pulsed optical excitation, however, for the system to reach the new equilibrium in the excited state (corresponding to the free energy minimum after complete solvation), the reorientational motions of the solvent molecules should be fast compared to the solute excited-state lifetime. Incomplete 'partial' solvation at low temperatures was concluded recently for styryl dyes **1** to **4** from cw emission experiments [8,9]. Upon lowering the temperature, from 200 K to 100 K, an appreciable decrease (to about 2,000 cm^{-1}) of the Stokes shift of the styryl dye systems dissolved in ethanol was found. Apparently, under low temperature conditions, the typical solvent rotational diffusion times slowed down to the extent that complete solvation no longer can be reached, and the cw emission is blue-shifted. Obviously, time-resolved studies of the solvation process might yield further information on the dynamic solute-solvent interactions [10]. Such solvation dynamics studies have in recent years been extensively performed using various methods, e.g., pump-probe and fluorescence upconversion spectroscopy [8,10-12]. Following pulsed laser excitation, the solvent molecules cannot adiabatically follow the changes induced in the electronic charge distribution of the solute. Due to this inertia, the time scale of the reorientational motions may vary from about 50 fs up to several hundred picoseconds. In this paper, we present results of femtosecond and picosecond fluorescence experiments of ionic styryl dyes in polar solution, at room temperature. The results show that the solvation dynamics [13-16] for the ionic styryl dye compounds actually can be probed by the measurement of dynamic Stokes shifts. The

data thus provide information about the solvation kinetics of the styryl dye systems in the excited state in polar solvents.

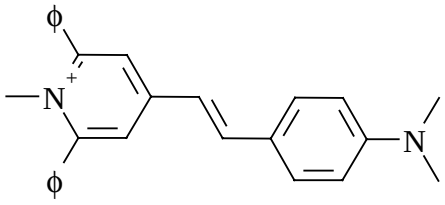

1 = *p*-DPD

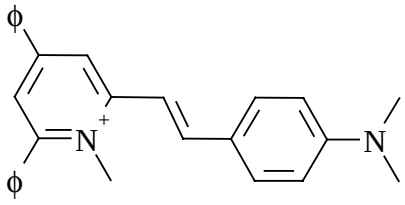

2 = *o*-DPD

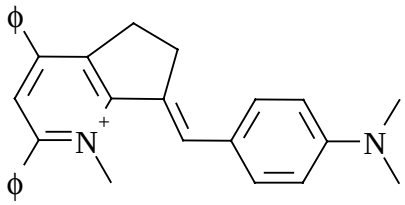

3 = *o*-DPD-b1

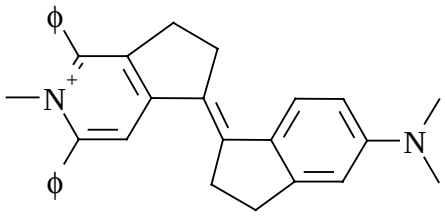

4 = *p*-DPD-b13

Figure 5.1. Schematic picture of structure of the ionic styryl dyes *p*-DPD (**1**), *o*-DPD (**2**), *o*-DPD-b1 (**3**) and *p*-DPD-b13 (**4**).

Another interesting recent observation for the DPD compounds (unbridged and bridged diphenyl derivatives of 1- or 4-(4'-dimethylaminostyryl)pyridinium dyes) concerns the temperature dependence of their relative nonradiative decay rate constants as concluded from fluorescence quantum yield and subnanosecond lifetime measurements [9]. For three members of the DPD family containing either one or two single bonds neighboring the styryl double bond, the relative nonradiative decay rates were determined at 298 K as 1, 1.3, and 0.8. For the double-bridged compound **4**, by contrast, a value of 0.1 is obtained. These results indicate that two-fold bridging of the single bonds might lead to a blocking of a rapid nonradiative decay mediated by single-bonded flexible groups. The presence of single-bonded flexible groups could lead to increased coupling of the excited state to the dense manifold vibrational levels of the ground state thus facilitating effective radiationless decay ('loose bolt theory' [17]). On the other hand, recently also examples of 'inverse loose bolt behavior' have been discussed for related cyanine dye systems [9,18]. In this work, we also report on lifetime measurements for the various DPD compounds in polar solution. The results

allow us to further substantiate the significance of the styryl single bonds in the nonradiative decay of the fluorescent excited state.

5.2 Experimental

The DPD compounds **1** to **4** (cf Figure 5.1) were synthesized as described elsewhere [19]. The solvents used were UV spectroscopy grade ethanol (Merck, μ = 1.7 D, η = 1.2 cP (20°C)), 99% GC-grade 1-decanol (Aldrich, μ = 1.7 D , η = 14.3 cP (20°C)) and 99.9% HPLC-grade benzonitrile (Aldrich, μ = 4.0 D, η = 1.24 cP (25°C)). Sample concentrations were about 10^{-3} M in the fluorescence upconversion experiments and about 10^{-4} M in the picosecond time-correlated single-photon counting measurements. All measurements were performed at room temperature.

The femtosecond fluorescence upconversion setup used for the measurements of the fluorescence transients in time windows from 12 ps up to 132 ps was described previously [11]. Briefly, a Spectra-Physics Millennia X diode laser pumped the Tsunami Ti:sapphire laser that delivered pulses with a typical width of ~50 fs and a wavelength of 840 nm (repetition rate is 82 MHz). Frequency doubling was achieved using a 1 mm thick BBO crystal. The pulses were split in pump and gating pulses by means of a dichroic beamsplitter. The pump pulses (λ = 420 nm, 1 nJ/pulse) excited the solution, contained in a 1 mm quartz cell. The latter was moved back and forth perpendicular to the excitation direction to prevent heating of the sample. The induced fluorescence was focused on a 1 mm thick BBO crystal (type I phase-matching conditions), together with the gating pulses. The latter were optically delayed with respect to the fluorescence beam by means of a translational stage. The upconverted signal was filtered by an UG11 filter (band pass 260-380 nm), focused on the entrance slit of a monochromator (spectral resolution < 5 nm) and detected by means of a photomultiplier (EMI 9863 QB/350) connected to a photon counting system. The up-conversion signal was accumulated for 1 s for each delay step of the translational stage. Fluorescence decays were measured using step sizes of 26.4, 66.6 or 264 fs. The instrumental response function, as determined from the cross correlation of the excitation and gating pulses, was estimated to be ~150 fs (FWHM).

The picosecond fluorescence transients in all samples were measured with a calibrated fluorescence setup outfitted with a time-correlated single-photon-counting

(SPC) detection system [20]. A mode-locked Ar^+-ion laser synchronously pumped a picosecond dye laser. The pulses from the dye laser were frequency doubled to a wavelength of 320 nm and used to photoexcite the sample. By measurement of the Raman scattered light from a water sample, the instrumental response was determined to be 16 ps (FWHM). Steady-state emission spectra were obtained by measurement of the time-integrated spectra with the same setup.

All measurements, with both set-ups, were performed under magic angle conditions.

5.3 Results

5.3.1 Steady-state emission spectra

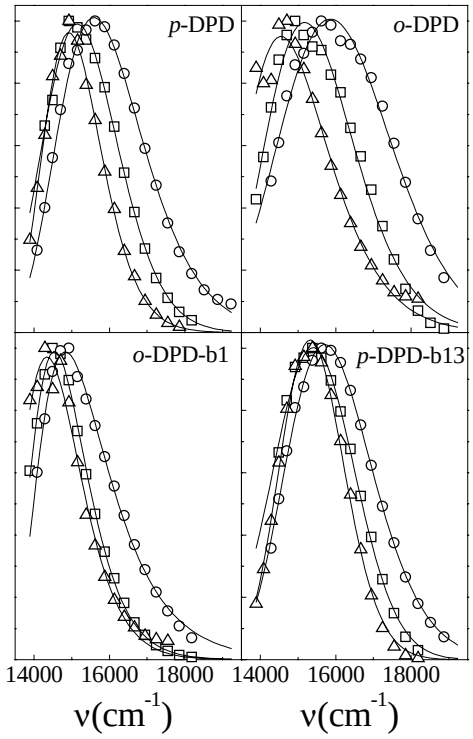

Figure 5.2. Steady-state emission spectra of the styryl dyes **1** to **4** dissolved in ethanol (□), decanol (O), and benzonitrile (Δ). Solid lines are best fits to log-normal line shape functions.

Figure 5.2 presents the steady-state emission spectra of the DPD compounds **1** to **4,** dissolved in ethanol, decanol and benzonitrile. The spectra are the same as reported previously [9]. For all compounds a similar broad band emission (maximum near 660 nm, FWHM about 2,500 cm^{-1}) is observed. In the highly polar solvent benzonitrile, the DPD-cation emissions are red-shifted compared to the emissions from the ethanol and decanol solutions, as expected for emission from a charge transfer state.

5.3.2 Femto- and picosecond fluorescence transients

Typical examples of *p*-DPD fluorescence transients measured by means of fluorescence upconversion and SPC detection are presented in Figure 5.3.

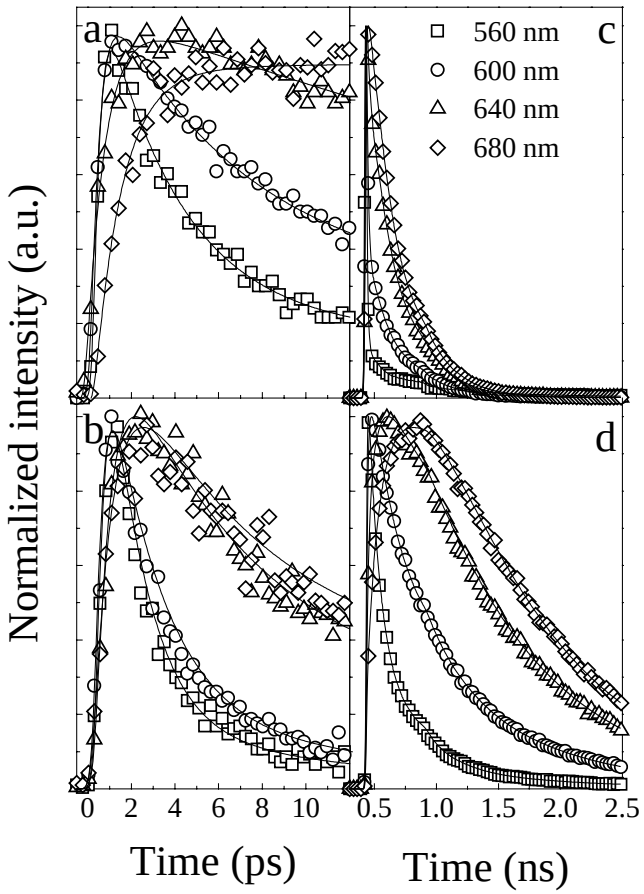

Figure 5.3. Fluorescence upconversion transients (time window: 12 ps) of *p*-DPD dissolved in ethanol (a) and benzonitrile (b). Fluorescence transients (time window: 2.5 ns) of *p*-DPD dissolved in benzonitrile (c) and decanol (d). Detection wavelengths are as indicated. Solid lines are best fits to a multi-exponential function.

The figure shows upconversion transients for a time window of 12 ps at a few detection wavelengths, for *p*-DPD in ethanol (Figure 5.3a) and benzonitrile (Figure 5.3b). As is evident from the figure, when detection is in the blue part of the emission band (λ < 610 nm), the fluorescence shows an instantaneous rise (within 100 fs), followed by a decay component on the picosecond time scale. At higher detection wavelengths (λ > 620 nm), the transients show picosecond rise components with time constants similar to those for the decay components measured at the blue emission side. Similar results were obtained for the *p*-DPD dissolved in decanol.

Table 5.1

Best fit values of the time constants and, in brackets, their relative pre-exponential factors of the multi-exponential fit functions of the femto- and picosecond fluorescence transients of *p*-DPD in ethanol, benzonitrile and decanol at room temperature

	λ_{fl} (nm)	τ_1 (ps)		τ_2 (ps)		τ_3 (ps)	
Ethanol	560	2.0	(0.6)	11	(0.4)		
	590	4.2	(0.7)	80	(0.3)		
	610	7.5	(0.5)	80	(0.5)		
	620	0.5	(-1)*	80	(1)		
	650	0.8	(-1)*	80	(1)		
	690	1.8	(-1)*	80	(1)		
Benzonitrile	560			1.7	(0.9)	210	(0.1)
	600			2.5	(0.9)	210	(0.1)
	620			6.3	(0.6)	210	(0.4)
	640	0.7	(-0.9)*	6.2	(0.8)	210	(0.2)
	680	0.9	(-0.9)*	6.1	(0.7)	210	(0.3)
	700	1.1	(-1)*	7.5	(0.5)	210	(0.5)
Decanol	530	34.9	(0.7)	149	(0.3)		
	560	57.8	(0.5)	215	(0.4)	900	(0.1)
	590	180.0	(0.5)	441	(0.4)	900	(0.1)
	620	30.9	(-0.4)*	548	(0.7)	900	(0.3)
	650	52.7	(-0.3)*	223	(-0.3)*	900	(1)
	680	74.1	(-0.2)*	302	(-0.6)*	900	(1)

*refers to rise components; positive pre-exponential factors refer to decay, their sum being normalized to 1.

The time span was expanded in the SPC measurements. As seen from Figure 5.3c, for *p*-DPD in benzonitrile, the picosecond rise components when $\lambda > 620$ nm are missing due to the limited instrumental time response (~16 ps) and only the decay components remain. However, for the higher viscous decanol solution, all kinetics becomes slower and the phenomenology of rise and decay components, analogous to the femtosecond upconversion experiments, is now resolved again (Figure 5.3d). Similar results with the same signal-to-noise ratio were obtained for *p*-DPD dissolved in ethanol (not shown).

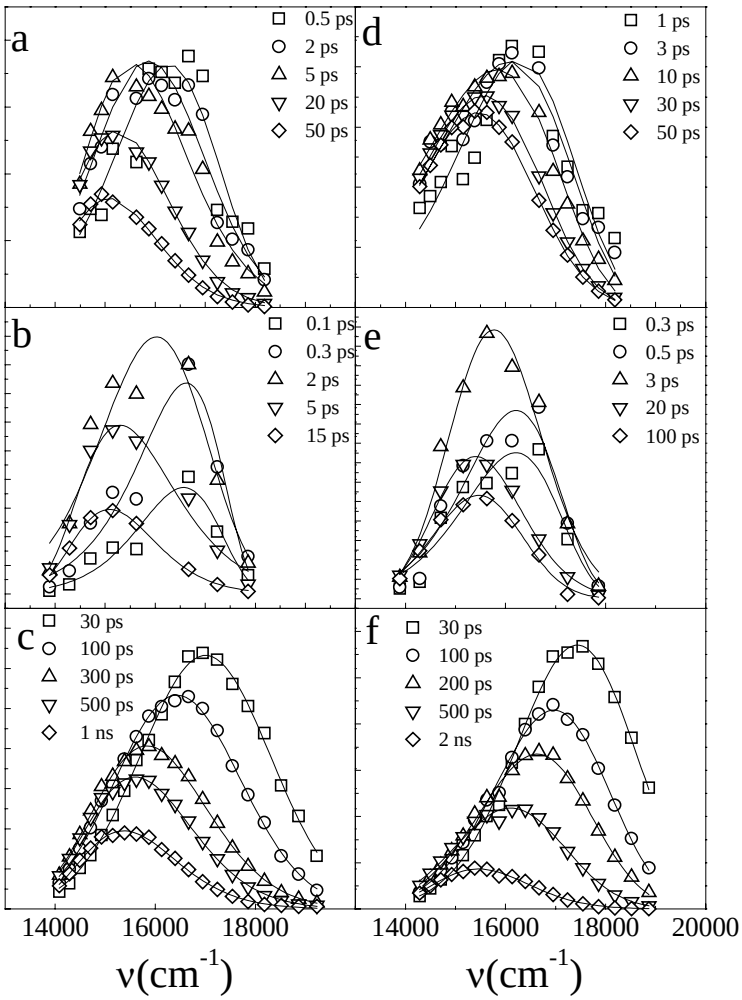

Figure 5.4. Reconstructed time-resolved emission spectra for *p*-DPD in ethanol (a), benzonitrile (b), decanol (c), and for *p*-DPD-b13 in ethanol (d), benzonitrile (e) and decanol (f). Solid lines are best fits of the point-to-point spectra to log-normal line shapes.

The femto- and picosecond transients, as obtained at the detection wavelengths between 530 nm and 700 nm, all could be fitted to a two- or three-exponential function convoluted with the instrumental response function. Table 5.1 comprises the resulting best-fit values of the time constants and relative amplitudes for *p*-DPD in ethanol, benzonitrile and decanol. (The longer characteristic times found for *p*-DPD in ethanol (80 ps) and benzonitrile (210 ps) and all time constants in decanol were determined from the transients measured with the SPC set-up). The solid curves in Figure 5.3 depict the multiexponential best-fits.

Table 5.2

Best fit values of the time constants and, in brackets, their relative pre-exponential factors of the multi-exponential fit functions of the femto- and picosecond fluorescence transients of *o*-DPD in ethanol and decanol at room temperature

	λ_{fl} (nm)	τ_1 (ps)		τ_2 (ps)		τ_3 (ps)	
Ethanol	540	1.1	(0.6)	2.3	(0.3)	8.4	(0.1)
	570	2.6	(0.7)	10.2	(0.2)	40	(0.1)
	590	0.2	(-0.8)*	3.9	(0.7)	40	(0.3)
	620	0.3	(-0.9)*	3.4	(0.7)	40	(0.3)
	650	0.4	(-1.0)*	6.1	(0.6)	40	(0.4)
	680	0.4	(-1.0)*	5.8	(0.6)	40	(0.4)
Decanol	530	23	(0.8)	103	(0.2)		
	570	38	(0.5)	148	(0.5)		
	620	227	(0.7)	400	(0.3)		
	650	28	(-0.4)*	400	(1)		
	680	57	(-0.6)*	400	(1)		
	700	70	(-0.7)*	400	(1)		

*refers to rise components; positive pre-exponential factors refer to decay, their sum being normalized to 1.

The variation of the fluorescence kinetics with the detection wavelength as illustrated by Figure 5.3 is characteristic of a dynamic Stokes shift [10]. This is also manifested after spectral reconstruction of the fluorescence transient data. Following the well-known procedure [21], time-resolved emission spectra represented as point-to-point plots of the fluorescence intensity at a certain delay time after the excitation pulse were obtained. Figure 5.4 shows the results for the time-resolved emission spectra of *p*-DPD in the solvents ethanol (a), benzonitrile (b), and decanol (c). The solid lines

represent the best fits to a log-normal line shape function [21]. The figure clearly demonstrates the resolved dynamic range for the Stokes shift for *p*-DPD in ethanol (~ 1600 cm^{-1} in about 20 ps, cf Figure 5.4a), benzonitrile (~1000 cm^{-1} in less than 10 ps, cf Figure 5.4b), and decanol (~1600 cm^{-1} in more than 500 ps, cf Figure 5.4c). The excited-state population decay to the ground state is much slower than the dynamic Stokes shift. Table 5.5 includes the variation of the lifetime of *p*-DPD in the three solvents.

Analogous results as for compound **1** were obtained for the kinetics of the fluorescence transients measured for **2** (*o*-DPD) and **3** (*o*-DPD-b1). Tables 5.2 and 5.3 summarize the results. After spectral reconstruction, a temporal behavior for the emission spectra of **2** and **3** in the various solvents similar to that of Figure 5.4 was obtained.

Table 5.3

Best fit values of the time constants and, in brackets, their relative pre-exponential factors of the multi-exponential fit functions of the femto- and picosecond fluorescence transients of *o*-DPD-b1 in ethanol and decanol at room temperature

	λ_{fl} (nm)	τ_1 (ps)		τ_2 (ps)		τ_3 (ps)	
Ethanol	550	0.5	(0.7)	2.1	(0.3)		
	570	0.8	(0.7)	4.3	(0.3)		
	590	1.9	(0.8)	13.5	(0.2)		
	610	2.5	(0.7)	65	(0.3)		
	640	2.3	(0.8)	65	(0.2)		
	690	4.1	(0.6)	65	(0.4)		
Decanol	560	20	(0.7)	89	(0.3)		
	590	29	(0.5)	112	(0.4)	500	(0.1)
	620	52	(0.3)	160	(0.5)	500	(0.2)
	650	5	(-0.8)*	180	(0.6)	500	(0.4)
	680	35	(-0.4)*	269	(0.4)	500	(0.6)
	710	58	(-0.6)*			500	(1)

*refers to rise components; positive pre-exponential factors refer to decay, their sum is normalized to 1.

For the double-bridged compound *p*-DPD,b13 (Figure 5.1), experiments similar to those for **1** to **3** were performed. The signal-to-noise ratio for the fluorescence transients are comparable to those of *p*-DPD. Table 5.4 summarizes the results for the time constants characteristic of the *p*-DPD-b13 fluorescence transients, after fitting to a three-exponential function convoluted with the system response function. Also for *p*-DPD-b13 a strong solvent dependence of its fluorescence kinetics was measured. This

is reflected in the temporal dependence of the emission spectrum of *p*-DPD-b13 as reconstructed from the fluorescence transient data. The reconstructed spectra represented as point-to-point plots for *p*-DPD-b13 in ethanol, benzonitrile and decanol are shown in Figure 5.4. The figure includes as solid curves the best-fit log-normal functions. Dynamic Stokes shifts are again apparent, the shifts being much faster for the ethanol and benzonitrile solutions than for the decanol solution. The excited-state lifetimes as determined for *p*-DPD-b13 in the three solvents are included in Table 5.5.

Table 5.4

Best fit values of the time constants and, in brackets, their pre-exponential factors of the multi-exponential fit functions of the femto- and picosecond fluorescence transients of *p*-DPD-b13 ethanol, benzonitrile and decanol at room temperature

	λ (nm)	τ_1 (ps)		τ_2 (ps)		τ_3 (ps)	
Ethanol	560	2.6	(0.3)	17	(0.6)		
	580	14.7	(0.5)	95	(0.5)		
	620	0.7	(-0.7)*	104	(1)		
	640	1.4	(-0.5)*	411	(1)		
	680	1.9	(-0.6)*	1400	(1)		
	720	2.4	(-0.6)*	1400	(1)		
Benzonitrile	560	4.6	(0.8)	50	(0.2)		
	580	4.9	(0.7)	51	(0.3)		
	620	0.8	(-0.8)*	9.0	(0.7)	2000	(0.3)
	660	1.1	(-0.7)*	12.7	(0.6)	2000	(0.4)
	680	1.5	(-0.7)*	12.2	(0.5)	2000	(0.5)
	720	2.7	(-0.8)*	10.0	(0.3)	2000	(0.7)
Decanol	530	36.2	(0.7)	142	(0.3)		
	560	66.4	(0.5)	219	(0.4)	943	(0.1)
	580	131.6	(0.5)	343	(0.4)	1386	(0.1)
	590	4.2	(-0.6)*	243	(0.7)	1185	(0.3)
	620	47.0	(-0.3)*	508	(0.6)	2136	(0.4)
	690	134.7	(-0.2)*	432	(-0.4)*	2402	(1)

* refers to rise components; positive pre-exponential factors refer to decay, their sum is normalized to 1.

5.4. Discussion

The temporal dependence of the emission spectra (cf Figure 5.4) is characteristic of Stokes shift dynamics. We first consider the possibility that the dynamics Stokes shift is caused by a twisting motion involving the rotation of one or more of the functional groups in the styryl compounds. Such fast, barrierless twisting

motions of phenyl groups about single bonds have for instance been extensively studied for di- and triphenylmethane dye molecules [22-25]. For these molecules it is well-known that the fluorescence quantum yield is high in highly viscous solvents whereas the quantum yield is drastically reduced in low-viscosity solution. Moreover, similar to the DPD dyes, the rotamer dynamics of these systems as manifested in the Stokes shift dynamics was also on the (sub)picosecond time scale [22,23]. A characteristic feature for the DPD compounds, however, is that bridging of both single bonds of the styryl dye has no significant influence on the rate of its dynamic Stokes shift (compare e.g. spectral dynamics of **1** and **4** in Figure 5.4). This result cannot be reconciled with the idea that the rate of the Stokes shift of styryl dyes is determined by twisting about a single styryl bond.

Alternatively, since for the ionic styryl dyes **1** to **4** it is observed that the Stokes shift dynamics varies with the nature of the solvent, and considering also that the probed molecules are chemically inert with respect to the solvents ethanol, benzonitrile and decanol, it is very likely that the observed dynamic Stokes shift is due to solvation. Then, one may expect little effect of the bridging of both single bonds, and this is what has actually been found experimentally. In the event of solvation, the dynamic Stokes shift may well be represented by the normalized spectral response function,

$$C(t) = \frac{\nu(t) - \nu(\infty)}{\nu(0) - \nu(\infty)} \qquad (5.1)$$

where $C(t)$ in linear response theory is equivalent to the time correlation function of the solvent-induced fluctuations of the optical transition frequency [26]. In Eq. (1), $\nu(t)$ is the first moment of the log-normal band shape function. In Figure 5.5 we have plotted the time dependence of the first moments of the emission bands of the DPD compounds **1** to **4** dissolved in ethanol, benzonitrile and decanol. The solid lines are the best fits to bi-exponential functions. The time constants and relative amplitudes characterizing these bi-exponential functions are given in Table 5.6. The table includes the average solvation times as known for the different polar solvents used here [8]. The weighted average times for the dynamic Stokes shifts of the styryl dye emission bands as discerned from the experimental $C(t)$ curves in Figure 5.5 compare well (to within a factor of about three) with the known solvation times of the solvents (Table 5.6) thus confirming that the dynamic Stokes shift is due to solvation dynamics in the excited state. A non-exponential decay behavior of the solvent response function is quite

common and is usually attributed to bimodal contributions of 'inertial free streaming' (~ 50-500 fs) and rotational diffusion motions (~ 1-100 ps) [27,28].

Table 5.5

Excited-state lifetimes (in picoseconds) for ionic styryl dyes **1** to **4** in the solvents indicated

	Ethanol	Benzonitrile	Decanol
p-DPD	80	215	900
o-DPD	40	85	400
o-DPD-b1	65	230	500
p-DPD-b13	1400	2000	2400

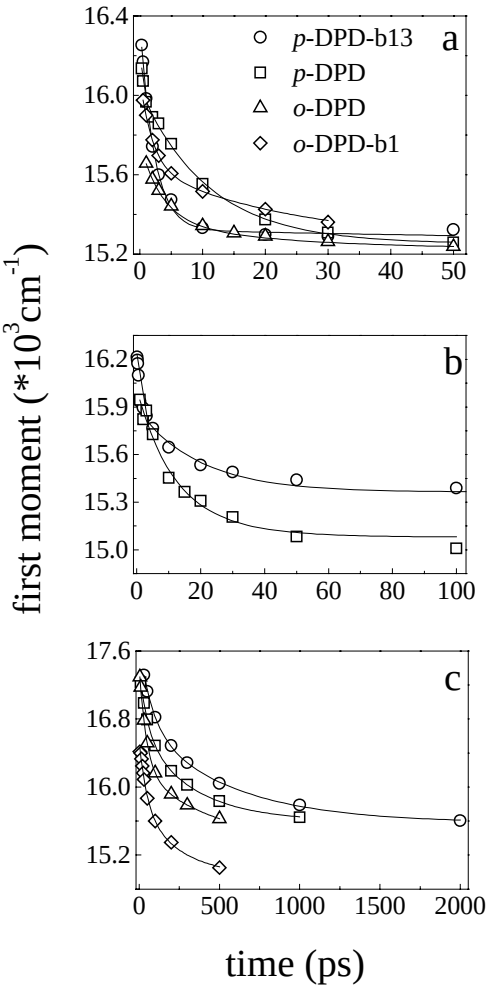

Figure 5.5. Time dependence of the first moment of the emission spectrum of **1** to **4** in ethanol (a), benzonitrile (b) and decanol (c). Solid lines are best fits to bi-exponential decay functions.

Interestingly, the total integrated fluorescence intensity of the DPD compounds at early times (t < 1 ps) shows an increase with time. This is perhaps best illustrated by Figures 5.4b and 5.4d for **1** and **4** dissolved in benzonitrile. The intensity rise, with a typical time of approximately 300 fs, probably is related to feeding from of the highly excited vibrational levels, due to IVR or energy transfer to the bath.

We now turn to the lifetime results for the DPD derivatives as presented in Table 5.5. Several features may be noted from this table. Firstly, as long as the styryl dye still has one unbridged single bond adjacent to the styryl-group double bond (compounds **1** to **3**), the lifetimes of the corresponding compounds, in a given solvent, are comparable. However, for compound **4** for which both single bonds are bridged, the excited-state lifetime is lengthened significantly (by a factor of at least ten when the solvent is ethanol). It is likely that the enhanced non-radiative decay of compounds **1** to **3** is related to the flexibility (torsional or bending) of functional groups that are linked by a single bond to the remainder of the molecule. The presence of single-bonded flexible groups could lead to increased coupling of the excited state to the dense manifold of vibrational levels of the ground state thus facilitating effective radiationless decay ('loose bolt theory' [17]). The flexible-group motions also depend on the viscosity of the solvent. As the viscosity of the solvent increases the torsional or bending motions slow down and this will reduce the rate of the radiationless decay process. This is indeed verified from the change of the excited-state lifetime of each of the styryl dyes with the viscosity of the solvent: in more viscous solutions longer lifetimes are found.

Table 5.6

Characteristic times (in ps) of the dynamic Stokes shift of the DPD emission bands. Relative intensities are given in brackets

	Ethanol			Benzonitrile			Decanol		
	τ_1	τ_2	τ_{av}	τ_1	τ_2	τ_{av}	τ_1	τ_2	τ_{av}
p-DPD	0.2 (0.3)	10 (0.7)	7.1	0.8 (0.4)	19 (0.6)	11.7	53 (0.3)	330 (0.7)	233
o-DPD	3.5 (0.7)	19 (0.3)	8.2				45 (0.6)	460 (0.4)	211
o-DPD-b1	1.9 (0.6)	24 (0.4)	10.7				45 (0.4)	210 (0.6)	136
p-DPD-b13	1.8 (0.8)	5.8 (0.2)	2.6	9.5 (0.5)	17.7 (0.5)	13.6	82 (0.5)	550 (0.5)	339
τ_{av} (Ref. 8)			16			5.1			245

In the context of the conjecture that the fast decay is connected to the possibility of single bond twisting it is of interest to note that previously analogous results were obtained for the structurally related compound *o*-DASPI [16]. The structure of the latter is similar to that of *o*-DPD, but without the phenyl groups attached to the pyridinium cation. Also for *o*-DASPI it was found that the initial fluorescence decay is determined by solvation in the time range from 100 fs up to about 10 ps. Our lifetime measurements yielded 21 ps (acetonitrile), 30 ps (methanol), 62 ps (ethanol), 110 ps (ethylene glycol), where the solvents have been given in brackets. The viscosity of ethylene glycol (η = 20 cP) is comparable to that for decanol (η = 14 cP) [29]. Yet, the lifetime of *o*-DASPI is shorter by a factor four compared to that of *o*-DPD (110 ps and 400 ps, respectively). This is understandable since the torsional motions in *o*-DPD should be slower on account of the increased inertia of the pyridinium cation containing the phenyl substituents.

Finally, we compare the lifetimes of unbridged *o*-DPD and singly bridged *o*-DPD-b1. As is seen from Table 5.5, in the three solvents used, the lifetime of the unbridged styryl dye is always shorter. Thus blocking one of the doorways for torsional relaxation causes a lengthening of the lifetime. The torsional motions involving the remaining single bond, however, also contribute to the radiationless decay process and thus the lifetime of the singly bridged compound, *o*-DPD-b1, is much shorter than that of *p*-DPD-b13. The latter compound probably relaxes due to *trans-cis* isomerization, which apparently is slower by at least a factor five (in the solvents ethanol and benzonitrile) as compared to the process leading to the nonradiative decay in **1-3**.

Acknowledgement

This research was financially supported by the Council for Chemical Sciences of the Netherlands Organization for Scientific Research (CW-NWO).

References

[1] W. Rettig, B. Strehmel, S. Schrader, H. Seifert (Eds.), Applied Fluorescence in Chemistry, Biology, and Medicine, Springer, Berlin, 1998.

[2] J. Fabian, H. Nakazumi, M. Matsuoka, Chem. Rev. **92**, 1197 (1992).

[3] U. Brackmann, Lambdachrome laser dyes, 2nd edn., Lambda Physik GmbH, Göttingen, 1994.

[4] S.R. Mujumdar, R.B. Mujumbar, C.M. Grant, A.S. Waggoner, Bioconjugate Chem. **7**, 356 (1996).

[5] P. Fromherz, K.H. Dambacher, H. Ephardt, A. Lambacher, C.O. Müller, R. Neigle, H. Schaden, O. Schenk, T. Vetter, Ber. Bunsenges. Phys. Chem. **95**, 1333 (1991).

[6] S. Fery-Forgues, M-T. Le Bris, J-C. Mialocq, J. Pouget, W. Rettig, B. Valeur, J. Phys. Chem. **96**, 701 (1992).

[7] U. Narang, C.F. Zhao, J.D. Bhawalkar, F.V. Bright, P.N. Prasad, J. Phys. Chem. **100**, 4521 (1996).

[8] M.L. Horng, J.A. Gardecki, A. Papazyan, M. Maroncelli, J. Phys. Chem. **99**, 17311 (1995).

[9] W. Rettig, K. Rurack, M. Sczepan, Proceedings of the international conference on methods and applications of fluorescence spectroscopy, Paris, 1999, B.Valeur and J.C. Brochon eds., Springer Verlag, Berlin, 2000.

[10] P.F. Barbara and W. Jarzeba, Adv. Photochem. **15**, 1 (1990).

[11] P. van der Meulen, H. Zhang, A.M. Jonkman, M. Glasbeek, J. Phys. Chem. **100**, 5367 (1996).

[12] S.A. Kovalenko, J. Ruthmann, N.P. Ernsting, Chem. Phys. Lett. **271**, 40 (1997).

[13] S.A. Kovalenko, N.P. Ernsting, J. Ruthmann, J. Chem. Phys. **106**, 3504 (1997).

[14] B. Strehmel, H. Seifert, W. Rettig, J. Phys. Chem. B **101**, 2232 (1997).

[15] H. Zhang, A.M. Jonkman, P. van der Meulen, M. Glasbeek, Chem. Phys. Lett. **224**, 551 (1994).

[16] A.M. Jonkman, P. van der Meulen, H. Zhang, M. Glasbeek, Chem. Phys. Lett. **256**, 21 (1996).

[17] G.N. Lewis, M. Calvin, Chem. Rev. **25**, 273 (1939); L.J.E. Hofer, R.J. Grabenstetter, E.O. Wiig, J. Am. Chem. Soc. **72**, 203 (1950).

[18] M. Sczepan, W. Rettig, Y.L. Bricks, Y.L. Slominski, A.I. Tolmachev, J. Photochem. Photobiol. A Chem. **124**, 75 (1999).

[19] M. Sczepan, W. Rettig, A.I. Tolmachev, to be published.

[20] E.R. Middelhoek, P. van der Meulen, J.W. Verhoeven, M. Glasbeek, Chem. Phys. **198**, 373 (1995).

[21] M. Maroncelli, G.R. Fleming, J. Chem. Phys. **86**, 6221 (1987).

[22] P. Changenet, H. Zhang, M.J. van der Meer, M. Glasbeek, P. Plaza, M.M. Martin, J. Phys. Chem. **102**, 6712 (1998).

[23] M.J. van der Meer, H. Zhang, M. Glasbeek, J. Chem. Phys. **112**, 2878 (2000).

[24] M.M. Martin, P. Plaza, P. Changenet, Y.H. Meyer, J. Photochem. Photobiol. A **105**, 197 (1997).

[25] M. Ishikawa, J.E. Ye, Y. Maruyama, H. Nakatsuka, J. Phys. Chem. A **103**, 4319 (1999), and references therein.

[26] A. Chandra, B. Bagchi, Chem. Phys. Lett. **165**, 93 (1990).

[27] R. Jimenez, G.R. Fleming, P.V. Kumar, M. Maroncelli, Nature **369**, 471 (1994).

[28] M. Maroncelli, J. Mol. Liq. **57**, 1 (1993).

[29] D.R. Lide (Ed.), Handbook of Chemistry and Physics, 78th edn., CRC Press, New York, 1998.

Chapter 6

Subpicosecond fluorescence upconversion measurements of primary events in yellow protein*

Abstract

The primary step in the photocycle of photoactive yellow protein (PYP) has been investigated by means of the subpicosecond fluorescence upconversion technique. The nature of the chromophore is found to affect the fluorescence decay dynamics: upon replacement of the coumaric acid chromophore by 7-hydroxy-coumarin-3-carboxylic acid, the fluorescence decay becomes much longer (with typical decay times larger than 60 ps), whereas the 700 fs and 3 ps components have disappeared. It is discussed that the obtained results are strong support for the idea that the initial step in the photocycle involves trans-cis isomerization inside the coumaric acid chromophore in native PYP.

* The contents of this chapter has been published as an article, P. Changenet, H. Zhang, M.J. van der Meer, K.J. Hellingwerf, M. Glasbeek, Chem. Phys. Lett. **282**, 276-282 (1998).

6.1 Introduction

The study of the photochemistry of photoactive proteins containing polyene chromophores has attracted great interest in recent years (see e.g. Ref. [1]). For rhodopsins and phytochromes, it is assumed that an ultrafast photoinduced *trans-cis* isomerization process occurring inside the chromophore molecule triggers a photocycle of reactions. Recently, similar photophysical behavior has been proposed for photoactive yellow protein (PYP) [2] isolated from the halophilic purple bacterium *Ectothiorhodospira halophila* [3]. PYP contains a coumaric acid chromophore [4-5] linked to the protein through a thiol ester bond [6], which is deprotonated in the ground state of PYP [5,7]. After blue light absorption, PYP undergoes a photocycle, which involves at least three intermediates. Two of these, pR and pB, were identified by transient absorption spectroscopy [8,9]. The red-shifted intermediate (pR), with an absorption maximum around 460 nm, appears first, in less than 5 ns after flash excitation of the ground state of PYP, pG (ε = 45.5 $mM^{-1}.cm^{-1}$). Subsequently, in a few hundred microseconds, a blue-shifted intermediate (pB) is formed, which absorbs near 335 nm and which returns to the ground state (pG) in about one second. In the pB intermediate the chromophore is protonated [10]. Additionally, from extraction and NMR spectroscopic studies, evidence was obtained that the chromophore in pG resides in a *trans* configuration whereas in pB it is in a *cis* configuration [2]. These observations led the authors to suggest that the pR intermediate may already be in a *cis* conformation and that the *trans-cis* isomerization in the chromophore may have occurred already during the earliest step of the photocycle of PYP, in analogy to the photochemistry of the rhodopsins [1].

Recently, several time-resolved studies of the primary events in PYP have been reported [9,11-13]. In a study of the temporal behavior of the spontaneous fluorescence of PYP it was shown that the transients exhibit a decay component faster than about 12 ps [11]. However, due to the limited time resolution of these experiments the relevant time constants could not yet be determined. In a recent transient absorption study, with a time resolution of 200 fs, it was reported that an intermediate excited state developed in 0.7 ps which evolved into a product in 3.6 ps [12]. Very recently, while our work was in progress, a fluorescence study of PYP with a time resolution of 200 fs was reported [13]. In the latter report, the fluorescence was shown to exhibit multiexponential decays only, with typical time constants of a few hundred femtoseconds to a few picoseconds.

In all aforementioned studies the (sub)picosecond fluorescence decay was interpreted to arise from fast barrierless *trans-cis* isomerization, taking place inside the protein chromophore. Naturally, one way to further test this idea is to examine the effect of the nature of the chromophore on the fluorescence decay dynamics. More specifically, one would expect that if the structure of the chromophore is modified such that the twisting motion around the relevant double bond in the probe molecule is hampered, this would in turn result in a reduction of the relative magnitude of the (sub)picosecond component in the decay kinetics of the probed fluorescence.

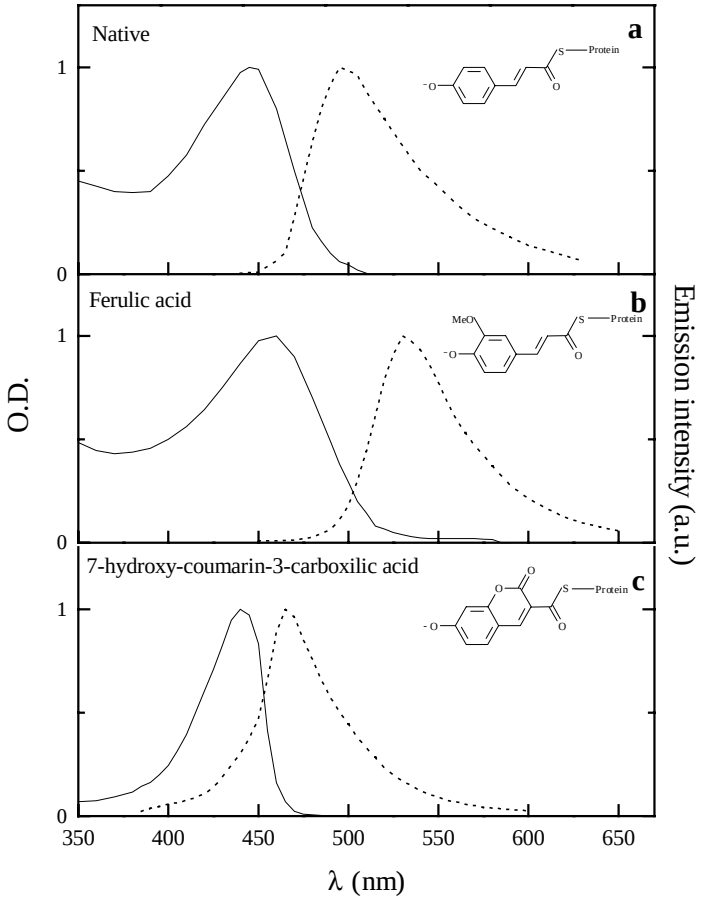

Figure 6.1. Normalized absorption and emission spectra of (a) native, (b) ferulic acid and (c) 7-hydroxy-coumarin-3-carboxylic acid PYP dissolved in water (10 mM Tris.HCl, pH=7.5). Schemes of the molecular structure of the chromophore of the PYP hybrids are given in the inserts.

In the present chapter, we compare the time-resolved fluorescence of native PYP and two of its artificial derivatives, which contain a ferulic acid chromophore and a 7-hydroxy-coumarin-3-carboxylic acid chromophore, respectively, instead of the *p*-

coumaric acid (for chromophore schematic structures, see inserts in Figure 6.1). In our experiments we applied the fluorescence upconversion technique, with a resolution of 150 fs, to cover a time window between 150 fs and 30 ps, whereas time-correlated single-photon-counting detection was applied for decays at longer time scales. Non-exponential fluorescence decays are obtained for all compounds. For native PYP, we confirm the recent results of Chosrowjan et al [13]. The most interesting result is however, that for the protein which contains the 7-hydroxy-coumarin-3-carboxylic acid chromophore, which because of its molecular structure cannot possibly exhibit the *trans-cis* isomerization, we do not observe the very fast decay components of 600 fs and 3 ps. This result is considered to be strong evidence that the intramolecular conformational changes of the chromophore are indeed responsible for the fast decay components in the PYP fluorescence.

6.2 Experimental

Reconstituted PYP samples were prepared in 10mM Tris.HCl, pH = 7.5, as described elsewhere [10]. All samples had a purity index lower than 2.5.

The femtosecond fluorescence transients were detected using a fluorescence upconversion set-up [14]. To this end, an all-line cw Ar^+-laser was used to pump a Tsunami Ti: sapphire laser (~ 50 fs pulse width) with a repetition rate of 82 MHz. The pulses were led through a 1 mm thick BBO frequency doubling crystal, after which the pulses were split by a dichroic beam-splitter into two beams, the first beam being the pump beam (at a wavelength of 420 nm, i.e., about 25 nm to the blue of the yellow protein absorption maximum) and the second beam being the gating beam (at 840 nm). Pulses with an energy of about 1 nJ/pulse were used to photoexcite the sample. The latter was contained in a cell of 2 mm thickness at room temperature, which was moving back and forth perpendicular to the excitation laser beam, in order to prevent heating of the sample. The gating beam passed a stepping motor-driven translational stage and was focussed together with the fluorescence induced by the pump-beam onto a 1 mm thick BBO crystal (type I phase match). The upconversion signal was filtered by an UG11 filter (band pass is from 260 nm to 380 nm), focussed on the entrance slit of the monochromator (spectral resolution < 5 nm) and detected by means of a photomultiplier (EMI 9863 QB/350) connected to a photon counting system linked to a

personal computer for data storage and analysis. To circumvent contributions to the probed fluorescence transients arising from reorientational motions of the probe, the transients were measured under magic angle conditions. The instrumental response function, as deduced from the measured cross correlation function of the excitation and the gating pulses (at 420 nm and 840 nm, respectively), was determined to be roughly 150 fs (FWHM).

The picosecond fluorescence transients of the yellow protein samples were measured using a calibrated emission spectrometer equipped with time-correlated single-photon-counting detection with a response of 16 ps [15]. The instrumental response function was determined by means of the Raman scattered light from a water sample.

In the picosecond fluorescence experiments the sample was excited by means of the frequency-doubled pulses from a synchronously pumped picosecond dye laser; the excitation wavelength was tuned at 322 nm. From the picosecond transients the time-resolved fluorescence spectra were reconstructed. Steady-state absorption spectra were recorded with a Shimadzu spectrometer UV 240 and steady-state fluorescence spectra were measured on a calibrated emission spectrometer.

6.3 Results

Steady-state absorption and emission spectra of PYP are presented in Figure 6.1a, for comparison [3,9,10]. The absorption band is centered near 446 nm. PYP exhibits an emission band centered around 495 nm. The fluorescence excitation spectrum fits the absorption band and shows no detection wavelength dependence. PYP is weakly fluorescent; its fluorescence quantum yield was estimated to be 0.2% [10,11].

The absorption and fluorescence band maxima of the PYP hybrid containing the ferulic acid chromophore, are at 460 nm and 527 nm, respectively, and thus are red shifted with respect to the transition wavelengths of native PYP (Figure 6.1b). The fluorescence quantum yield of this PYP hybrid is somewhat larger than for native PYP and estimated to be 5.4% [10]. For the hybrid containing 7-hydroxy-coumarin-3-carboxylic acid, the absorption band peaks at about 443 nm, and the emission band maximum is near 465 nm (Figure 6.1c).

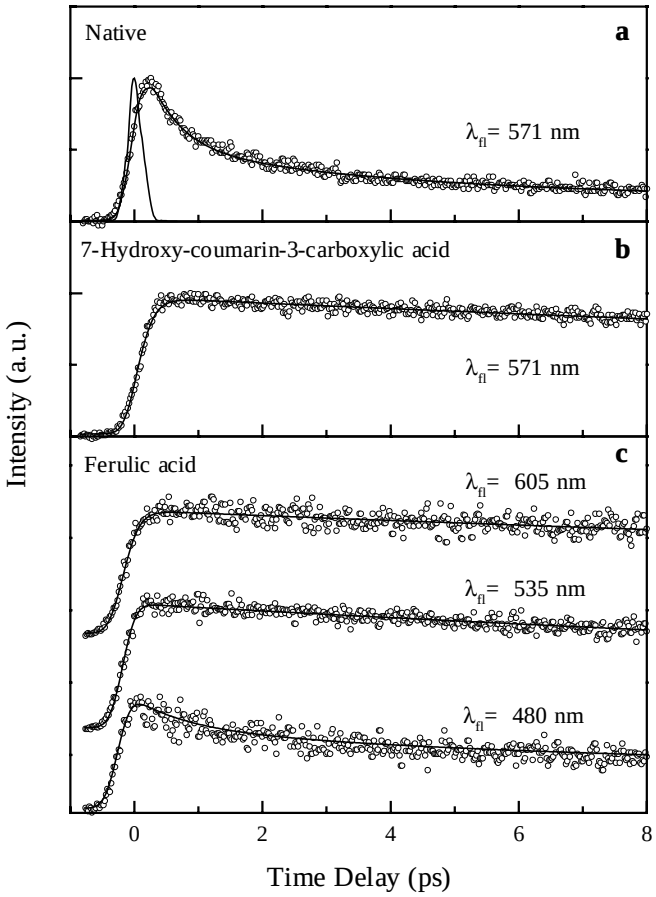

Figure 6.2. Representative fluorescence transients of (a) native, (b) 7-hydroxy-coumarin-3-carboxylic acid, and (c) ferulic acid PYPs dissolved in water (10 mM Tris.HCl, pH=7.5). Solid curves represent best fits as described in text. The system response function is included in (a).

For each protein, upconversion fluorescence transients were measured at ten different wavelengths in the 150 fs - 30 ps time window. When performing time-correlated single-photon-counting measurements, transients were monitored at an interval of 10 nm within the emission band in the 16 ps - 5 ns time window. Representative fluorescence decays measured for native and the hybrid PYPs at different wavelengths are shown in Figure 6.2. Fluorescence decay transients were fitted to a multiexponential function, convoluted with the system response.

Table 6.1

Time components (τ_i) and pre-exponential factors (a_i) obtained from the fit of fluorescence decays of native PYP, measured by upconversion technique in a time-window of 30ps, at a few representative wavelengths (λ_{exc} = 420 nm, λ_{gating} = 840 nm).

λ nm	τ_1 (a_1)	τ_2 (a_2)	τ_3 (a_3)
455	0.7 ps (52%)	4.3 ps (32%)	68.5 ps (16%)
480	0.7 ps (40%)	4.3 ps (35%)	38.3 ps (25%)
505	1.0 ps (47%)	3.7 ps (30%)	47.2 ps (23%)
530	0.7 ps (49%)	3.9 ps (29%)	41.6 ps (22%)
570	0.4 ps (60%)	3.1 ps (26%)	53.8 ps (14%)

The different lifetimes and their amplitudes obtained for the native PYP at a few representative detection wavelengths are given in Tables 6.1 and 6.2. It is seen that the fluorescence decay kinetics is characterized by a non-exponential decay with two dominating short components of about 700 fs and 3 ps, respectively. In contrast to the transient absorption results of Baltuška et al [12], in all fluorescence transients no rapid rise component was detected. It should be added that in the fluorescence upconversion experiment, we selectively probe the temporal evolution of the excited state population without any interference from the ground-state population dynamics. Moreover, our experimental data for the native PYP are in full agreement with those reported by Chosrowjan et al [13].

The fluorescence decay of the hybrid containing 7-hydroxy-coumarin-3-carboxylic acid could be fitted to a multi-exponential function, in which the three fastest decay components have lifetimes of 58 ps (75%), 450 ps (9%), and 3.4 ns (16 %). It is emphasized that the upconversion measurements show that the decay kinetics of this locked hybrid does not contain lifetime components shorter than 60 ps (cf Figure 6.2b).

Following the method given by Maroncelli and Fleming [16], time-resolved emission spectra of the hybrid proteins were reconstructed from the fluorescence decays. Representative results for native PYP are given in Figure 6.3. As illustrated by the spectra of Figure 6.3, a spectral broadening amounting to 1300 cm^{-1} (FWHM) is observed, over the whole time range. No significant dynamic spectral changes were resolved for the 7-hydroxy-coumarin-3-carboxylic acid hybrid.

Table 6.2

Time components (τ_i) and pre-exponential factors (a_i) obtained from the fit of fluorescence decays of native PYP measured by single photon counting in a time-window of 5 ns at a few representative wavelengths (λ_{exc} = 322 nm).

λ nm	τ_1 (a_1)	τ_2 (a_2)	τ_3 (a_3)	τ_4 (a_4)
460	10 ps (64%)	56 ps (27%)	331 ps (7%)	2.5 ns (2%)
480	20 ps (71%)	100 ps (22%)	400 ps (5%)	2.4 ns (2%)
500	21 ps (66%)	97 ps (27%)	431 ps (5%)	2.6 ns (2%)
520	17 ps (59%)	79 ps (33%)	389 ps (6%)	2.6 ns (2%)
540	10 ps (51%)	61 ps (38%)	344 ps (8%)	2.6 ns (3%)
560	13 ps (56%)	73 ps (32%)	384 ps (9%)	2.7 ns (3%)
580	20 ps (57%)	72 ps (30%)	401 ps (9%)	2.8 ns (4%)
600	18 ps (61%)	105 ps (25%)	469 ps (10%)	2.8 ns 4%)

In contrast with the results mentioned above for the native protein and the 7-hydroxy-coumarin-3-carboxylic acid hybrid, for the hybrid containing ferulic acid a wavelength dependence was found in its fluorescence kinetics (see Figure 6.2c). The fluorescence transient for the ferulic acid hybrid, when detected at 480 nm, could be fitted to a multi-exponential function with characteristic times of 700 fs (30%), 3 ps (20%), 60 ps (25%), 400 ps (20%), and 1.2 ns (5%). When the measurements are performed at longer wavelengths, the fit of the fluorescence decays always contains the latter three slow components. The contribution to the fluorescence decay of the two fastest components (700 fs and 3 ps) gradually becomes less for longer detection wavelengths; for wavelengths larger than 545 nm, these components have disappeared.

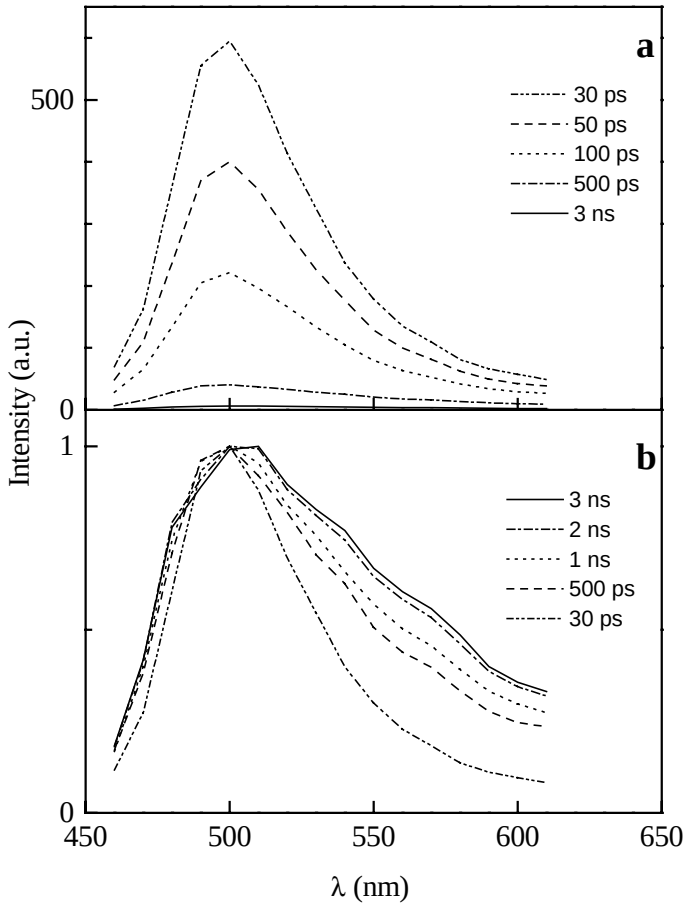

Figure 6.3. Reconstructed time-resolved emission spectra of native PYP dissolved in water (10 mM Tris.HCl, pH=7.5), in the time window from 30 ps to 3 ns. (a) unnormalized, (b) normalized to same maximum intensity at all times.

6.4 Discussion

The ultrafast appearance, the fast non-exponential decay, and the negligible red-shift of the spontaneous emission show that native PYP behaves very similar to bacteriorhodopsin (bR) [17-19]. For retinal in bR a two-state model has been proposed to explain the fast photoisomerization process [1]. In that model, excitation of the population in a repulsive Franck-Condon region was assumed to give rise to an ultrafast conformational relaxation of the retinal (150 fs). The model could not explain the absence of a dynamic Stokes shift in the experiments, however. It has recently been discussed that the excited-state dynamics of retinal in bR is compatible with a three-state model [19]. In this model, upon pulsed photoexcitation, the decay out of the Franck-Condon regime is assumed to be very fast (< 50 fs) and into an almost flat (non-repulsive) excited state potential, S_1. The initially formed emissive state, S_1, decays into

a reactive region typical of the twisted retinal molecule, where it anticrosses with S_2, after which the molecule may decay non-radiatively into the all-*trans* or 13-*cis* retinal. Due to inhomogeneous broadening effects, caused by the protein pocket, the lifetime of the emissive state, S_1, may vary from 500 fs up to the picosecond time regime. Similar results and a similar picture have been reported by Haran et al [18].

Likewise, we infer that in the case of native PYP a similar model is applicable. Thus we attribute the rapid decay components with time constants in the range from 600 fs up to 4.4 ps to the decay of the S_1 state into a twisted conformation. Inhomogeneous broadening of the anticrossing region of the S_1 and S_2 levels, caused by ill-defined surroundings in the protein pocket, is held responsible for the spread in the S_1 lifetime. This is further illustrated by the time-resolved spectra of Figure 6.3a. These spectra show that, as time progresses, the total intensity of the emission decays on a time scale of about 70 ps. Since we do not resolve a dynamic Stokes shift, the emissive state responsible for the observed emission must be formed within about 150 fs (i.e., the experimental resolution) and it is very unlikely that the rapid decay in the total emission intensity of Figure 6.3a is caused by a relaxation of this state into electronic state(s) of different radiative character (no spectral diffusion). On the other hand, if the observed emission spectrum is composed of an inhomogeneous distribution of emission bands, each band contributing according to its own lifetime, then it is understood that the total intensity will decay in accordance with the distribution of the characteristic decay times of the inhomogeneous ensemble. We thus conclude that the time dependence of the integrated emission intensity of the native PYP is characteristic of an inhomogeneous distribution in the emission-band lifetime indeed. Furthermore, it is of interest to note that the inhomogeneous spread in lifetime is accompanied by a slight change in the emission spectrum: a broadening of the emission with time occurs on the red edge of the spectrum (cf Figure 6.3b). It is likely, in analogy with bR, that the emission of the native PYP arises from the chromophore in a slightly twisted conformation at S_1 out of the Franck-Condon regime. A strong dependence of the excited-state lifetime on the twisting angle is expected [17]. We thus tentatively propose for the native PYP that the inhomogeneous spread in the fluorescence–state lifetime may be connected to an inhomogeneous spread in the twisting angle of the chromophore in its excited state, thus giving rise to slight inhomogeneous broadening effects as well. Remark that the three-state model has previously also been considered by Todd et al [20] when

discussing the rapid decay of the fluorescence of photoexcited *cis*-stilbene in liquid solution. Simulations on the basis of a modified Smoluchowski equation for the diffusion of the population out of the Franck-Condon regime, assuming an almost flat decaying potential and a rapidly decaying sink function, could explain the lack of dynamic Stokes shift and the occurrence of picosecond transients characterized by a sum of exponentials [21].

Remarkably different temporal fluorescence behavior is obtained for the other two PYP hybrids. As is evident from Figure 6.2, for the 7-hydroxy-coumarin-3-carboxylic acid hybrid the very fast (700 fs and 3 ps) decay components, which are characteristic of the native PYP fluorescence decay, are missing. Obviously, due to its rigid ring structure, *trans-cis* isomerization around a vinyl bond does not come into play for this hybrid. In accordance with the model discussed above regarding the crucial role of the twisting motion around the vinyl bond in determining the excited-state lifetime, it is to be expected that for the 7-hydroxy-coumarin-3-carboxylic acid chromophore a rapid decay into the reactive state cannot take place and thus decay time constants faster than 10 ps are not found.

As was mentioned in the results section, in the case of the ferulic acid hybrid the fluorescence decay shows a detection wavelength dependence. The rapid decay components are more prominent in the blue part of the emission ($\lambda < 530$ nm) and the less rapidly decaying components with lifetimes longer than 60 ps are the only remaining components when $\lambda > 530$ nm. However, it is emphasized that although the amplitudes of the exponential terms in the best fit multi-exponentially decaying function change with the emission wavelength, the best fit values for the time constants of the exponential terms in the multi-exponential do not. Thus, in analogy to the case of the native PYP system, we conclude that a dynamic Stokes shift is not observed for the ferulic acid hybrid system. Since the short-living components, with time constants of only a few picoseconds or less, apparently emit at the blue edge of the emission band and are not found on the red edge, it seems that the inhomogeneous spread in the case of the ferulic acid hybrid is more outspoken than in the case of the native PYP system. We tentatively propose that, in native PYP the structure is such that the chromophore fits pretty well in the protein pocket; a slight structural change of the chromophore, for instance by attaching a methoxy-group to one of the rings, may affect the excited state potential and therefore also the inhomogeneous broadening. A more detailed study of

the effect of structural changes on the dynamics of the photocycle is currently in progress in this laboratory.

In summary, the fluorescence behavior of native PYP, as established from fluorescence upconversion measurements with 150 fs time resolution, is very similar to that of retinal in bR: after the pulsed excitation, no dynamic Stokes shift is resolved in the fluorescence and a very fast initial decay (although somewhat slower than for retinal in bR) is observed. From the lack of the very rapid initial decay components when the coumaric acid pigment in native PYP has been substituted by the artificial 7-hydroxy-coumarin-3-carboxylic acid, it is confirmed that *trans-cis* isomerization inside the chromophore is indeed pertinent to the observation of the very rapid decay components in the fluorescence of photoactive proteins.

Acknowledgement

This work was supported in part by the Netherlands Foundation for Chemical Research (SON) with financial aid from Netherlands Organization for Scientific Research (NWO). We thank Robert Cordfunke, Remco Kort and Herman Vennema for preparing the PYP samples.

References

[1] G.G. Kochendoerfer, R.A. Mathies, Israel J. of Chemistry **35**, 211 (1996).

[2] R. Kort, H. Vonk, X. Xu, W.D. Hoff, W. Crielaard, K.J. Hellingwerf, FEBS Letters **382**, 73 (1996).

[3] T.E. Meyer, Biochim. Biophys. Acta **806**, 175 (1985).

[4] W.D. Hoff, P. Dux, K. Hard, B. Devreese, I.M. Nugteren-Roodzant, W. Crielaard, R. Boelen, R. Kaptein, J. van Beeumen, K.J. Hellingwerf, Biochem. **33**, 13959 (1994).

[5] M. Baca, G.E.O. Borgstahl, M. Boissinot, P.M. Burke, D.R. Williams, K.A. Slater, E.D. Getzoff, Biochem. **33**, 14369 (1994).

[6] W.D. Hoff, B. Devreese, R. Fokkens, I.M. Nugteren-Roodzant, J. van Beeumen, N. Nibbering, K.J. Hellingwerf, Biochem. **35**, 1274 (1996).

[7] M. Kim, R. A. Mathies, W. D. Hoff, K. J. Hellingwerf, Biochem. **34**, 12669 (1995).

[8] T.E. Meyer, E. Yakali, M.A. Cusanovich, G. Tollin, Biochem. **26**, 418 (1987).

[9] W.D. Hoff, I.H.M. van Stokkum, H.J. van Ramesdonk, M.E. van Brederode, A.M. Brouwer, J.C. Fitch, T.E. Meyer, R. van Grondelle, K.J. Hellingwerf, Biophys. J. **67**, 1691 (1994).

[10] A.R. Kroon, W.D. Hoff, H. Fennema, G.J. Koomen, J.W. Verhoeven, W. Crielaard, K.J. Hellingwerf, J. Biol. Chem. **271**, 31949 (1996).

[11] T.E. Meyer, G. Tollin, T.P. Causgrove, P. Cheng, R.E. Blankenship, Biophys. J. **59**, 988 (1991).

[12] A. Baltuska, I.H.M. van Stokkum, A. Kroon, R. Monshouwer, K.J. Hellingwerf, R. van Grondelle, Chem. Phys. Lett. **270**, 263 (1997).

[13] H. Chosrowjan, N. Mataga, N. Nakashima, Y. Imamoto, F. Tokunaga, Chem. Phys. Lett. **270**, 267 (1997).

[14] P. van der Meulen, H. Zhang, A. M. Jonkman, M. Glasbeek, J. Phys. Chem. **100**, 5367 (1996).

[15] E.R. Middelhoek, P. van der Meulen, J.W. Verhoeven, M. Glasbeek, Chem. Phys. **198**, 373 (1995).

[16] M. Maroncelli, G.R. Fleming, J. Chem. Phys. **86**, 6221 (1987).

[17] M. Du, G.R. Fleming, Biophys. Chem. **48**, 101 (1993).

[18] G. Haran, K. Wynne, A. Xie, Q. He, M. Chance, R.M. Hochstrasser, Chem. Phys. Lett. **261**, 389 (1996).

[19] K.C. Hasson, F. Gai, P.A. Anfinrud, Proc. Natl. Acad. Sci. USA **93**, 15124 (1996).

[20] D.C. Todd, J.M. Rosenthal, A.J. Ruggiero, D. Yang, G.R. Fleming, J. Chem. Phys. **93**, 8658 (1990).

[21] B. Bagchi, Chem. Phys. Lett. **135**, 558 (1987).

Chapter 7

Femtosecond fluorescence up-conversion studies of photoactive yellow protein and derivatives

Abstract

The effect of substitutional groups in the chromophore of photoactive yellow protein (PYP) on the ultrafast isomerization process of the chromophore has been investigated by comparing the femtosecond fluorescence dynamics with native PYP. Deuteration of the double bond of the chromophore was found to have no influence on the fluorescence dynamics. Bromination of the chromophore on one side of the double bond red-shifted the emission spectrum. The fluorescence decay times were not affected. Attaching a hydroxyl-group to the phenyl-ring of the coumaric acid chromophore, changing it to a caffeic acid, led to an enhanced spectral broadening, also observed for ferulic acid (see Chapter 6). From these observations we conclude that the driving force for the trans-cis isomerization is provided by the backbone of the protein.

7.1. Introduction

Photoactive proteins are of great importance in many biological systems. Ultrafast photoinduced isomerization has been considered as the start of a photocycle of reactions in rhodopsins [1], phytochromes [2] and photoactive yellow protein (PYP) [3]. The chromophore of PYP is deprotonated coumaric acid [4,5], which is linked to the protein by a thiol ester bond [6,7]. During the photocycle, which starts after blue light absorption, several interesting features can be observed [8-10]. First, in less than 5 ns, a red-shifted intermediate state (pR) is reached with an absorption maximum of 460 nm. After a few hundred microseconds a second intermediate state (pB) is formed, that is blue-shifted, and that has an absorption maximum at 335 nm. In this pB state the chromophore is protonated. From NMR studies it is known that its double bond is in a cis configuration, while the chromophore in the ground state (pG) resides in a trans configuration [2]. The return to the ground state (pG) takes about 1 second.

In a former study (Chapter 6), by means of time-resolved fluorescence upconversion measurements, it was argued that the first intermediate state (pR) is already in a cis configuration [11]. Fluorescence transient measurements for the coumaric acid chromophore of PYP showed ultrafast decay components in the fluorescence intensity. The transients could be fitted to a bi-exponential function with time constants of approximately 0.7 and 3 ps. A similar ultrafast relaxation behavior has been observed for bacteriorhodopsin (bR) [12-14], which was attributed to the isomerization of the retinal chromophore molecule from all-trans to 13-cis. It was suggested that trans-cis isomerization of the double bond of coumaric acid in PYP also occurs during the first few picoseconds of the photocycle [11]. To study the isomerization process we replaced the coumaric acid chromophore with a bridged molecule, called 7-hydroxy-coumarin-3-carboxylic acid. The bridge prevents rotational motions about the double bond. The fluorescence decay time constants of this compound were much larger (about 60 ps) than the time constants of native PYP. The ultrafast decay components of 0.7 and 3 ps were absent. In another modification of the chromophore molecule, a methoxygroup was attached to the phenyl ring of the coumaric acid, changing it to a ferulic acid chromophore. The fluorescence transients of the ferulic acid PYP sample showed a wavelength-dependent decay behavior. Ultrafast decay components of about 0.7 and 3 picoseconds were present on the blue side of the emission spectrum. At the red edge no ultrafast decay components were

measured. An enhanced spectral broadening is observed for the ferulic acid compound due to the inhomogeneous spread in decay times. It was discussed that the ferulic acid chromophore fits less well in the protein pocket, causing an inhomogeneous spread in the decay times and inhomogeneous spectral broadening of the emission.

A trans-cis isomerization process of the chromophore inside the protein is much more complicated in a protein environment than in a solvent. By means of FTIR spectroscopy it was shown that the isomerization process may not only involve isomerization about the chromophore double bond but reorientation of functional groups about the single bond. The breaking of one hydrogen bond of the carbonyl-oxygen and the formation of another is involved in this process [15,16]. In Figure 7.1, the double isomerization process is illustrated. It is assumed that upon pulsed excitation of the chromophore the double isomerization occurs as the primary step of the photocycle. A recent study by Chosrowjan et al. [17,18] showed that the protein environment has a large influence on the isomerization process. They showed that modifications of the protein pocket, by side-directed mutagenesis, influences the rate of the isomerization. Changing functional groups on the chromophore, which affect the isomerization process, is another option to further investigate the isomerization processes of the PYP chromophore.

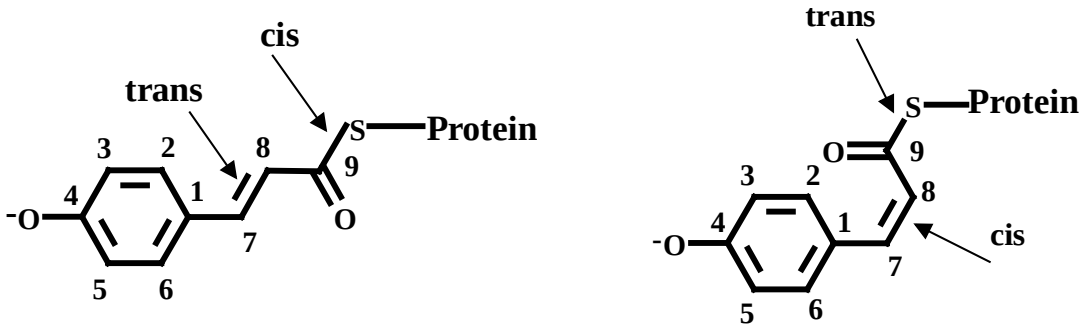

Figure 7.1. On the left the ground state conformer is shown (7-trans 9-s cis). The right conformer is double isomerized (7-cis 9-s trans).

In this chapter, we present ultrafast time-resolved fluorescence studies of three PYP samples, in which the coumaric acid chromophore has been replaced by derivative compounds. We compare the temporal behavior of the fluorescence of these chromophores with that of native PYP. In the first derivative both carbon atoms 7 and

8 (Figure 7.1) of the double bond are deuterated. The second derivative is brominated on carbon 8 of the chromophore; it is called α-Br PYP. The third derivative compound contains a caffeic acid chromophore instead of a coumaric acid. The chemical structures of all chromophores are included in Figure 7.2. Femtosecond upconversion experiments, with a time resolution of about 150 fs, were performed to measure the temporal behavior of the fluorescence in a time window of 30 ps. The long time behavior of the fluorescence was measured using a time-correlated single-photon counting setup with a time resolution of 16 ps.

7.2. Experimental

Reconstituted PYP samples were prepared in 10 mM tris.HCl, pH=8, as described elsewhere [10]. All samples had a purity index lower than 2.5.

The femtosecond fluorescence upconversion setup used for the measurements in time windows from 10 to 130 ps was described previously [19]. Briefly, a Spectra-Physics Millennia X diode laser pumped the Tsunami Ti:sapphire laser that delivered pulses with a typical width of ~50 fs and a wavelength of 840 nm (repetition rate is 82 MHz). Frequency doubling was achieved using a 1 mm thick BBO crystal. The pulses were split in pump and gating pulses by means of a dichroic beamsplitter. The pump pulses (λ = 420 nm, 1 nJ/pulse) excited the solution, contained in a 2 mm quartz cell. The latter was moved back and forth perpendicular to the excitation direction to prevent heating of the sample. The induced fluorescence was focused on a 1 mm thick BBO crystal (type I phase-matching conditions), together with the gating pulses. The latter were optically delayed with respect to the fluorescence beam by means of a translational stage. The upconverted signal was filtered by an UG11 filter (band pass 260-380 nm), focused on the entrance slit of a monochromator (spectral resolution < 5 nm) and detected by means of a photomultiplier (EMI 9863 QB/350) connected to a photon counting system. The up-conversion signal was accumulated for 1 s for each delay step of the translational stage. The instrumental response function, as determined from the cross correlation of the excitation and gating pulses, was estimated to be ~150 fs (FWHM).

The picosecond fluorescence transients in all samples were measured with a calibrated fluorescence setup outfitted with a time-correlated single-photon-counting (SPC) detection system [20]. A mode-locked Ar^+-ion laser synchronously pumped a picosecond dye laser. The pulses from the dye laser were frequency doubled to a wavelength of 322 nm and used to photoexcite the sample. By measurement of the Raman scattered light from a water sample, the instrumental response was determined to be 16 ps (FWHM). Steady-state emission spectra were obtained by measurement of the time-integrated spectra with the same setup.

All measurements, with both set-ups, were performed under magic angle conditions.

7.3. Results

Steady-state absorption and emission spectra of PYP samples are presented in Figure 7.2. In Figure 7.2a the results for native PYP are included for comparison. The absorption spectra of the PYP samples containing the double deuterated or the brominated chromophore are similar to the absorption spectrum of native PYP. The emission band maximum of the double deuterated sample is at 480 nm, which is slightly blue shifted with respect to 495 nm of the native sample. The fluorescence of the brominated PYP sample is red shifted and has its maximum at about 520 nm. The peak positions of the absorption and emission bands of the caffeic acid PYP are 460 nm and 550 nm respectively. Both bands are red-shifted compared to the native PYP absorption and emission spectra.

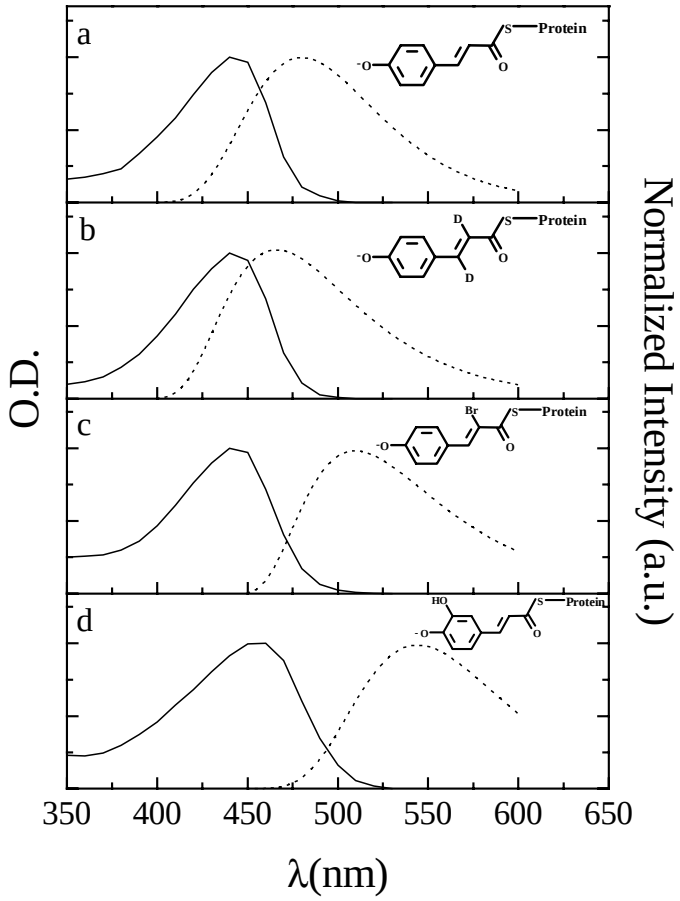

Figure 7.2. Normalized absorption and emission spectra of (a) native, (b) double deuterated coumaric acid, (c) α-brominated coumaric acid and (d) caffeic acid PYP dissolved in water (10 mM Tris.HCl, pH=8). Schemes of the molecular structure of the chromophore of the PYP hybrids are given in the inserts.

For all PYP samples, femtosecond fluorescence transients were measured at different wavelengths with 10 nm intervals over the entire emission band. The time windows used were 10, 30 or 130 ps. The picosecond fluorescence measurements were taken in a time window of 5 ns in order to determine decay components longer than 130 ps. In Figure 7.3 typical femtosecond fluorescence transients in a 10 ps time window are shown for all PYP derivatives. The transients were all fitted to multiexponential decay functions convoluted with the system response function. For the PYP sample with the deuterated chromophore, the best fit values of the multiexponential decay functions are presented in Tables 7.1 (upconversion measurements) and 7.2 (single photon counting results).

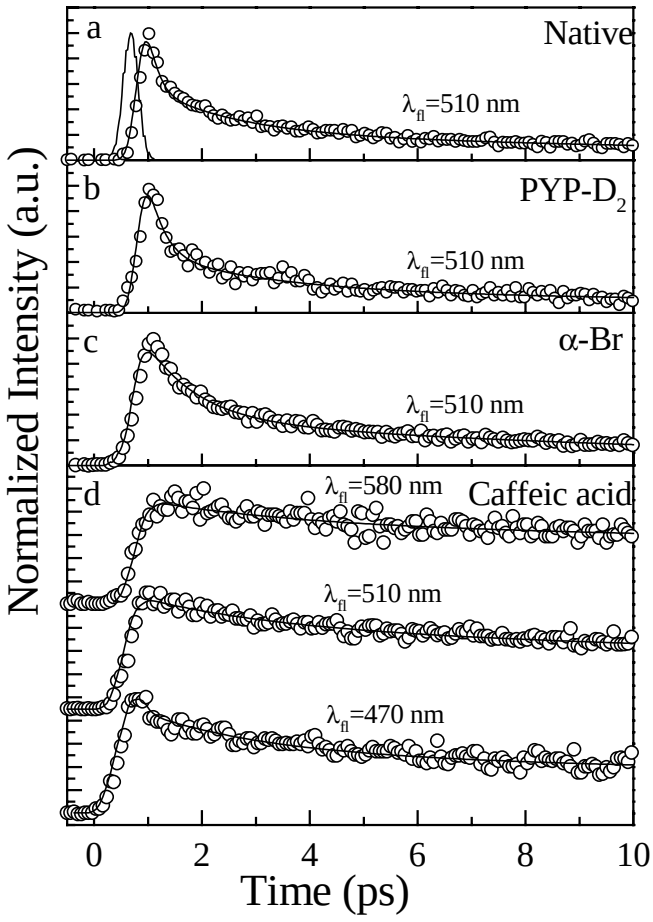

Figure 7.3. Representative fluorescence transients of (a) native, (b) double deuterated coumaric acid, (c) α-brominated coumaric acid and (d) caffeic acid PYP dissolved in water (10 mM Tris.HCl, pH=8). Solid curves represent best fits as described in text. The system response function is included in (a).

Table 7.1

Best fit values for (τ_i) and (a_i) of multi-exponential decay functions obtained from the fluorescence upconversion transients of double deuterated PYP, measured in a 10 ps time window, at several detection wavelengths (λ_{exc} = 420 nm)

λ (nm)	τ_1 (a_1)		τ_2 (a_2)		τ_3 (a_3)	
470	0.1 ps	(71%)	1.1 ps	(19%)	10.1 ps	(11%)
490	0.2 ps	(74%)	2.0 ps	(17%)	16.9 ps	(10%)
510	0.3 ps	(68%)	2.4 ps	(22%)	29.2 ps	(10%)
530	0.3 ps	(57%)	2.7 ps	(30%)	29.1 ps	(12%)

Two dominant decay time components, about 300 fs and 2 ps, are found from the femtosecond fluorescence upconversion transients. The longer decay times are best fitted with the single-photon counting results. They are determined as 90 ps and 1 ns. Similar behavior was already observed for the native PYP [11]. The temporal behavior of the fluorescence intensity of the α-brominated sample appeared comparable to that of the native and the double deuterated sample, as can also be seen from Figure 7.2.

The fluorescence upconversion results for the PYP sample containing the caffeic acid chromophore are different from the aforementioned derivatives. In this case, as can be seen in Figure 7.3d, a wavelength dependence of the fluorescence intensity decay was found. The longer decay time components (130 ps and 0.9 ns) are present at all detection wavelengths and more or less similar to those for the other PYP hybrids. However, the shorter decay components (0.6 and 2 ps), which are present at the blue edge of the emission band, disappear when changing the detection wavelength toward the red side of the fluorescence spectrum.

Table 7.2

Best fit values for (τ_i) and (a_i) of multi-exponential decay functions obtained from the single photon counting fluorescence transients of double deuterated PYP, measured in a 5 ns time window, at several detection wavelengths (λ_{exc} = 322 nm)

λ (nm)	τ_1 (a_1)		τ_2 (a_2)		τ_3 (a_3)	
460	15.2 ps	(78%)	100.5 ps	(18%)	1052 ps	(4%)
480	15.4 ps	(76%)	91.0 ps	(21%)	1020 ps	(3%)
500	14.9 ps	(75%)	85.2 ps	(23%)	989 ps	(2%)
520	14.2 ps	(75%)	84.8 ps	(23%)	1056 ps	(2%)
540	13.7 ps	(75%)	85.0 ps	(22%)	1067 ps	(3%)
560	13.4 ps	(75%)	88.4 ps	(21%)	1119 ps	(4%)

7.4. Discussion

From the observed ultrafast fluorescence dynamics of the native PYP and derivatives in our former study (Chapter 6), we were able to obtain several conclusions [11]. The unbridged native PYP showed ultrafast fluorescence decay components, while the bridged derivative of PYP showed no such fast behavior. From this we

concluded that bridging led to the prevention of isomerization involving torsion about the double bond and therefore this isomerization process then no longer could enhance the fluorescence dynamics. From the enhanced spectral broadening, observed for the PYP sample containing the ferulic acid chromophore, it was concluded that the ferulic acid chromophore fits less well in the protein pocket due to the attachment of a methoxy group on the phenyl ring.

In this chapter, we study the isomerization in further detail by changing the groups directly attached to the chromophore double bond. Furthermore, the results of the ferulic acid PYP, are now complemented by those of caffeic acid PYP.

As remarked in Section 7.3 (see also Figure 7.3b), the fluorescence decay kinetics of the deuterated sample are not different from that for native PYP. This indicates that the reaction rate of the isomerization process is not influenced by the replacement of protons to deuterons. Several theoretical and experimental studies have previously been performed to investigate the deuterium isotope effect on isomerization rates. In different systems with C-C bond isomerization, k(H)/k(D) ratios between 1.15 and 1.46 have been predicted [21,22]. Experimentally 1.47 has been found for stilbene [21]. The fact that we did not observe an isotope effect on the isomerization rate of coumaric acid indicates that here the isoptope effect is reduced, possibly by the protein environment.

In the case of the α-brominated sample, the steady-state emission spectrum in Figure 7.2c shows a red shift of about 2000 cm^{-1} compared to the native PYP emission. This indicates that energy levels in the chromophore are influenced somewhat by bromination. This result is in agreement with earlier studies of halogen substitution showing that electron-withdrawing substituents (like bromine) lower the excited state energy levels [23,24]. From Figure 7.3c it can be seen that the fluorescence decay kinetics of α-Br PYP is comparable to that for native PYP (Figure 7.3a). Apparently, the kinetics of the isomerization process of the chromophore in PYP is barely influenced by Br-substitution of the vinyl hydrogen atoms. We conclude that changing the inertial moment of the vinyl group is not a determining factor for the isomerization dynamics, thus suggesting that the isomerization process may involve a rearrangement involving motions other than a simple rotation about the C=C double bond. Likewise, the possibility of sterical hindrance by the Br-atom in the isomerization process can be

neglected.

In a recent report on nanosecond time-resolved X-ray crystallography of PYP it was discussed how the PYP chromophore is moving inside the protein pocket upon photo-excitation [25]. From the crystallographic data, the atomic positions of the chromophore in the ground (pG) state and, after the first step in the photocycle, the (pR) state were compared. It was found that the breaking and forming of H-bonds between the protein and the chromophore are rate-determining steps in the primary process. In another study it was shown that the protein environment has a large influence on the isomerization process [17,18]. More specifically, it was shown that modifications of the protein pocket, by side-directed mutagenesis, influences the rate of trans-cis isomerization. On the other hand, our observations show that substituents neighboring the double bond in the chromophore molecule have no influence on the rate of the isomerization process. It is likely therefore that the protein backbone provides the driving force for the isomerization process.

In the case of the caffeic acid chromophore, the temporal behavior of the fluorescence largely resembles that for the ferulic acid PYP hybrid [11]. As mentioned in Section 7.3, the multi-exponential decay times of the fluorescence intensity are detection wavelength dependent. The ultrafast components are only present at the blue edge of the emission spectrum. For the ferulic acid this behavior was discussed in terms of inhomogeneous broadening. As seen from Figure 6.1a and b (Chapter 6), the steady-state absorption band of ferulic acid is slightly broader than that for the native coumaric acid chromophore. The structural change on the ring may affect the excited state potential and therefore the inhomogeneous broadening. The same explanation might hold for caffeic acid. The size of the substituted group can result in a less well fit of the chromophore in the protein pocket. This leads to increased inhomogeneous spectral broadening and therefore to an enhanced variation in decay times over the emission band. The shortest decay times may then have disappeared when detecting at the red edge of the emission.

In summary, the influence of substituents near the double bond of the chromophore of photoactive yellow protein is as follows. Bridging of the double bond of the chromophore, which prevents the isomerization process, eliminates the ultrafast decay components. Such decay components can thus be associated with the isomerization process in the unbridged compounds. Subgroups directly attached to the

double bond have negligible effect on the isomerization kinetics. From this we infer that the protein backbone largely determines the trans-cis isomerization process.

References

[1] G. G. Kochendoerfer and R. A. Mathies, Israel J. of Chemistry **35**, 211 (1996).

[2] F. Andel , K.C. Hasson F. Gai , P.A. Anfinrud , R.A. Mathies, Biospec. **3**, 421 (1997).

[3] R. Kort, H. Vonk, X. Xu, W.D. Hoff, W. Crielaard, and K.J. Hellingwerf, FEBS Letters **382**, 73 (1996).

[4] W.D. Hoff, P. Dux, K. Hard, B. Devreese, I.M. Nugteren-Roodzant, W. Crielaard, R. Boelen, R. Kaptein, J. van Beeumen, and K.J. Hellingwerf, Biochem. **33**, 13959 (1994).

[5] M. Baca, G.E.O. Borgstahl, M. Boissinot, P.M. Burke, D.R. Williams, K.A. Slater, and E.D. Getzoff, Biochem. **33**, 14369 (1994).

[6] W.D. Hoff, B. Devreese, R. Fokkens, I.M. Nugteren-Roodzant, J. van Beeumen, N. Nibbering, and K.J. Hellingwerf, Biochemistry **35**, 1274 (1996).

[7] M. Kim, R. A. Mathies, W. D. Hoff, and K. J. Hellingwerf, Biochem. **34**, 12669 (1995).

[8] T.E. Meyer, E. Yakali, M.A. Cusanovich, and G. Tollin, Biochemistry **26**, 418 (1987).

[9] W.D. Hoff, I.H.M. van Stokkum, H.J. van Ramesdonk, M.E. van Brederode, A.M. Brouwer, J.C. Fitch, T.E. Meyer, R. van Grondelle, and K.J. Hellingwerf, Biophys. J. **67**, 1691 (1994).

[10] A.R. Kroon, W.D. Hoff, H. Fennema, G.J. Koomen, J.W. Verhoeven, W. Crielaard, and K.J. Hellingwerf, J. Biol. Chem. **271**, 31949 (1996).

[11] P. Changenet, H. Zhang, M.J. van der Meer, K.J. Hellingwerf, M. Glasbeek, Chem. Phys. Lett. **282**, 276 (1998).

[12] M. Du, G.R. Fleming, Biophys. Chem. **48**, 101 (1993).

[13] G. Haran, K. Wynne, A. Xie, Q. He, M. Chance, R.M. Hochstrasser, Chem. Phys. Lett. **261**, 389 (1996).

[14] K.C. Hasson, F. Gai, P.A. Anfinrud, Proc. Natl. Acad. Sci. USA **93**, 15124 (1996).

[15] A. Xie, W.D. Hoff, A.R. Kroon, K.J. Hellingwerf, Biochemistry **35**, 14671 (1996).

[16] Y. Imamoto, K. Mihara, O. Hisatomi, M. Katoaka, F. Tokunaga, N. Bojkova, K. Yoshihara, J. Biol. Chem. **272**, 12905 (1997).

[17] H. Chosrowjan, N. Mataga, Y. Shibata, Y. Imamoto, F. Tokunaga, J. Phys. Chem. B **102**, 7695 (1998).

[18] N. Mataga, H. Chosrowjan, Y. Shibata, Y. Imamoto, F. Tokunaga, J. Phys. Chem. B **104**, 5191 (2000).

[19] P. van der Meulen, H. Zhang, A. M. Jonkman, and M. Glasbeek, J. Phys. Chem. **100**, 5367 (1996).

[20] E.R. Middelhoek, P. van der Meulen, J.W. Verhoeven, and M. Glasbeek, Chem. Phys. **198**, 373 (1995).

[21] L.P. Olsen, S. Niwayama, H.Y. Yoo, K.N. Houk, N.J. Harris, J.J. Gajewski, J. Am. Chem. Soc. **118**, 886 (1996).

[22] F. Negri, G. Orlandi, J. Phys. Chem. **95**, 748 (1991).

[23] R.S. Murphy, C.P. Moorlag, W.H. Green, C. Bohne, J. Photochem. Photobiol. A Chem. **110**, 123 (1997).

[24] C. Burgdorff, S. Ehrhardt, H.G. Lohmannsroben, J. Phys. Chem. **95**, 4246 (1991).

[25] B. Perman, V. Srajer, Z. Ren, T.Y. Teng, C. Pradervand, T. Ursby, D. Bourgeois, F. Schotte, M. Wulff, R. Kort, K. Hellingwerf, K. Moffat, Science **279**, 1946 (1998).

Samenvatting

Om het verloop van een chemische reactie te begrijpen, wordt meestal uitgegaan van een potentiële-energiefunctie als functie van een reactiecoördinaat. Deze reactiecoördinaat wordt doorgaans bepaald door intramoleculaire vibraties of rotaties en, in het geval dat de moleculen in oplossing zijn, door bewegingen van de oplosmiddelmoleculen. De reacties waar wij in het bijzonder onze aandacht op hebben gericht zijn ultrasnelle intramoleculaire reoriëntatiebewegingen van moleculen in oplossing. De invloed van verschillende oplosmiddeleigenschappen zoals viscositeit en polariteit op de intramoleculaire reoriëntatiebewegingen zijn bestudeerd. Onze belangrijkste aandachtspunten zijn de aard van de reactiecoördinaat en de vorm en samenstelling van de potentiële energiefunctie van de reactie. Met behulp van tijdsopgeloste fluorescentie spectroscopie met een tijdresolutie in het picoseconde en het femtoseconde tijdsdomein zijn verschillende moleculaire systemen in oplossing bestudeerd. De metingen in het femtoseconde tijdsdomein werden uitgevoerd met behulp van de fluorescentie up-conversie techniek waarbij de moleculen geëxciteerd werden door een femtoseconde gepulste titaan:saffier laser (tijdresolutie ~150 fs). De picoseconde metingen werden uitgevoerd met een fluorescentie single-photon-counting opstelling met een tijdresolutie van ± 16 ps.

In Hoofdstuk 1 wordt een inleiding gepresenteerd over het vakgebied van de ultrasnelle tijdsopgeloste spectroscopie. Begrippen als solvatatie dynamica, intramoleculaire bewegingen en isomerisatie komen aan de orde. Ook wordt er teruggeblikt op (recente) literatuur op dit gebied. Er is aandacht voor zowel de experimentele als de theoretische kant van ultrasnelle foto-geïnduceerde reacties.

In Hoofdstuk 2 geven we een beschrijving van de twee gebruikte experimentele opstellingen (de femtoseconde up-conversie en de picoseconde single-photon-counting opstelling). Het principe van beide opstellingen en de gebruikte lasersystemen worden kort uitgelegd. Ook wordt een overzicht gegeven van de gebruikte chemicaliën en de wijze waarop deze gebruikt zijn.

In Hoofdstuk 3 rapporteren we over onze resultaten van femto- en picoseconde tijdsopgeloste fluorescentie metingen aan auramine, een laserdye, als functie van de viscositeit van het oplosmiddel. De ultrasnelle exponentiële vervaltijden

in laag visceuze oplosmiddelen (bijv. ethanol) worden vertienvoudigd in oplosmiddelen met een hoge viscositeit (bijv. decanol). Een interne rotatie van een functionele groep van het molecuul wordt verondersteld het snelle verval te veroorzaken. De rotatie ondervindt een grotere tegenwerking in een meer visceus oplosmiddel.

In Hoofdstuk 4 wordt de invloed van het oplosmiddel op de ultrasnelle dynamica van auramine in oplossing verder onderzocht. In dit geval wordt de viscositeit van het oplosmiddel (ethanol) veranderd door het verlagen van de temperatuur. Om de experimentele resultaten te simuleren wordt een theoretisch model bediscussieerd. Uit de simulaties volgt dat de geëxciteerde electronen toestand van auramine een adiabatisch gekoppelde toestand is van twee elektronen toestanden waarvan de eerste wel emitteert en de tweede een zogenoemde donkere toestand is. De rotatie van de phenyl-groepen van auramine zorgt voor het overgaan van de stralende (emitterende) toestand naar de donkere toestand. Een verhoogde viscositeit zorgt voor een frictie die het rotatieproces vertraagt, waardoor de snelheid van het relaxatieproces van de stralende naar de donkere toestand afneemt.

In Hoofstuk 5 worden verschillende gebrugde en ongebrugde ionische styryl moleculen onderzocht in oplosmiddelen met verschillende viscositeit en polariteit. Uit de pico- en femtoseconde tijdsopgeloste fluorescentie metingen blijkt dat de waargenomen ultrasnelle dynamische Stokes verschuiving bepaald wordt door solvatatie dynamica. Dit geldt zowel voor de gebrugde als de ongebrugde verbindingen. Wel blijkt dat de levensduur van de elektronische toestanden enorm toeneemt naarmate de moleculaire groepen minder flexibel zijn. Torsie bewegingen binnen het molecuul hebben dus alleen invloed op het niet-stralende verval van de elektronisch aangeslagen fluorescerende toestand.

In Hoofdstuk 6 presenteren we de resultaten van onze tijdsopgeloste studie aan het fluorescerende photo-active yellow protein (PYP). Het kleurencentrum (chromofoor) van dit eiwit bevat een dubbele binding waarvan men aanneemt dat een trans-cis isomerisatieproces het begin vormt van een fotocyclus, zoals bij andere soortgelijke eiwitten is waargenomen. Door een brug over de dubbele binding in het molecuul in te bouwen kan worden voorkomen dat de isomerisatie plaats vindt. Uit de resultaten van onze experimenten blijkt dat de ultrasnelle verval componenten die bij het wild-type PYP voorkomen niet aanwezig zijn in de metingen van het eiwit met het

gebrugde chromofoor. Dit is een verdere ondersteuning voor het idee dat er een trans-cis isomerisatie op picoseconde tijdschaal plaatsvindt in het wild-type PYP.

Hoofdstuk 7 is een verdere uitbreiding op onze studie van het fluorescerende eiwit PYP. In dit hoofdstuk worden verschillende derivaten van PYP onderzocht, waarbij in één geval de protonen rond de dubbele binding van de chromofoor zijn vervangen door deuteronen, en in een tweede geval een waterstofatoom aan de dubbele binding is vervangen door een broomatoom. Uit de resultaten blijkt dat deze vervangingen geen invloed hebben op de ultrasnelle dynamica van het chromofoor. Dit impliceert, tezamen met bevindingen van anderen in de recente literatuur, dat de eiwitomgeving van het chromofoor de drijvende kracht is achter het trans-cis isomerisatieproces.

Nawoord

Aan het einde van dit proefschrift wil ik graag nog van wat bladzijden gebruik maken om een aantal mensen te bedanken. Door de hulp en aanwezigheid van hen kan ik op een leuke en geslaagde vier jaar Amsterdam terugkijken.

Als eerste wil ik mijn promotor Max Glasbeek bedanken dat hij mij de gelegenheid heeft gegeven binnen zijn groep te promoveren. Ook heeft hij mij bijzonder goed geholpen in het verwoorden van mijn resultaten, zowel in de artikelen als in dit proefschrift.

Zonder de technische hulp van Hong Zhang was dit boekje er helemaal niet geweest. Hem wil ik dan ook heel erg bedanken voor alle hulp in ons donkere femto-lab en ook voor het feit dat hij het vier jaar met me op één kamer heeft uitgehouden. Ik bedank hem uitdrukkelijk niet in het Engels, want het wordt nu echt tijd dat hij een keer Nederlands leert.

De ondersteuning van onze technische medewerkers heeft er voor gezorgd dat er de afgelopen vier jaar überhaupt iets te meten was. Aan allen van hen heb ik veel te danken en om geen onderscheid te maken noem ik hen in alfabetische volgorde. Dick Bebelaar, bedankt voor al je hulp op het pico-lab. Het feit dat je altijd kritisch blijft over de metingen en de apparatuur en de meetomstandigheden heeft zeker bijgedragen aan de kwaliteit van mijn metingen. Michiel Groeneveld wil ik bedanken voor alle optische hulpmiddelen die hij voor ons gemaakt heeft en ook voor de gezellige koffie en bier tijd. Jos Scheijde, inmiddels van papa- naar opa-Jos gepromoveerd, wil ik bedanken voor de digitale ondersteuning en voor de vele wandelingen in Amsterdam-Oost. Eigenlijk zouden we ook eens een biertje met elkaar moeten drinken. Rolf Sitters, zeker niet in de laatste plaats, kan ik eigenlijk wel op alle gebieden bedanken. In het chemisch lab, maar zeker ook bij de femto-opstelling heeft hij me het werk bijzonder makkelijk en aangenaam gemaakt. De gezellige uurtjes in de Krater hebben hier zeker ook hun bijdrage aan geleverd. Ton Vronik wil ik bedanken voor het fabriceren van enkele hele handige hulpmiddelen voor onze beide opstellingen.

I owe two chapters of my thesis to Pascale Changenet who worked with us for two years as a postdoc. I would like to thank her for her work on PYP and auramine. I

enjoyed working with her and her knowledge helped me with the rest of my chapters as well.

Johnny Hendriks van de vakgroep microbiologie bedank ik voor het maken van mijn PYP-samples.

De leden van de manuscript/promotie-commisie wil ik bedanken voor het zorgvuldig nakijken van mijn manuscript. Ook mijn broer Rob bedank ik voor het uiterst nauwkeurig nakijken van mijn manuscript. Na het vinden van zoveel fouten zou ik bijna zeggen dat de fouten die er nu nog in zitten hem toegerekend kunnen worden.

De directe (ex-)collega's van onze groep, de postdocs Paolo Prosposito en Werner Humbs en de aio's David Marks en Emile van Veldhoven wil ik bedanken voor de prettige samenwerking en de goede werksfeer. Ik bedank hen en de medewerkers en aio's van de andere fysische groepen Dick ter Steege, Arjan Rijkenberg, Anouk Rijs, Marc Smits, Conny Scheper en Wybren-Jan Buma voor de leuke tijd die ik op de vierde verdieping heb gehad. Het was daar en in de Roetertoeter behoorlijk gezellig. De twee barre tochten die ik met Werner, Arjan en Dick heb gemaakt naar de Schneibstein en de Watzmann mogen ook wel even vermeld worden. Ik heb die tochten geweldig gevonden en hoop dat er nog meer volgen.

Clara, Monique en Adriaan wil ik bedanken voor de leuke en leerzame tijd die we samen in het CHAOS-bestuur hebben gehad.

Zeker niet in de laatste plaats bedank ik het thuisfront. Saskia, bedankt voor de steun en het geduld van de afgelopen vier jaar. Ook wil ik je bedanken voor de prachtige zoon die we hebben gekregen. Lars, bedankt voor je lach en je traan. Door jou kwamen alle mee- en tegenvallers weer eens in het juiste perspectief te staan.

Michiel.